HELSINKI INSTITUTE OF PHYSICS INTERNAL REPORT SERIES

HIP-2012-02

On the Effects of Cosmic Structures in the Late Universe

Maria Mattsson

Helsinki Institute of Physics
P.O. Box 64, FIN-00014 University of Helsinki, Finland

ACADEMIC DISSERTATION
To be presented, with the permission of the Faculty of Science of the University of Helsinki, for public criticism in the Auditorium XV of the University Main building (Fabianinkatu 33), on the 2nd of July 2012 at one o'clock.

Helsinki 2012

ISBN 978-952-10-5333-7
ISSN 1455-0563
ISBN 978-952-10-5334-4 (pdf version)
http://ethesis.helsinki.fi
Yliopistopaino
Helsinki 2012

Contents

Mattsson, Maria: On the Effects of Cosmic Structures in the Late Universe, University of Helsinki, 2012, 79 p. + appendices, Helsinki Institute of Physics Internal Report Series, HIP-2012-02, ISSN 1455-0563, ISBN 978-952-10-5333-7 (printed version), ISBN 978-952-10-5334-4 (pdf version).
INSPEC classification: A9880, A9880D, A9880L, A0420.
Keywords: cosmology, gravitation, general relativity, accelerating Universe, large scale structure (cosmological), dark energy.

Abstract

During the last decade, the cosmological observations have indicated that the homogeneous and isotropic Friedmann models with linear perturbations fail to describe our universe at late times unless a dominant energy component with negative pressure called dark energy is introduced. In this thesis, we study the implications of the nonlinear nature of general relativity on the cosmological model building beyond the standard Friedmann models. Despite the well-established observational status of cosmic structures, their effects have gained more attention only along with the dark energy debate. In particular, the fact that the start of the supposed dark energy domination coincides with the time the nonlinear inhomogeneities started to form on larger scales, motivates the study of the dynamics of the cosmic structures.

In cosmology, the implication of the nonlinearity of gravity is that averages of inhomogeneous quantities do not evolve in time like the corresponding homogeneous quantities – a phenomenon referred to as the backreaction. Due to the new precision observations during the recent years, the evaluation of the backreaction in our universe is a topical, but complex task. In this thesis, rather than trying to fully quantify the backreaction, the emphasis is on the model building. We explicitly demonstrate the importance of the exact matching conditions in the solutions representing cosmic structures in the context of backreaction evaluation. Indeed, the cosmic web of structures is made of very differently behaving regions and the shear on the interface between the different regions seems to play an important role.

The backreaction term emerging from averaging the Einstein equation is not the only effect that cosmic structures can have on the observations. Indeed, we also demonstrate that even though the backreaction would remain small, large effects can arise from the choice of the smoothing scale and, perhaps surprisingly, from perturbative models as well. As we find, at least the supernova data can be explained within a linearly perturbed Friedmann model – without dark energy. The key point is to take into account the effects of structures on the observable distance measures, ignored in the standard cosmological perturbation theory. Further inspection shows that the model is actually equivalent to a nonperturbative inhomogeneous solution, confirming that the supernova data does not necessarily imply additional nonperturbative corrections.

Considering physical quantities such as the expansion rate of space and the matter density, there are large local variations in the cosmic web. The main question to answer is whether (and to what extent) the effects of the local variations average out or accumulate in the observables. It appears likely that when combining all the cosmological data, more sophisticated models than the perturbed Friedmann or the simplest spherically symmetric exact inhomogeneous solutions are required to fully quantify the effects of the structures on the cosmological observations.

Acknowledgements

This thesis is based on research carried out in the Helsinki Institute of Physics at the University of Helsinki and in the University of Canterbury in New Zealand. The financial support from the Academy of Finland, the Graduate School in Particle and Nuclear Physics (GRASPANP), the Vilho, Yrjö and Kalle Väisälä Foundation, the Magnus Ehrnrooth Foundation and the EU 6th Framework Marie Curie Research and Training network "UniverseNet" (MRTN-CT-2006-035863), is gratefully acknowledged.

Firstly, I thank my supervisor Prof. Kari Enqvist for his support, guidance and advices, as well as allowing me for the opportunity to do a major part of this thesis work in New Zealand. I consider myself fortunate to have had Kari as my supervisor during both my undergraduate and graduate studies. It is also a pleasure to thank the lecturers of the theoretical physics courses at the University of Helsinki, in particular Dr. Hannu Kurki-Suonio for his inspiring courses in general relativity and cosmology. Furthermore, my high school teachers Eija Keronen, Jyrki Pihlman and Juhani Luoma are warmly acknowledged for awakening my enthusiasm in physics. I also thank the pre-examiners of my thesis, Prof. Kimmo Kainulainen and Dr. Valerio Marra, for their valuable comments.

I am very grateful for the time I have been able to spend in the University of Canterbury. Prof. David Wiltshire deserves special thanks for his hospitality and providing me with all the facilities needed to pursue my research.

With all my love, I thank my husband Dr. Teppo Mattsson for always being with me and continuously supporting me. From Teppo, I have learned physics perhaps the most. It has been a privilege to collaborate with him and his excellent physical intuition has been of great help for me. I also thank my collaborator Dr. Gerasimos Rigopoulos for interesting discussions and for sharing his experience.

Finally, I express my gratitude to my beloved family, especially to my mother Marjatta and father Raimo, for their loving care and support during all of my life.

Maria Mattsson

Christchurch, April 2012

List of included papers

The four articles included in this thesis are:

1. T. Mattsson and M. Mattsson, "Exploiting scale dependence in cosmological averaging", JCAP **0802** (2008) 004 [arXiv:0708.3673 [astro-ph]].
2. K. Enqvist, M. Mattsson and G. Rigopoulos, "Supernovae data and perturbative deviation from homogeneity", JCAP **0909** (2009) 022 [arXiv:0907.4003 [astro-ph.CO]].
3. M. Mattsson and T. Mattsson, "On the role of shear in cosmological averaging", JCAP **1010** (2010) 021 [arXiv:1007.2939 [astro-ph.CO]].
4. M. Mattsson and T. Mattsson, "On the role of shear in cosmological averaging II: large voids, non-empty voids and a network of different voids", JCAP **1105** (2011) 003 [arXiv:1012.4008 [astro-ph.CO]].

The contribution of the present author to the joint publications

1. The idea of testing the scale-dependence in the Buchert averaging method within the LTB models came from Teppo Mattsson. All the calculations were performed independently by both authors. The plots were mainly done by the present author. The paper was written through joint efforts, the present author contributing mainly to Sections 3 and 4.
2. The initial idea to deduce the gravitational potential perturbation from the supernova observations and compare the resulting model to the LTB models came from Kari Enqvist and Gerasimos Rigopoulos. The idea was then elaborated on through discussions between all authors. The calculations were done by the present author, and part of them also by Gerasimos Rigopoulos. The plots were done by the present author. All authors took part in writing the paper.
3. Teppo Mattsson suggested to evaluate the shear in the boundaries of voids and walls within the LTB models. The idea was subsequently developed through discussions. All the calculations were performed independently by both authors. Both authors took part in writing the paper.
4. The idea to generalize the study of Paper 3 originated in the discussions between the authors. All the calculations were performed independently by both authors. The draft was written mainly by Teppo Mattsson, and shaped into its final form by joint efforts of both authors.

Chapter 1

Introduction

Cosmology is a science, which tries to understand and explain the universe as a whole − its history, present state, future and the origin. Our theoretical understanding of the cosmos relies on general relativity, a classical theory of gravitation which Einstein completed in 1915 [1]. With given initial conditions, general relativity uniquely determines the evolution of the universe. However, even if we knew the exact initial conditions for our universe, solving the exact equations of general relativity is unfeasible for such a complex system. Therefore, some coarse graining has to be introduced in our theoretical description.

In the standard cosmological picture, the universe is modeled by the spatially homogeneous and isotropic Friedmann-Robertson-Walker (FRW) solution of general relativity, with linear perturbations describing the evolution of structure. The structure is believed to have originated during inflation [2, 3] in the very early universe in the form of small irregularities with simple statistical properties. In addition, until the type Ia supernova observations published in 1998 [4, 5], the standard assumption was that the universe is made of ordinary energy forms with positive pressure, such as matter and radiation. However, the supernova observations suggested that the expansion of the universe has accelerated during the latter part of its lifetime, which would be impossible in the suggested matter-dominated FRW model.

Dark energy, an energy form with negative pressure, is nowadays widely accepted as the missing link to match our theoretical understanding of the evolution history of the universe to the current cosmological observations that suggest late-time acceleration [6–8], as highlighted by the 2011 Nobel prize in physics. Indeed, the standard ΛCDM model of cosmology, capable of successfully explaining all the most important cosmological observations, is an FRW model containing the simplest dark energy candidate, vacuum energy or the cosmological constant Λ [9]. However, dark energy has not been directly observed − its presumed existence is based on producing the otherwise impossible accelerated expansion within the homogeneous FRW models. Moreover, the enormous fine-tuning needed to explain both the size and the timing of such an energy component has raised doubts about its correctness and thus given rise to the search for alternatives [10–14].

The unresolved question of the nature of dark energy, or whether dark energy even exists, affects our overall understanding of the universe and the fundamental laws of physics. Indeed, the need for dark energy could be just an illusion created by a failure of the assumptions in our theoretical description: Firstly, the inconsistency of the homogeneous matter-dominated FRW model with the observations could be a manifestation of our incomplete theory of gravity in describing the universe as a whole [11]. Secondly, dark energy could be an artefact of a too

simple homogeneous model used to describe our universe: in the standard FRW models, the assumption is that the matter distribution in the universe is homogeneous on large distance scales $\gtrsim 100$ Mpc. The validity of this assumption, i.e. the effects of the cosmological structures both on smaller and larger scales, needs to be evaluated thoroughly – after all, there are nonlinear inhomogeneities on smaller scales, and, on larger scales, the universe is homogeneous possibly only in a statistical sense. This thesis has been devoted to the latter alternative – studying the dynamical and observational effects of the nonlinear cosmic structures using inhomogeneous cosmological models of general relativity without the problematic dark energy.

The potential inadequacy of the simplest homogeneous models in describing the complex, inhomogeneous universe was criticized already around the same time when these models were first studied [15, 16]. However, it was not until the supernova observations of the late 1990's when the failure of the simple matter-dominated FRW models to describe our universe became clear. Along with the ensuing dark energy debate, the potential observational consequences of nonlinear structures have gained more attention. As has been demonstrated during recent years (see e.g. Refs. [17–23]), the cosmic structures can have a similar effect on the observations as dark energy. Therefore, a detailed understanding of the effects of the observed structures is essential for the correct interpretation of the cosmological data.

An issue addressed in this thesis is that if the nonlinear structures really are responsible for the observed effect, what is the precise physical interpretation of how they do it and how to model it. Indeed, both the complexity of our universe and the complexity of the underlying theory of gravity have presented considerable challenges for constructing a realistic cosmological model capable of accounting for the effects of the nonlinear inhomogeneities. One possibility is to use exact inhomogeneous solutions of general relativity [15], where the coarse graining shows up implicitly in the form of the symmetries of the solution. After introducing the standard framework in Chapter 2, we discuss exact inhomogeneous cosmological models in the first part of Chapter 3. Within the exact solutions, it has been demonstrated that the accelerated expansion can arise from a faster local expansion rate due to a large local void, see e.g. Refs. [18, 20, 24–33].

Another way to find an appropriate coarse-grained description of the universe is to explicitly average the cosmic structures. In this context, the effect of the nonlinear inhomogeneities is called backreaction. The crucial point is that, in general, an inhomogeneous model of the universe does not evolve on average like a homogeneous one − an issue which the current observations might indicate, an issue which Shirokov and Fisher pointed out already in the 1960's [34] and Ellis made more popular in the 1980's [35, 36]. A problem has been the unambiguous specification of an appropriate averaging procedure [36]; for a recent review, see Ref. [37]. In the latter part of Chapter 3, we shed light on the issue of averaging a cosmological system of general relativity and present the Buchert averaging method [12, 38], which is one of the most widely used averaging methods in cosmology.

Research Papers 1–4 [22, 39–41] are discussed in Chapter 4. We elaborate the Buchert averaging formalism in Papers 1, 3 and 4. In Paper 2, a perturbative alternative is presented and tested against the supernova observations. The central feature of this work is in making an effort towards a more realistic modeling of the cosmic structures. In Chapter 5, we summarize the main results of the research.

Chapter 2

Standard cosmology

In 1929, Edwin Hubble made the cornerstone observation of modern cosmology: distant objects in all directions on the sky are receding from us, the faster the further away they are [42]. Together with the Copernican principle (or the cosmological principle), which states that our position in the universe is not special, this leads to the conclusion that the universe is expanding. From the expansion it in turn follows that in the distant past the universe must have been denser and hotter, giving rise to the idea of Big Bang.

As predicted by Gamow, Alpher and Herman in 1948 [43, 44], according to the hot Big Bang scenario, there should be observable redshifted relic radiation from the time when the universe was only a few hundred thousand years old: The energy content of the early universe was in thermal equilibrium under the extreme temperature and density. The expansion of the universe cooled down the plasma and eventually allowed the electrons and nuclei of the plasma to form neutral atoms in the process called recombination. Soon after recombination, as the number of free electrons decreased, photons decoupled from matter. Since decoupling, those primordial photons, exhibiting a blackbody spectrum, were left to traverse the universe almost freely, cooling down with the expansion.

The presence of this cosmic microwave background (CMB) radiation that baths the Earth from every direction was detected in 1965 by radio astronomers Penzias and Wilson [45], for which they were awarded the physics Nobel prize in 1978. The radiation has closest to the blackbody spectrum ever observed with temperature today $T_0 = 2.725 \pm 0.002$ K and with anisotropies only[1] of the order of 10^{-5}, as measured in 1992 by the COBE satellite [46, 47]. For the COBE measurements, the physics Nobel prize was awarded in 2006. The existence of the CMB is one of the strongest evidence for the Big Bang theory.

The observed slight anisotropies in the CMB spectrum are a consequence of the inhomogeneities in the primordial plasma. A popular hypothesis in modern cosmology is that these tiny density variations originate from close to Gaussian random fluctuations around a homogeneous and isotropic background generated by inflation in the very early universe. The perturbations are thereafter amplified by gravitational attraction to eventually form the structures in the universe [48–50].

The largest observed structures in the universe consist of clusters and filaments of galaxies with nearly empty voids in between them [51–54]. Mappings of the large scale structure, such as

[1] Excluding the 10^{-3} dipole anisotropy.

the Two-degree-Field Galaxy Redshift Survey (2dFGRS) [55] and the Sloan Digital Sky Survey (SDSS) [56], seem to indicate spatial homogeneity of the universe on scales $\gtrsim 100h^{-1}$ Mpc, where $h = H_0/(100$ km/s/Mpc).

The observations above have led one to consider expanding universe models, which are to a first approximation homogeneous as well as isotropic. Within these models, the growth of structures is described as linear perturbations evolving on the smooth background. Before presenting these models, we first briefly discuss the theory of gravitation needed to determine the cosmological dynamics.

2.1 General relativity

Einstein's general theory of relativity [1] – the most accurate description of gravitation so far [57] – determines the dynamics for the spacetime metric g with components $g_{\mu\nu}$[2]. It describes gravity not as a classical force between particles, but as the curving of spacetime due to the distribution of energy in space and time. General relativity is a deterministic classical theory of gravitation: given the initial conditions in the early universe, the later evolution is uniquely determined.

In general relativity, the gravitational field is described by a rank four tensor, the Riemann curvature tensor

$$R^{\alpha}{}_{\sigma\mu\nu} = \partial_\mu \Gamma^{\alpha}_{\nu\sigma} - \partial_\nu \Gamma^{\alpha}_{\mu\sigma} + \Gamma^{\alpha}_{\mu\lambda}\Gamma^{\lambda}_{\nu\sigma} - \Gamma^{\alpha}_{\nu\lambda}\Gamma^{\lambda}_{\mu\sigma} \ , \tag{2.1}$$

where the quantities $\Gamma^{\alpha}{}_{\mu\nu}$ are known as the Christoffel symbols, related to the metric through

$$\Gamma^{\alpha}{}_{\mu\nu} = \frac{1}{2} g^{\alpha\sigma}(\partial_\mu g_{\nu\sigma} + \partial_\nu g_{\mu\sigma} - \partial_\sigma g_{\mu\nu}) \ . \tag{2.2}$$

The Riemann tensor (2.1) contains the full information about the curvature of spacetime. Eqs. (2.1) and (2.2) tell us that the Riemann tensor is given by the metric and its first and second derivatives, in accordance with the interpretation of the metric as a gravitational tensor potential. As the metric thus uniquely determines the spacetime curvature, it can be regarded as a fundamental variable.

One can decompose the Riemann tensor (2.1) into the trace

$$R_{\sigma\nu} \equiv R^{\alpha}{}_{\sigma\alpha\nu} \ , \tag{2.3}$$

called the Ricci tensor, and the traceless part

$$C_{\alpha\sigma\mu\nu} \equiv R_{\alpha\sigma\mu\nu} - (g_{\alpha[\mu}R_{\nu]\sigma} - g_{\sigma[\mu}R_{\nu]\alpha}) + \frac{1}{3} g_{\alpha[\mu}g_{\nu]\sigma}R \ , \tag{2.4}$$

called the Weyl tensor (written in four dimensions), and we have further defined the Ricci scalar as

$$R \equiv g^{\mu\nu}R_{\mu\nu} \ . \tag{2.5}$$

The square brackets in Eq. (2.4) denote antisymmetrization:

$$A_{[\mu\nu]} \equiv \frac{1}{2!}\left(A_{\mu\nu} - A_{\nu\mu}\right) \tag{2.6}$$

[2] In this thesis, the metric signature is chosen to be $\{-,+,+,+\}$. A Greek letter $\alpha, \beta, ...$ as an index gets values from 0 to 3, and Latin letters $i, j, ...$ get values from 1 to 3, referring to the spatial parts of the quantities in question. We assume the Einstein summation convention, where applicable. Furthermore, we use natural units where the speed of light, the Planck constant and the Boltzmann constant are set to one: $c = \hbar = k_B = 1$.

$$B_{[\mu\nu\sigma]} \equiv \frac{1}{3!}\left(B_{\mu\nu\sigma} - B_{\nu\mu\sigma} + B_{\sigma\mu\nu} - B_{\sigma\nu\mu} + B_{\nu\sigma\mu} - B_{\mu\sigma\nu}\right) \ , \tag{2.7}$$

and similarly for objects with more indices.

The local part of the relation between energy and the geometry of the spacetime is provided by the Einstein equation

$$G_{\mu\nu} = 8\pi G T_{\mu\nu} \ , \tag{2.8}$$

where $G_{\mu\nu}$ is the Einstein tensor corresponding to the geometry,

$$G_{\mu\nu} \equiv R_{\mu\nu} - \frac{1}{2} g_{\mu\nu} R \ , \tag{2.9}$$

and $T_{\mu\nu}$ is the energy-momentum tensor carrying the information on energy density, momentum density, pressure and stress. The Weyl tensor (2.4) provides the non-local part of the relation through the Bianchi identity [58].

The Einstein equation (2.8) is a set of ten coupled nonlinear second-order partial differential equations for the ten independent metric components $g_{\mu\nu}$. However, by virtue of the twice-contracted Bianchi identity [58]

$$\nabla_\mu G^{\mu\nu} = 0 \ , \tag{2.10}$$

the number of independent functions is reduced to six. The physical embodiment of Eq. (2.10) together with the Einstein equation (2.8) is the local conservation of energy and momentum:

$$u^\nu \nabla_\mu T^\mu_\nu = 0 \ , \tag{2.11}$$

where $u^\mu \equiv \mathrm{d}x^\mu/\mathrm{d}\tau$ is the four-velocity of the fluid, τ being the proper time of the fluid particles.

2.2 FRW model

In cosmology, we are interested in the time evolution of the universe, leading to the need to artificially break the symmetry between time and space inherent in general relativity: the four-dimensional curved spacetime manifold has to be split into time and 3-space. A physically well justified choice is to divide the spacetime into spatial hypersurfaces of constant time coordinate t measuring the proper time of the freely-falling observers. The most general metric describing a time-evolving, exactly spatially homogeneous and isotropic spacetime is the Robertson-Walker (RW) metric for which the spacetime line-element,

$$\mathrm{d}s^2 = g_{\mu\nu}\mathrm{d}x^\mu \mathrm{d}x^\nu \ , \tag{2.12}$$

in the comoving synchronous coordinates reads as[3] [58]

$$\mathrm{d}s^2 = -\mathrm{d}t^2 + a^2(t)\left[\frac{\mathrm{d}r^2}{1-kr^2} + r^2(\mathrm{d}\theta^2 + \sin^2\theta \mathrm{d}\varphi^2)\right] \ , \tag{2.13}$$

Here $a(t)$ is a dimensionless scale factor describing the volume expansion (or contraction) of spatial hypersurfaces, whereas the dimensionful parameter k describes the curvature of spatial hypersurfaces. The cases $k < 0, k = 0, k > 0$ correspond to negative spatial curvature (open), zero spatial curvature (flat) and positive spatial curvature (closed), respectively. Note that

[3] In Sect. 3.2, we present a class of more general metrics, from which the RW metric (2.13) is a special case.

there is a freedom to rescale the radial coordinate r. This freedom is commonly used to make k dimensionless and normalize it to $k \in \{-1, 0, +1\}$. In this case, $a(t)$ has the dimension of distance since the rescaled r is dimensionless. A common alternative is to choose the normalization such that $a(t_0) \equiv a_0 = 1$, where t_0 is some reference time[4].

2.2.1 The Friedmann equations

The dynamics of the metric (2.13) is given by the Einstein equation (2.8).

The energy content of a homogeneous and isotropic universe is described by the ideal fluid [58], whose energy-momentum tensor has the following form

$$T_{\mu\nu} = (\rho + p)u_\mu u_\nu + p g_{\mu\nu} \ , \tag{2.14}$$

where $u^\mu \equiv \mathrm{d}x^\mu/\mathrm{d}\tau$ is the four-velocity of the fluid which, in the comoving coordinates of the metric (2.13), is at rest $u^\mu = \delta^\mu_0$ by definition and orthogonal to the spatial hypersurfaces. The symbols $\rho \equiv \rho(t) \equiv \sum_i \rho_i(t)$ and $p \equiv p(t) \equiv \sum_i p_i(t)$ stand for the energy density and pressure respectively, where the sums run over different non-interacting fluid components labeled by the index i. For the ideal fluid, the continuity equation (2.11) in the comoving coordinates reads as

$$\dot{\rho} + 3H(\rho + p) = 0 \ . \tag{2.15}$$

The nonzero Einstein tensor (2.9) components for the RW metric (2.13) are

$$G^0{}_0 = -\frac{3}{a^2}(\dot{a}^2 + k) \tag{2.16}$$

$$G^i{}_j = -\frac{1}{a^2}(2\ddot{a}a + \dot{a}^2 + k)\delta^i_j \ , \tag{2.17}$$

where the dot indicates a derivative with respect to the time coordinate. By applying the energy-momentum tensor (2.14) to the Einstein equation (2.8), we arrive at the Friedmann equations that determine the evolution of the scale factor in terms of the energy density and the pressure:

$$H^2 + \frac{k}{a^2} = \frac{8\pi G}{3}\rho \tag{2.18}$$

$$\frac{\ddot{a}}{a} = -\frac{4\pi G}{3}(\rho + 3p) \ , \tag{2.19}$$

where $H(t) \equiv \dot{a}/a$ is the Hubble parameter describing the volume expansion of the fluid. The value of the Hubble parameter at some reference time t_0, usually taken to be the present time, is called the Hubble constant and denoted by $H_0 \equiv H(t_0)$. Eq. (2.18) is often referred to as the Friedmann equation and Eq. (2.19) as the acceleration equation. The continuity equation (2.15) can be derived also from the Friedmann equations (2.18) and (2.19), thus providing no independent additional information.

Altogether, the Friedmann universe contains three dynamical degrees of freedom, the scale factor $a(t)$, the density $\rho(t)$ and the pressure $p(t)$, and only two independent equations governing their evolution. In order to solve the system, we thus need e.g. the equation of state $p = p(\rho)$, which, in the case of the ideal fluid has the form

$$p(t) = w(t)\rho(t) \ , \tag{2.20}$$

[4]Note that the normalizations of k and a_0 cannot be applied simultaneously.

where $w(t)$ is the equation of state parameter. For a constant equation of state parameter w, the continuity equation (2.15) can be integrated for the energy density to yield

$$\rho = \rho_0 \left(\frac{a_0}{a}\right)^{3(1+w)} \ , \tag{2.21}$$

where the subscript 0 refers to the value at the reference time t_0. For a spatially flat universe (i.e. $k = 0$), plugging Eq. (2.21) into the Friedmann equation (2.18) yields for the evolution of the scale factor:

$$a = a_0 \left(\frac{t}{t_0}\right)^{\frac{2}{3(1+w)}} \tag{2.22}$$

for $w \neq -1$ and

$$a = a_0 e^{H(t-t_0)} \tag{2.23}$$

for $w = -1$, where the Hubble parameter H is a constant.

It is common to measure the energy density relative to the value needed to make the universe flat. The critical density is thus given by

$$\rho_c(t) = \frac{3H^2}{8\pi G} \ , \tag{2.24}$$

and the relative energy densities are denoted by

$$\Omega_i(t) = \frac{\rho_i(t)}{\rho_c(t)} \ , \tag{2.25}$$

where the index i labels different components. The total density parameter in units of the critical density (2.24) is defined as

$$\Omega(t) \equiv \frac{\rho(t)}{\rho_c(t)} \ , \tag{2.26}$$

so that $\Omega = \sum_i \Omega_i$. In terms of the density parameter (2.26), the Friedmann equation can be rewritten as

$$\Omega - 1 = \frac{k}{(aH)^2} \ . \tag{2.27}$$

It thus follows that the nature of the curvature depends on the density parameter Ω as

$$\begin{aligned} \Omega < 1 \quad &\Leftrightarrow \quad k < 0 \\ \Omega = 1 \quad &\Leftrightarrow \quad k = 0 \\ \Omega > 1 \quad &\Leftrightarrow \quad k > 0 \ . \end{aligned} \tag{2.28}$$

It is compatible with the standard model of particle physics to assume that the cosmic fluid in the early universe consists of essentially two components: non-relativistic matter with $w = 0$ and highly relativistic matter or radiation with $w = 1/3$. In addition, in the standard model of cosmology, vacuum energy or the cosmological constant Λ with $w = -1$ is included at late times, as discussed in Sect. 2.4. According to Eq. (2.21), the energy densities thus behave as

$$\rho_m(t) = \rho_m(t_0) \left(\frac{a_0}{a}\right)^3 \tag{2.29}$$

$$\rho_r(t) = \rho_r(t_0) \left(\frac{a_0}{a}\right)^4 \tag{2.30}$$

$$\rho_\Lambda = \text{const.}, \tag{2.31}$$

for radiation, matter and vacuum energy, respectively. The energy density of matter scales inversely with volume, as can be expected from the mass conservation. The energy density of radiation decreases with a factor of a^{-1} compared to matter due to the gravitational redshift

$$z \equiv \frac{\lambda_o - \lambda_e}{\lambda_e} = \frac{a_0}{a} - 1 \ , \tag{2.32}$$

where the subscripts o and e refer to the observer and emitter, respectively. Radiation thus only accounts for a very small fraction of the total energy density in the universe today. A constant energy density will inevitably become dominant at late times.

The Friedmann equation (2.18) can be cast into yet another useful form in terms of the density parameters by using the definitions (2.24) and (2.25) and Eqs. (2.27) and (2.29) – (2.31): substituting $\rho_m(t) = (3H_0^2\Omega_m)/(8\pi G)\,(a_0/a)^3$, $\rho_r(t) = (3H_0^2\Omega_r)/(8\pi G)\,(a_0/a)^4$, $\rho_\Lambda = (3H_0^2\Omega_\Lambda)/(8\pi G)$ and $k = H_0^2(\Omega_0 - 1)a_0^2$ into the Friedmann equation (2.18), yields

$$H^2(t) = H_0^2 \left[\Omega_m \left(\frac{a_0}{a}\right)^3 + \Omega_r \left(\frac{a_0}{a}\right)^4 + \Omega_\Lambda + (1 - \Omega_0)\left(\frac{a_0}{a}\right)^2\right] \ , \tag{2.33}$$

where $\Omega_i \equiv \Omega_i(t_0)$ and $\Omega_0 = \Omega_m + \Omega_r + \Omega_\Lambda$.

We will follow the convention to refer to the flat matter-dominated ($\Omega_0 = \Omega_m = 1, k = 0$) FRW model as the Einstein-de Sitter (EdS) model, and the empty model ($\Omega_0 = 0$) as the Milne model.

2.3 Cosmological observations

In order to build a cosmological model that closely describes our universe, we must determine the values of the free parameters by testing the model against observations. The testing is done mainly against astrophysical observations, but also against data from particle physics experiments, such as the Large Hadron Collider (LHC) at Cern [59]. The different astrophysical observations provide small bits of information each; no single experiment is able to constrain all of the parameters alone and the combination of different data sets gives more strict constraints on the parameters than a single data set. In addition, there are usually degeneracies among the different parameters. The three most important astrophysical sources of observations in cosmology are the type Ia supernovae (SNIa), the cosmic microwave background (CMB) radiation and the distribution of galaxies on large scales.

2.3.1 Type Ia supernovae

Using supernovae, particularly of type Ia, has turned out to be a good way of determining the relation between redshifts and distances, and thus the expansion history of the universe. Light emitted at the supernova explosion will be redshifted along its path towards the observer due to the expansion of the universe. Furthermore, the light will appear dimmer due to the distance to the supernova, with the exact amount of dimming depending on the expansion of the universe along our line of sight to the object. Thus, by measuring the redshifts and energy fluxes from supernovae at different distances from us, we can constrain the expansion of the universe along our line of sight from today back until the time corresponding to the emission of light from the farthest supernova.

The fact enabling this procedure is that the type Ia supernovae are believed to be so-called standardizable candles [60]. This means that the absolute or intrinsic luminosity L, that is the total power emitted by the source, can be deduced quite accurately by observing the light curves of the supernovae. If this intrinsic luminosity is known, the distance to the object can be found by measuring the apparent luminosity l, that is the received power per unit area (intensity or the energy flux), of the incoming radiation. This defines the luminosity distance through

$$d_L \equiv \sqrt{L/4\pi l} \ , \tag{2.34}$$

which in the static Euclidean space would also correspond to the physical distance of the object. What is still needed is to calculate the theoretical relation between the luminosity distance and the redshift, $d_L(z)$, for a specific cosmological model in question and then to compare it with the observed relation.

Also another distance measure, called the angular diameter distance d_A, can be defined as

$$d_A \equiv \frac{s}{\Theta} \ , \tag{2.35}$$

where s is the proper size of the object and Θ its observed angular diameter on the sky. There is a general relation between the angular diameter and luminosity distances,

$$d_L(z) = (1+z)^2 d_A(z) \ , \tag{2.36}$$

which holds for geodesic light in any spacetime as proved by Etherington in 1933 [61,62]. We can thus speak simply about an observable distance-redshift relation $d(z)$ which can refer to both $d_A(z)$ and $d_L(z)$.

In 1998 two independent groups, the High-z Supernova Search Team (HZT) and Supernova Cosmology Project (SCP) headed by B. Schmidt and S. Perlmutter respectively, announced the observations of 16 type Ia supernovae. When interpreted within the FRW models, these supernovae indicated a presence of the cosmological constant Λ which would dominate the energy density of the universe [4, 5]. The observation leading to this conclusion was that the type Ia supernovae at large redshifts appear fainter than expected in a perfectly homogeneous and isotropic matter-dominated FRW universe [4]. For this discovery, the 2011 physics Nobel prize was awarded to Perlmutter, Schmidt and Riess. The suggested interpretation for this excess dimming of the distant supernovae is that the expansion of the universe has accelerated during the latter part of its lifetime due to the cosmological constant term with negative pressure (for further discussion, see Sect. 2.4). Allowing a contribution in the form of Λ to the energy density and assuming a flat[5] FRW universe, the best-fit values for the densities were found to be $\Omega_M \sim 0.3$ and $\Omega_\Lambda \sim 0.7$. Since then, more accurate observations of supernovae have confirmed these ratios [6, 63–66]. Of the different observations, the supernovae provide the most direct evidence for the acceleration, as they probe the integrated cosmic expansion to several redshifts in the range $z = 0 \ldots 2$.

2.3.2 CMB observations

The CMB radiation that baths the earth from all directions consists of photons that have propagated almost freely to us from the last scattering sphere in about 380000-year-old universe, when

[5]The shape of the CMB spectrum from the WMAP analysis combined with the data from the Hubble Space Telescope (HST), which gives an independent estimate of the Hubble parameter, is usually taken as evidence for the flatness of the universe.

the matter and radiation decoupled. The temperature of the decoupled photons has diminished from about 3000 K by the enormous factor the universe has expanded since the early stages so that the average temperature today is $T_0 = 2.725 \pm 0.002$ K, as measured in 1992 by the COBE satellite [46].

The frequency distribution of the CMB is the most precisely measured blackbody spectrum in nature. The CMB temperature is highly isotropic to roughly one part in 10^5, after subtracting out the dipole anisotropy with the observed maximum value $\Delta T/T = 10^{-3}$. The origin of the dipole can be both kinematical, i.e. due to the Doppler shift of the background radiation, which is caused by the peculiar motion of our local galaxy group relative to the CMB rest frame, and cosmological, i.e. due to inhomogeneities the light encounters when traversing the universe, see e.g. Refs. [67, 68]. The small anisotropies in the background temperature were first detected in 1992 by the COBE satellite [47].

By measuring the detailed temperature distribution over the sky, we can gain knowledge about the expansion history of the universe. Furthermore, the observed anisotropy carries a record of the small inhomogeneities in the matter distribution at the time of decoupling and thus the origin of structure in the universe we see today – hotter regions correspond to underdense, colder to overdense regions. Inflation [2, 3] predicts the existence of these initial irregularities with close to Gaussian statistics, arising from quantum fluctuations in the inflaton field during the inflation which took place in the very early universe (roughly from 10^{-36} to 10^{-32} seconds after the Big Bang) [69–71]. The primary anisotropy is due to effects occurring at the last scattering surface and before – most importantly the acoustic oscillations of the baryon-photon fluid (BAO) and the Silk damping [72]. In addition, the cosmological conditions in the later universe affect the observed temperature variations. This secondary anisotropy, occurring between the last scattering surface and the observer, is mainly due to two effects [72]: Firstly, interactions of the background radiation with ionized gas, which happens at reionization and later via the Sunyaev-Zel'dovich effect. Secondly, the Sachs-Wolfe effect, which causes the CMB photons to be gravitationally redshifted or blueshifted due to changing gravitational potentials in the expanding universe.

The CMB temperature distribution over the sky can be written as

$$T(\theta, \phi) = T_0 + \delta T(\theta, \phi) \ , \tag{2.37}$$

where $T_0 = 2.725 \pm 0.002$ K is the observed average temperature and the function $\delta T(\theta, \phi)$ represents the small anisotropy. Conventionally, the observed anisotropy is expanded in terms of spherical harmonics $Y_{lm}(\theta, \phi)$, a complete set of functions on a sphere [73],

$$\frac{\delta T}{T_0}(\theta, \phi) = \sum_{l=1}^{\infty} \sum_{m=-l}^{l} a_{lm} Y_{lm}(\theta, \phi) \ . \tag{2.38}$$

A standard assumption is that the statistical properties of the temperature distribution do not depend on the orientation described by m. One can thus average the observed a_{lm} over the index m to obtain the observed temperature power spectrum:

$$C_l = \frac{1}{2l+1} \sum_{m=-l}^{l} |a_{lm}|^2 \ . \tag{2.39}$$

By assuming the small anisotropy to be a (Gaussian) random variable, one then compares the observed spectrum (2.39) with the theoretical one,

$$\tilde{C}_l \equiv \langle |\tilde{a}_{lm}(P_i)|^2 \rangle = \frac{1}{2l+1} \sum_{m=-l}^{l} \langle |\tilde{a}_{lm}(P_i)|^2 \rangle \ , \tag{2.40}$$

where $\langle \ \cdot \ \rangle$ stands for an average over an ensemble of universes representing all possible realizations of the initial conditions, and P_i represents the cosmological parameters of the model; a comparison between the observed and a theoretical power spectra is plotted in Fig. 2.1.

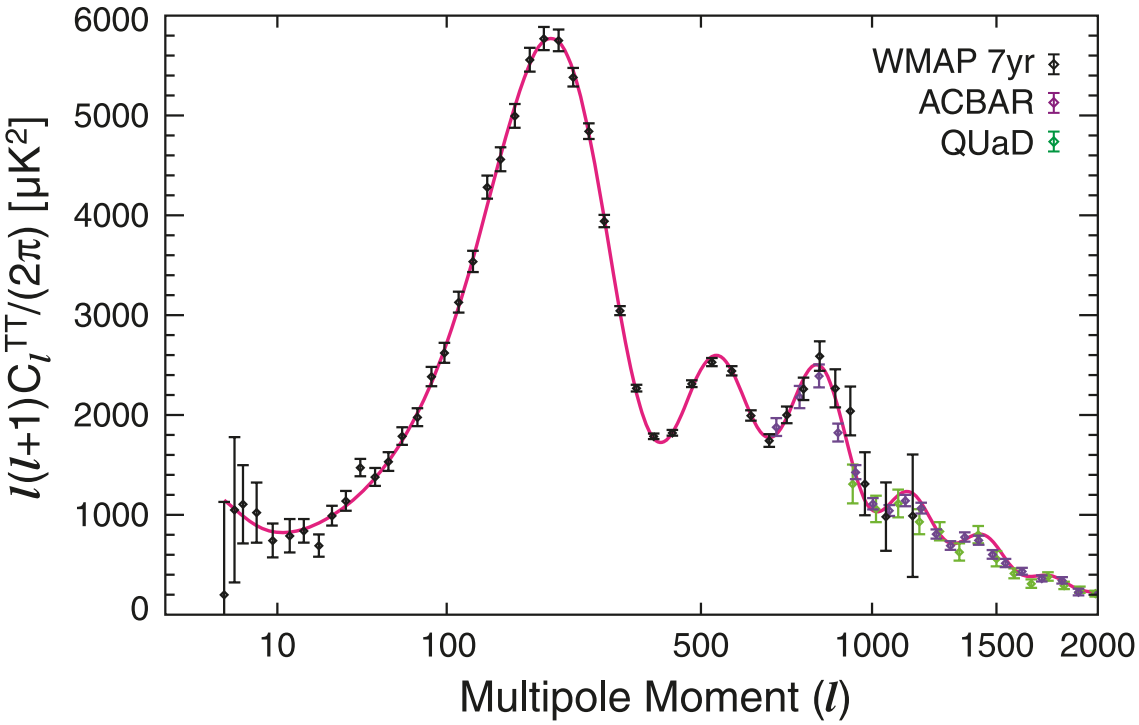

Figure 2.1: The theoretical CMB temperature power spectrum (solid line) of the best fit 6-parameter flat ΛCDM model to the 7-year WMAP data. There are also included data points from other recent CMB experiments. Figure by the 7-year WMAP Collaboration [7].

The restriction that we cannot carry out a real ensemble average when calculating the observed power spectrum, as we can observe only one set of a_{lm} in our sky, is represented by the cosmic variance. It is defined as the expected squared difference between C_l and $\tilde{C}_l$:

$$\langle (C_l - \tilde{C}_l)^2 \rangle = \frac{2}{2l+1} \tilde{C}_l^2 \ . \tag{2.41}$$

Especially for low values of l, there will be a smaller (size $2l+1$) statistical sample of a_{lm} to average over for calculating the C_l, meaning the approximation to the true ensemble average becomes worse. The cosmic variance thus limits the accuracy of the comparison of the CMB observations with theory.

2.3.3 Large scale structure

The slight inhomogeneities in the matter distribution in the early universe have been enhanced in time, primarily by the influence of gravity, to form the structures in the universe. The structure appears to be organized hierarchically up to the scale of superclusters and filaments with nearly empty voids between them [51–54]. On even larger scales, galaxy surveys seem to indicate that the lumpiness is homogenized and isotropized to a smooth distribution. This is believed to happen roughly at the scale of $100h^{-1}$ Mpc, the so-called homogeneity scale [55, 56]. However, there has been debate whether such a scale exists at all [74–79], and even if the scale exists, it means that the universe is homogeneous on larger scales possibly only in a statistical sense. We discuss this issue in little more detail in Sect. 3.3.2.

By studying the large scale structure, we can learn about the total density of matter and how matter clusters. Moreover, the clustering of matter depends on the expansion history of the universe; by comparing the observed sound horizon scale today as inferred from galaxy clustering data to the sound horizon at decoupling imprinted in the CMB, the large scale structure surveys provide us with important knowledge about the expansion history. The two largest galaxy surveys are the Sloan Digital Sky Survey (SDSS), and the Two-degree-Field Galaxy Redshift Survey (2dFGRS), which has already been completed.

The clustering properties of the galaxies can be analyzed statistically by looking at how the density of the galaxies is correlated. A quantitative measure of this is the two-point correlation function $\xi(x)$, which is defined as the excess probability, relative to a homogeneous distribution, of finding a galaxy at a comoving distance x from another galaxy. The baryon acoustic oscillation signal would show up as a bump in the correlation function at a comoving separation equal to the sound horizon. By writing the deviation from a homogeneous matter distribution as $\rho(\mathbf{x}) = \rho_0(1 + \delta(\mathbf{x}))$, where ρ_0 is the background FRW density and $\delta(\mathbf{x})$ is the perturbed density contrast, the two-point correlation function reads as

$$\xi(x) \equiv \langle \delta(\mathbf{x}_1)\delta(\mathbf{x}_2) \rangle \ , \tag{2.42}$$

where the average is taken over all realizations of the density field under the condition $x = |\mathbf{x}_1 - \mathbf{x}_2|$. The two-point correlation function from the SDSS survey is plotted in Fig. 2.2, showing the detected baryon acoustic oscillation peak [8].

In practice, one often deals with the matter power spectrum $P(k)$, which is the Fourier transform of $\xi(x)$:

$$P(k) = \int \xi(x) e^{-i\mathbf{k}\cdot\mathbf{x}} \mathrm{d}\mathbf{x} \ . \tag{2.43}$$

The power spectrum of Eq. (2.43) thus gives the contribution of scale k to the two-point correlation function of Eq. (2.42) through

$$\xi(x) = \int_0^\infty \mathcal{P}(k) \frac{\sin(kx)}{kx} \frac{\mathrm{d}k}{k} \ , \tag{2.44}$$

where $\mathcal{P}(k) = k^3/(2\pi^2)P(k)$.

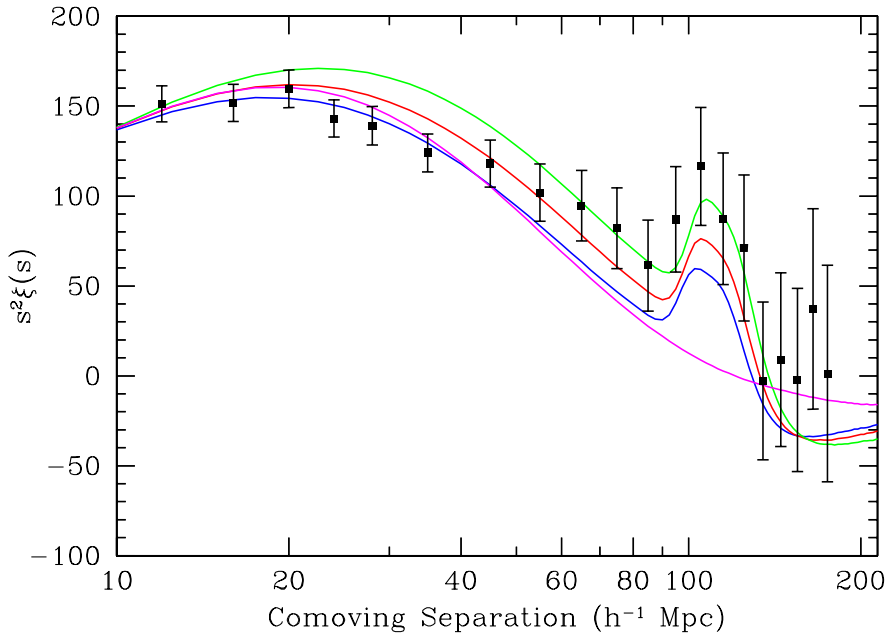

Figure 2.2: The two-point correlation function from the SDSS data. The curve with no peak represents a matter-dominated model with no acceleration; other curves correspond to accelerating models with different total matter densities. Figure from Ref. [8].

2.4 Dark energy

Newtonian gravity is always attractive, whereas in general relativity gravity can also be repulsive, as e.g. Eq. (2.19) demonstrates: by having $p < -\rho/3$ accelerated expansion can be achieved within the FRW models. With ordinary energy forms, locally accelerating expansion of space is thus still impossible in general relativity. Yet, as suggested by the observations of light from distant type Ia supernovae in the late 1990's [4, 5], during the latter part of its lifetime, the expansion of the universe seems to have increased roughly by a factor of 3/2 along our line of sight, relative to the expectation from the perfectly homogeneous and isotropic FRW models based on ordinary energy forms [21]. When interpreted within the FRW models, observations thus seemed to imply that there had to be something else besides the ordinary energy forms in the universe to cause it to accelerate. Moreover, the observations suggested this new dark energy component would have to be dominant.

2.4.1 The cosmological constant Λ

The simplest candidate for the new energy component with negative pressure already existed in theory, introduced by Einstein himself – the cosmological constant Λ with $w = -1$. Indeed, Einstein applied his general relativity to cosmology already in 1917 [80]. The original motivation for the use of a cosmological constant term was different, however: Einstein considered the universe to be static in line with the astronomical observations of the time. But as matter attracts gravitationally, he thought the theory of gravity as he first formulated it did not permit

a static universe – in order to arrange a static universe, he added a constant term into the field equation (2.8):

$$G_{\mu\nu} + \Lambda g_{\mu\nu} = 8\pi G T_{\mu\nu} \ . \tag{2.45}$$

Although Einstein thought the cosmological constant as an extra term to the geometry of the universe, it can alternatively be thought of as an extra term to the energy content of the universe, as the constant energy density of vacuum with $\rho_\Lambda = \Lambda/(8\pi G)$ [81–83].

The cosmological constant had been reconsidered also before the supernova measurements published in 1998, for example in the context of the CMB observations by the COBE satellite in 1992, which implicated inconsistency between the CMB anisotropies and the large scale structure [84]. The cosmological constant was also invoked to provide a solution to the age crisis in the mid-1990's: the age of the EdS universe (the flat matter-dominated FRW universe), would be less than the age of the oldest stars in globular clusters. However, the supernova observations at the latest established Λ in cosmology.

Ever since the supernova observations in the late 1990's, also the CMB observations [7], the large scale structure surveys [8, 85] as well as more recent supernova analysis [6, 65, 86], when interpreted in the context of the FRW models, all seem to imply that the universe is undergoing an accelerated expansion and would thus be dominated by a dark energy component. When these three data sets are combined, the current best fit estimate for the dark energy equation of state parameter is[6] $w_{\rm DE} = -0.980 \pm 0.053$ [87], thus favouring the simplest dark energy candidate, the cosmological constant. Models with more general forms of dark energy are not, however, excluded by the data.

Besides dark energy, astrophysical observations suggest the existence of another non-standard ingredient: dark matter [88]. The idea of dark matter dates back to the 1930's, when it was deduced from the motions of galaxies that the matter we can directly observe, such as stars, is just a small fraction of the total mass which affects the galaxy motions through gravity. The rest would be dark matter, probably made of (yet unknown) weakly interacting particles and something that can be observed only through its gravitational effect. From the later observations it has turned out that baryonic matter could not alone have had enough time to form the kind of structures in the universe we see today.

When looking at the different data sets, the following information for the density parameters is obtained[7]:

- CMB alone: $\Omega_0 = \Omega_m + \Omega_\Lambda \sim 1$
- Galaxy surveys alone: $\Omega_m \sim 0.3$
- CMB + BAO scale from galaxy surveys: $\Omega_\Lambda \sim 0.7$
- Type Ia supernovae: $\Omega_m \sim 0.3$ and $\Omega_\Lambda \sim 0.7$

The best fit value for the total density parameter from the combined data[8] is $\Omega_0 = 1.0023^{+0.0056}_{-0.0054}$ [87], thus favouring a spatially flat Friedmann model. Moreover, at least the supernova data alone seems to require $\Omega_\Lambda > 0$ at a high confidence level [6, 65]. Independently from the supernova

[6] The obtained value assumes constant w and spatial flatness.

[7] These parameter constraints involve additional assumptions; for example, in the supernova data analysis spatial flatness ($\Omega_0 = 1$) has been assumed.

[8] WMAP+BAO+H_0.

data, also the combined CMB+BAO+H_0 data implies $\Omega_\Lambda > 0$ at high confidence, assuming close to scale invariant primordial perturbations.

Altogether, the analysis of the cosmological data within FRW models with both the vacuum energy and matter components included yields a consistent picture of the universe, known as the concordance ΛCDM model: a spatially flat Friedmann model with the cosmological constant as the dark energy component [10]. By combining WMAP data [7], the BAO scale inferred from the galaxy distribution statistics [85] and Hubble constant measurements [89], the current best-fit shares of the energy components in the present-day universe are found to be[9] [87]

$$\begin{aligned} \Omega_b &= 0.0456 \pm 0.0016 \\ \Omega_{cdm} &= 0.227 \pm 0.014 \\ \Omega_\Lambda &= 0.728^{+0.015}_{-0.016} \ , \end{aligned} \tag{2.46}$$

where b stands for baryonic matter and cdm for cold dark matter. The uncertainties are given at 1σ level.

2.4.2 Problems with dark energy

What should be kept in mind is that the target in cosmology is to understand the universe; to describe its properties and evolution as accurately as possible. A question to be asked then is whether the ΛCDM model really is a successful model in understanding our universe, not just a phenomenological fit to the data: can we really say we understand the universe if about 95% of its energy density is made up of unknown components in the form of dark matter and dark energy?

The evidence for dark matter as well as dark energy is indirect. The cosmological constant (or more general forms of dark energy) is inferred indirectly under the assumptions of homogeneity and isotropy and the validity of Einstein's general theory of relativity. There is no evidence from local physics for dark energy, all of the indications involve integrals over large scales. However, the situation with dark matter is rather different, for which the evidence is both observationally, including local physics, and theoretically more solid: Suggested extensions to the standard model of particle physics predict possible candidates for dark matter particles. Observationally, there are several independent sources supporting dark matter, such as the motions of stars in galaxies (rotation curves of galaxies), the motions of clusters, the peak structure of the CMB power spectrum, the early formation of structures, gravitational lensing, as well as direct measurements of the matter density combined with the baryon density from the Big Bang nucleosynthesis. Indeed, dark matter is relevant through the expansion history of the universe, all the way from the radiation dominated epoch, whereas dark energy in the form of a cosmological constant would be relevant only at the latest stage of the cosmic evolution.

Besides the lack of stronger observational evidence for the cosmological constant, there are various issues associated with it that should be given natural dynamical explanations – explanations that the ΛCDM model does not provide. Firstly, the value for the cosmological constant, $\Lambda \sim 10^{-123}\ G^{-1}$, as required to explain the observations is unnaturally tiny when compared to the estimate from naive dimensional analysis, which suggests $\Lambda \sim G^{-1}$. Secondly, as a naive expectation for the probability of a quantum field to arise at a temperature T is given by the

[9] Assuming the standard 6 parameter spatially flat ΛCDM model.

Boltzmann factor $P \sim e^{-T_{\rm Planck}/T}$, the appearance of dark energy seems to happen at an unnaturally low temperature of $T \simeq 4$ K, taking into account that it has had the huge temperature range from $T_{\rm Planck} \gtrsim 10^{32}$ K to $T_0 \simeq 2.7$ K available. Why should we be witnessing this special and brief dynamical phase in the evolution of the universe – a transition from matter domination to vacuum energy domination? Indeed, it is strange that dark energy has exactly the value that makes it important today; a significantly lower or higher value would either have made no impact on the cosmic expansion today or conversely prevented the structures to form. Related to this, Λ seems to be fine-tuned also in the sense that today the universe appears to undergo nearly free expansion, $H_0 t_0 \lesssim 1$, whereas only a slightly bigger Λ would yield $H_0 t_0 > 1$.

Let us discuss the last point a little more closely. A convenient measure of the expansion rate is given by the dimensionless factor obtained by multiplying the Hubble parameter H with the age of the universe t. By integrating the Friedmann equation (2.18), we find the following expressions:

$$Ht = 1 \qquad \text{if} \quad \Omega_m = \Omega_0 \simeq 0 \tag{2.47}$$

$$Ht = \frac{2}{3} \qquad \text{if} \quad \Omega_m = \Omega_0 = 1 \tag{2.48}$$

$$H = H_0 \sqrt{\Omega_\Lambda} \coth\left\{\frac{3}{2} H_0 t \sqrt{\Omega_\Lambda}\right\} \qquad \text{if} \quad \Omega_\Lambda + \Omega_m = 1 \ . \tag{2.49}$$

When the CMB data is combined with the BAO scale inferred from the galaxy distribution statistics, we obtain a constraint that the expansion of the universe should have increased along our line of sight such that $Ht \sim 2/3$ at large redshifts whereas today $H_0 t_0 \sim 1$. Independently from these two, a similar conclusion comes from the type Ia supernova data. From Eq. (2.49), we can see that at early times ($z \sim 10^3$) when the matter dominates over the cosmological constant, the ΛCDM model evolution reduces to $Ht \simeq 2/3$, whereas the present-day value with $\Omega_\Lambda \simeq 0.7$ is

$$H_0 t_0 = \frac{2}{3\sqrt{\Omega_\Lambda}} \mathrm{arsinh} \sqrt{\frac{\Omega_\Lambda}{1 - \Omega_\Lambda}} \simeq 1 \ . \tag{2.50}$$

Interestingly enough, the ΛCDM present-day value coincides with the (nearly) empty Milne solution (2.47), which is the maximum value for Ht in the FRW model with ordinary energy forms. On the other hand, in the ΛCDM model, Ht is not restricted from above. Indeed, if the value for $H_0 t_0$ deduced from the observations were greater than one, it could thus serve as an implication for dark energy by disfavouring or even ruling out some other explanations for acceleration. However, the best fit value (2.50) being exactly slightly below than one seems coincidental, taken the huge range of values it could take. On the other hand, structure formation could provide a natural dynamical explanation for the increase of the expansion rate from 2/3 to 1: due to the formation of the cosmic web of voids, the light propagates through emptier and emptier regions, yielding the present value $H_0 t_0 \simeq 1$, see e.g. Ref. [21].

Many efforts have been made towards the physical understanding of dark energy so that its coincidental nature would get a natural dynamical explanation. For example, to alleviate the timing problem associated with the cosmological constant, various dynamical dark energy models have been proposed (see e.g. Refs. [10, 90]). Indeed, the observations do allow the dark energy equation of state parameter to vary instead of imposing $w_{\rm DE} = -1$ as a starting point of the data analysis. In these models, the late time acceleration is caused by a slowly spacetime varying scalar field, the quintessence. However, such models seem to fail in their original mission but require similar fine-tuning as the cosmological constant and they are not compelling from particle physics point of view either [10, 90]. Indeed, attempts to deduce dark energy from extensions

of the standard model of particle physics have not been successful. The fine-tuning seems to be present also in the widely explored modified gravity models [11, 91, 92]. In this thesis, the focus is on the remark unifying all the above described problems: why would the effects of dark energy appear just when nonlinear structures at cosmologically significant scales start to form? Indeed, unlike the assumptions of ordinary matter and general relativity, the assumption of only linear deviations from homogeneity and isotropy is known to be violated at late times due to the formation of nonlinear structures; at least in the matter distribution and the expansion rate, there are large local deviations. It is thus crucial to carefully evaluate whether the standard FRW approach is able to capture the effects of the cosmic web on the observations or whether dark energy is just a manifestation of its failure to do so.

Chapter 3

Inhomogeneous cosmology

3.1 Different levels of coarse graining in cosmology

Nature is extremely complex with huge amount of degrees of freedom so that only rarely our theories in physics are able to describe even some specific parts of the whole exactly – theories are coarse-grained descriptions of the reality. Even more coarse graining steps into the picture when applying the theories; even though it is possible to write down the dynamical equations governing the phenomena, solving them is only rarely straightforward. The level of coarse graining depends on the phenomenon in question and the level of description wanted.

In spite of the complexity of nature and our theories, the investigation of the laws of nature has been very successful; we have the standard model of particle physics and general relativity, and all the experiments and observations performed on Earth and in the solar system agree with these theories within the current level of accuracy[1]. We can say that there are two main levels of understanding classical physical phenomena, microscopic and macroscopic. Physically, a macroscopic theory has often a direct observational status whereas microscopic features may often be beyond measurement and also beyond computation. In macroscopic description, the idea is that although the physical system of interest may be extremely complicated microscopically, its average properties can be described to a good approximation.

The cool and sparse late universe forms perhaps the purest gravitational system possible, so from that perspective it is plausible to assume general relativity as the theory to begin with in cosmology. However, as general relativity is likely to be a microscopic theory which is physically adequate and realistic for treatment of the gravitational field created by a point-like discrete matter distribution, the microscopic description in cosmology is beyond limits – an appropriate macroscopic description of gravitation that is simple enough to solve is needed. Indeed, the question then is how to smooth the complex detailed behaviour of the inhomogeneities without changing the relevant physical content of the solution? We have discussed in Sect. 2.4 how the homogeneous and isotropic FRW models might be too coarse to describe the late universe with nonlinear structures.

The derivation of a macroscopic description of gravity from the microscopic one is not straightforward in cosmology. The task can be approached from two slightly different perspectives:

[1]The inherent inconsistency between the two theories above the Planck energy $E_P \sim 10^{19}$ GeV does not seem to pose a practical problem to their validity, as this energy scale is vastly beyond our direct experiments.

coarse graining can be applied implicitly via symmetries in the exact solutions of general relativity, or via explicit averaging of the Einstein equation[2]. We have already given an example of the first case by considering the homogeneous and isotropic FRW models in Sect. 2.2. In Sect. 3.2, we present a more general class of exact solutions of general relativity with a wide range of applicability in cosmology – the Lemaître-Tolman-Bondi (LTB) model – from which the RW metric (2.13) is a special case. For more discussion about exact inhomogeneous solutions, see e.g. Ref. [15], and Ref. [93] for a recent review. In Sect. 3.3, we consider the averaging approach.

3.2 LTB model

The limitation in the FRW models is the spatial homogeneity. On the other hand, as we the observers gather light from all directions around us, the spherical symmetry is a natural simplifying symmetry. The general form of the line-element in coordinates respecting the spherical symmetry can be written as

$$\mathrm{d}s^2 = -b^2(\tilde{r},\tilde{t})\mathrm{d}\tilde{t}^2 + c(\tilde{r},\tilde{t})\mathrm{d}\tilde{r}\mathrm{d}\tilde{t} + \tilde{X}^2(\tilde{r},\tilde{t})\mathrm{d}\tilde{r}^2 + \tilde{A}^2(\tilde{r},\tilde{t})(\mathrm{d}\theta^2 + \sin^2\theta\mathrm{d}\phi^2) \ , \tag{3.1}$$

where $b(\tilde{r},\tilde{t})$, $c(\tilde{r},\tilde{t})$, $\tilde{X}(\tilde{r},\tilde{t})$ and $\tilde{A}(\tilde{r},\tilde{t})$ are functions of the radial and time coordinates and the spatial origin $\tilde{r}=0$ has been chosen as the symmetry center. The coordinates r and t can be subjected to a transformation $\tilde{r}=f_r(r,t)$, $\tilde{t}=f_t(r,t)$ that makes the term $c(\tilde{r},\tilde{t})\mathrm{d}\tilde{r}\mathrm{d}\tilde{t}$ vanish. Furthermore, the spherical symmetry implies vanishing vorticity so that in the case of a dust universe[3], we can choose the time coordinate t to measure the proper time of the comoving dust particles. The line-element then takes the form

$$\mathrm{d}s^2 = -\mathrm{d}t^2 + X^2(r,t)\mathrm{d}r^2 + A^2(r,t)(\mathrm{d}\theta^2 + \sin^2\theta\mathrm{d}\phi^2) \ . \tag{3.2}$$

Note that the scale functions $A(r,t)$ and $X(r,t)$ have both temporal and spatial dependence. This exact spherically symmetric dust solution of the Einstein equation was discovered by Lemaître in 1933 [81, 94] and was also studied by Tolman [95] and Bondi [96]; later, it has been used in various astronomical and cosmological contexts [15, 16]. The Schwarzschild and RW metrics are special cases of Eq. (3.2). For example, the homogeneous RW metric (2.13) follows when: $X(r,t)\to a(t)/\sqrt{1-kr^2}$ and $A(r,t)\to a(t)r$.

The nonzero Christoffel symbols (2.2) for the metric (3.2) are given in Eq. (A.1) of Appendix A. The nonvanishing Einstein tensor (2.9) components are:

$$G^0{}_0 = \frac{2A''}{AX^2} - \frac{2\dot{A}\dot{X}}{AX} - \frac{2A'X'}{AX^3} - \frac{(1+\dot{A}^2)}{A^2} + \frac{A'^2}{A^2X^2} \tag{3.3}$$

$$G^0{}_1 = \frac{2\dot{A}'}{A} - \frac{2A'\dot{X}}{AX} \tag{3.4}$$

$$G^1{}_1 = \frac{A'^2}{A^2X^2} - \frac{2\ddot{A}}{A} - \frac{(1+\dot{A}^2)}{A^2} \tag{3.5}$$

$$G^2{}_2 = G^3{}_3 = \frac{A''}{AX^2} - \frac{\ddot{A}}{A} - \frac{\ddot{X}}{X} - \frac{\dot{A}\dot{X}}{AX} - \frac{A'X'}{AX^3} \ . \tag{3.6}$$

[2]This distinction between the two coarse graining approaches is somewhat artificial; usually a combination of them is applied.

[3]The approximation that matter is irrotational breaks down at small scales, as vorticity is closely associated with structure formation. However, this small-scale breakdown of the approximation has been argued to be cosmologically less important [19].

The energy-momentum tensor in the above defined coordinates is given by

$$T^{\mu}{}_{\nu} = -\rho_m(r,t)\delta^{\mu}_0\delta^0_{\nu} - \rho_\Lambda \delta^{\mu}{}_{\nu} \ , \tag{3.7}$$

where $\rho_m(r,t)$ is the energy density of dust, $u^\mu = \delta^\mu_0$ represents the components of the 4-velocity-field of the dust and we have kept the vacuum energy ρ_Λ for generality.

When Eqs. (3.3) – (3.7) are applied to the Einstein equation (2.8), the following four algebraically different equations arise:

$$-2\frac{A''}{AX^2} + 2\frac{A'X'}{AX^3} + 2\frac{\dot{A}\dot{X}}{AX} + \frac{1}{A^2} + \left(\frac{\dot{A}}{A}\right)^2 - \left(\frac{A'}{AX}\right)^2 = 8\pi G(\rho_m + \rho_\Lambda) \tag{3.8}$$

$$\dot{A}' = A'\frac{\dot{X}}{X} \tag{3.9}$$

$$2\frac{\ddot{A}}{A} + \frac{1}{A^2} + \left(\frac{\dot{A}}{A}\right)^2 - \left(\frac{A'}{AX}\right)^2 = 8\pi G\rho_\Lambda \tag{3.10}$$

$$-\frac{A''}{AX^2} + \frac{\ddot{A}}{A} + \frac{\dot{A}}{A}\frac{\dot{X}}{X} + \frac{A'X'}{AX^3} + \frac{\ddot{X}}{X} = 8\pi G\rho_\Lambda \ . \tag{3.11}$$

This set of equations (3.8) – (3.11) contains only three independent differential equations: by solving the functions $\dot{X}$ and $\ddot{X}$ from Eq. (3.9), and the functions A'^2 and A'' from Eq. (3.10), we find that Eq. (3.11) is trivially satisfied, leaving only two of Eqs. (3.9) – (3.11) independent. Integrating Eq. (3.9) over time yields

$$X(r,t) = \frac{A'(r,t)}{\sqrt{1-k(r)}} \ , \tag{3.12}$$

where $k(r)$ is a function determined by the boundary conditions. The metric (3.2) can now be written in the following form:

$$\mathrm{d}s^2 = -\mathrm{d}t^2 + \frac{(A'(r,t))^2}{1-k(r)}\mathrm{d}r^2 + A^2(r,t)\left(\mathrm{d}\theta^2 + \sin^2\theta\mathrm{d}\varphi^2\right) \ . \tag{3.13}$$

The solved equation (3.12) reduces the number of independent differential equations in (3.8) – (3.11) from three to two:

$$\frac{\dot{A}^2 + k(r)}{A^2} + \frac{2\dot{A}\dot{A}' + k'(r)}{AA'} = 8\pi G(\rho_m + \rho_\Lambda) \tag{3.14}$$

$$\dot{A}^2 + 2A\ddot{A} + k(r) = 8\pi G\rho_\Lambda A^2 \ . \tag{3.15}$$

By combining Eqs. (3.14) and (3.15), we can construct a generalized acceleration equation:

$$\frac{2}{3}\frac{\ddot{A}}{A} + \frac{1}{3}\frac{\ddot{A}'}{A'} = -\frac{4\pi G}{3}(\rho_m - 2\rho_\Lambda) \ . \tag{3.16}$$

In the LTB models, there can be acceleration both in the radial and angular directions, represented by $\ddot{A}'(r,t)$ and $\ddot{A}(r,t)$ respectively. Eq. (3.16) tells us that the total acceleration, given by the left hand side, is everywhere negative unless the vacuum energy is large enough: $\rho_\Lambda > \rho_m/2$. However, there can still be radial acceleration $\ddot{A}'(r,t) > 0$ even in the pure dust universe, if

the angular scale factor $A(r,t)$ is decelerating enough and vice versa. Already a simple example like this demonstrates how the very notion of accelerated expansion becomes ambiguous in the presence of the inhomogeneities; see also Ref. [97] for a discussion.

The first time integral of Eq. (3.15) is

$$\frac{\dot{A}^2}{A^2} = \frac{F(r)}{A^3} + \frac{8\pi G}{3}\rho_\Lambda - \frac{k(r)}{A^2} \ , \tag{3.17}$$

where $F(r)$ is a non-negative function. Substituting Eq. (3.17) into Eq. (3.14) gives

$$\frac{F'}{A'A^2} = 8\pi G\rho_m \ . \tag{3.18}$$

The boundary condition functions $F(r)$ and $k(r)$ are specified by the exact inhomogeneity profile, conveniently given on a spatial hypersurface $t = t_0$. For intuition, it is convenient to relate $F(r)$ and $k(r)$ to the analogous FRW quantities – the Hubble constant H_0 and the density parameter Ω_m – by comparing Eq. (3.17) with the Friedmann equation (2.33). Indeed, the similarity between Eqs. (3.17) and (2.33) motivates us to define a local angular Hubble rate

$$H(r,t) \equiv \frac{\dot{A}(r,t)}{A(r,t)} \ , \tag{3.19}$$

and matter density through

$$F(r) \equiv H_0^2(r)\Omega_m(r)A_0^3(r) \ , \tag{3.20}$$

with

$$k(r) \equiv H_0^2(r)(\Omega_m(r) + \Omega_\Lambda(r) - 1)A_0^2(r) \ , \tag{3.21}$$

where $A_0(r) \equiv A(r,t_0)$, $H_0(r) \equiv H(r,t_0)$, $\Omega_\Lambda(r) \equiv 8\pi G\rho_\Lambda/3H_0^2(r)$ and $\Omega_m(r)$ is a measure of the matter density at $t = t_0$, given by a spatial integral over Eq. (3.18) as:

$$\Omega_m(r) \equiv \frac{\langle\rho_m(r,t_0)\rangle_{\mathbb{B}(r)}}{\rho_{\rm crit}(r,t_0)} \equiv \frac{8\pi G}{3H_0^2(r)}\frac{\int_{\mathbb{B}(r)}\rho_m(r,t_0)\mathrm{d}^3x}{\int_{\mathbb{B}(r)}\mathrm{d}^3x} \ , \tag{3.22}$$

where $\int_{\mathbb{B}(r)}$ denotes Euclidean space integral over an origin-centered ball of radius r so $\mathrm{d}^3x \equiv r^2\sin\theta\mathrm{d}r\mathrm{d}\theta\mathrm{d}\varphi$. Inversely, using Eqs. (3.18) and (3.20), $\rho_m(r,t_0) \equiv \rho_0(r)$ can be written in terms of $\Omega_m(r)$ and $H_0(r)$ as

$$\rho_0(r) = \frac{3H_0^2(r)}{8\pi G}\Omega_m(r)\left[1 + \frac{A_0(r)}{3A_0'(r)}\left(\frac{\Omega_m'(r)}{\Omega_m(r)} + 2\frac{H_0'(r)}{H_0(r)}\right)\right] \ . \tag{3.23}$$

With the definitions of Eqs. (3.19) – (3.21), Eq. (3.17) takes the physically more transparent form

$$H^2(r,t) = H_0^2(r)\left[\Omega_m(r)\left(\frac{A_0}{A}\right)^3 + \Omega_\Lambda(r) + \Omega_c(r)\left(\frac{A_0}{A}\right)^2\right] \ , \tag{3.24}$$

where $\Omega_c(r) \equiv 1 - \Omega_\Lambda(r) - \Omega_m(r)$. The difference between the homogeneous Friedmann equation (2.33) and its LTB generalization (3.24) is that all the quantities in the LTB case depend on the r-coordinate. Similar to the scaling freedom of the scale factor $a(t_0)$ present in the FRW models,

the corresponding present-day scale function $A_0(r)$ of the LTB models can be chosen to be any smooth and invertible positive function. In this thesis, we employ the conventional choice:

$$A_0(r) = r \ . \tag{3.25}$$

Although the vacuum energy density ρ_Λ is constant, its value in the units of critical density $\Omega_\Lambda(r) \equiv \rho_\Lambda/\rho_{\rm crit}(r)$ is not. This is because the critical density itself has spatial dependence: $\rho_{\rm crit}(r) \equiv 3H_0^2(r)/8\pi G$. The converse is also true: if e.g. $\Omega_m(r) = $ constant, the matter distribution $\rho_m(r,t)$ has spatial dependence as long as $H_0(r) \neq$ constant.

The integration of Eq. (3.24) w.r.t. time gives the second integral of Eq. (3.15):

$$t_0 - t = \frac{1}{H_0(r)} \int_{\frac{A(r,t)}{A_0(r)}}^{1} \frac{{\rm d}x}{x\sqrt{\Omega_m(r)x^{-3} + \Omega_c(r)x^{-2} + \Omega_\Lambda(r)}} \ . \tag{3.26}$$

For any spacetime point with coordinates (t, r, θ, φ), Eq. (3.26) determines the function $A(r,t)$ and all its derivatives. This uniquely specifies the metric (3.13), so given the inhomogeneities $H_0(r)$ and $\Omega_m(r)$ (and ρ_Λ), all the observable quantities can be computed.

In general, Eq. (3.26) has to be integrated numerically. However, in the special cases when $\Omega_\Lambda(r) = 0$ or $\Omega_\Lambda(r) + \Omega_m(r) = 1$ the result can be given in terms of elementary functions:

1. $\Omega_m(r) = 1$ and $\Omega_\Lambda(r) = 0$:

$$A(r,t) = A_0(r)\left[1 + \frac{3}{2}(t - t_0)H_0(r)\right]^{2/3} \ . \tag{3.27}$$

2. $\Omega_m(r) \equiv \Omega(r) < 1$ and $\Omega_\Lambda(r) = 0$:

$$(t - t_0)H_0(r) = \frac{\Omega(r)}{(1-\Omega(r))^{3/2}}\left[{\rm arsinh}\sqrt{\frac{1-\Omega(r)}{\Omega(r)}} - {\rm arsinh}\sqrt{\frac{1-\Omega(r)}{\Omega(r)}\left(\frac{A(r,t)}{A_0(r)}\right)}\right] +$$

$$-\frac{1}{(1-\Omega(r))}\left[1 - \sqrt{\Omega(r)\left(\frac{A(r,t)}{A_0(r)}\right) - (\Omega(r)-1)\left(\frac{A(r,t)}{A_0(r)}\right)^2}\right] \ , \tag{3.28}$$

which can alternatively be written as

$$(t - t_0)H_0(r) = \frac{\Omega(r)}{(1-\Omega(r))^{3/2}}\ln\left(\frac{\sqrt{1-\Omega(r)}+1}{\sqrt{(1-\Omega(r))\frac{A(r,t)}{A_0(r)}} + \sqrt{(1-\Omega(r))\frac{A(r,t)}{A_0(r)} + \Omega(r)}}\right) +$$

$$-\frac{1}{(1-\Omega(r))}\left[1 - \sqrt{\Omega(r)\left(\frac{A(r,t)}{A_0(r)}\right) - (\Omega(r)-1)\left(\frac{A(r,t)}{A_0(r)}\right)^2}\right] \ . \tag{3.29}$$

Eq. (3.29) is more useful in numerical applications, as it behaves well also in the limit $\Omega(r) \to 0$.

3. $\Omega_m(r) \equiv \Omega(r) > 1$ and $\Omega_\Lambda(r) = 0$:

$$(t - t_0)H_0(r) = \frac{\Omega(r)}{(\Omega(r)-1)^{3/2}} \left[\arcsin\sqrt{\frac{\Omega(r)-1}{\Omega(r)}\left(\frac{A(r,t)}{A_0(r)}\right)} - \arcsin\sqrt{\frac{\Omega(r)-1}{\Omega(r)}} \right] + \\ + \frac{1}{(\Omega(r)-1)} \left[1 - \sqrt{\Omega(r)\left(\frac{A(r,t)}{A_0(r)}\right) - (\Omega(r)-1)\left(\frac{A(r,t)}{A_0(r)}\right)^2} \right] . \tag{3.30}$$

4. $\Omega_m(r) + \Omega_\Lambda(r) = 1$:

$$A(r,t) = A_0(r) \left[\cosh\left[\frac{3}{2} H_0(r) \Omega_\Lambda^{1/2}(r)(t - t_0) \right] + \frac{\sinh\left[\frac{3}{2} H_0(r) \Omega_\Lambda^{1/2}(r)(t - t_0) \right]}{\Omega_\Lambda^{1/2}(r)} \right]^{\frac{2}{3}} . \tag{3.31}$$

3.2.1 Useful LTB results

Let us calculate some LTB results useful for the research presented in this thesis. We refer to these results in the forthcoming sections. From here on, we only consider the case $\rho_\Lambda = 0$ and write $\Omega_m(r) \equiv \Omega_0(r)$.

There are different ways to classify the inhomogeneities of the LTB spacetime. Firstly, they can be classified according to their physical interpretation on a spatial hypersurface at $t = t_0$: Inhomogeneities in the matter distribution $\rho_m(r, t_0)$ and inhomogeneities in the expansion scalar $\theta(r, t_0) = \nabla_\mu u^\mu(r, t_0)$ (see Eq. (3.74)) or, equivalently, in the velocity distribution of the matter. Note that it is equivalent to use the functions $\Omega_0(r)$ and $H_0(r)$ instead of ρ_m and θ. Secondly, we can consider differences in the time evolution, i.e. divide the inhomogeneities to growing and decaying modes, meaning that the inhomogeneities in the model grow or decay with time, respectively [98]. For general functions $\Omega_0(r)$ and $H_0(r)$ that are independent of each other, the LTB solution contains both decaying and growing inhomogeneities. Although our quantitative discussion concentrates only on the spherically symmetric LTB solution, the same division applies to arbitrary inhomogeneities.

The growing modes can be found by demanding homogeneity in the early universe or simultaneity of the Big Bang (BB). In a simultaneous Big Bang, the divergent curvature of the initial singularity or the condition $A(r, t_{BB}) = 0$ coexists everywhere at the same time coordinate $t = t_{BB}$ whereas in an inhomogeneous Big Bang, $t_{BB}(r)$ is a function of the spatial location. Thus, for a simultaneous Big Bang, the age of the universe must be independent of the spatial coordinates: $t_{\rm age} \equiv t_0 - t_{BB} =$ constant. To obtain this constraint we need the expression for the age of the LTB universe which can be calculated by performing the integral in Eq. (3.26) with $A(r, t) = 0$. In the cases where the result is an elementary function of the boundary conditions, the results are:

1. $\Omega_0(r) = 1$ and $\Omega_\Lambda(r) = 0$:

$$t_{\rm age}(r) = \frac{2}{3H_0(r)} . \tag{3.32}$$

2. $\Omega_0(r) < 1$ and $\Omega_\Lambda(r) = 0$:

$$t_{\rm age}(r) = \frac{\sqrt{1-\Omega_0(r)} - \Omega_0(r)\text{arsinh}\sqrt{\frac{1-\Omega_0(r)}{\Omega_0(r)}}}{H_0(r)(1-\Omega_0(r))^{3/2}} \ . \tag{3.33}$$

3. $\Omega_0(r) > 1$ and $\Omega_\Lambda(r) = 0$:

$$t_{\rm age}(r) = \frac{\Omega_0(r)\text{arcsin}\sqrt{\frac{\Omega_0(r)-1}{\Omega_0(r)}} - \sqrt{\Omega_0(r)-1}}{H_0(r)(\Omega_0(r)-1)^{3/2}} \ . \tag{3.34}$$

4. $\Omega_0(r) + \Omega_\Lambda(r) = 1$:

$$t_{\rm age}(r) = \frac{2}{3H_0(r)} \frac{\text{arsinh}\sqrt{\frac{1-\Omega_0(r)}{\Omega_0(r)}}}{\sqrt{1-\Omega_0(r)}} \ . \tag{3.35}$$

In each case, the requirement $t_{\rm age}(r) =$ constant sets the constraint between the boundary condition functions $\Omega_0(r)$ and $H_0(r)$ that preserves only the growing modes. If the condition $t_{\rm age}(r) =$ constant is violated instead, decaying modes are present as well. In the first case above where $\Omega_0(r) = 1$, we have only decaying modes. This case is commonly referred to as the flat LTB model, as from Eq. (3.21) we obtain $k(r) = 0$ and the spatial Ricci scalar ${}^{(3)}R$, given by Eq. (2.5) as

$${}^{(3)}R = 2\frac{\partial_r(A(r,t)k(r))}{A^2(r,t)A'(r,t)} \ , \tag{3.36}$$

thus vanishes. For a more detailed discussion on growing and decaying modes in the LTB model, see Ref. [98].

As an example, applying the simultaneous Big Bang condition $t_{\rm age}(r) =$ const. into Eq. (3.33) implies the following constraint between the boundary condition functions $\Omega(r)$ and $H_0(r)$ for the second case above:

$$H_0(r) = \frac{1}{t_0}\left[\frac{\sqrt{1-\Omega_0(r)} - \Omega_0(r)\text{arsinh}\sqrt{\frac{1-\Omega_0(r)}{\Omega_0(r)}}}{(1-\Omega_0(r))^{3/2}}\right] \ , \tag{3.37}$$

where $t_0 =$ constant is the age of the universe. This model can thus be determined by a free dimensionless function, $\Omega_0(r)$, and a free parameter, t_0. In order to simplify analytic calculations, we have utilized the following formula in Papers 3 and 4

$$H_0(r) = \frac{1}{t_0}\left(1 - \frac{\sqrt{\Omega_0(r)}}{3}\right) \ , \tag{3.38}$$

which approximates the simultaneous Big Bang condition (3.37) such that the $|\text{error}| < 1.5\%$ in the interval $0 \leq \Omega_0 \leq 1$ we consider and no error at the extremes $\Omega_0 = 0$ and $\Omega_0 = 1$. Alternatively, Eq. (3.38) can be understood as an exact LTB solution where the age of the universe can have small ($< 1.5\%$) spatial variations.

The models with (approximately) simultaneous Big Bang form perhaps the most relevant subcase of LTB solutions, because in these models, the inhomogeneities are growing modes as e.g. the near isotropy of the CMB suggests is also the case in the real universe. In this thesis, we have

used both the model with $\Omega_0(r) \leq 1$ (Papers 2 – 4) and the flat model $\Omega_0(r) = 1$ (Paper 1). The flat model most likely cannot give a realistic description of our universe as the model evolves towards homogeneity at late times – just the opposite to the observed structure formation in the real universe. However, for low-redshift observations, this should not make a difference when serving as a toy model for demonstrative purposes.

The volume expansion scalar $\theta(r,t)$ defined in Eq. (3.74) for the LTB model reads as

$$\begin{aligned}\theta(r,t) &= \nabla_\mu u^\mu = \Gamma^1_{10} + \Gamma^2_{20} + \Gamma^3_{30} = \frac{\dot{X}(r,t)}{X(r,t)} + 2\frac{\dot{A}(r,t)}{A(r,t)} = 2\frac{\dot{A}(r,t)}{A(r,t)} + \frac{\dot{A}'(r,t)}{A'(r,t)} \\ &= \frac{1}{A'(r,t)A^2(r,t)}\frac{\partial}{\partial r}\left(A^2(r,t)\dot{A}(r,t)\right) \ , \end{aligned} \tag{3.39}$$

where we have used Eqs. (A.1) and (3.12). A radial Hubble function $H_r(r,t) \equiv \dot{A}'(r,t)/A'(r,t)$ can be defined via Eq. (3.39) as

$$\theta(r,t) \equiv 2H(r,t) + H_r(r,t) \ . \tag{3.40}$$

The shear scalar $\sigma^2(r,t) \equiv \sigma^{\mu\nu}\sigma_{\mu\nu}$ can be calculated from the definition of the shear tensor $\sigma_{\mu\nu}$

$$\sigma_{\mu\nu} \equiv \frac{1}{2}(\nabla_\mu u_\nu + \nabla_\nu u_\mu) - \frac{1}{3}(g_{\mu\nu} + u_\mu u_\nu)\nabla_\alpha u^\alpha \ , \tag{3.41}$$

yielding

$$\sigma^2(r,t) = \frac{2}{3}\left(\frac{\dot{A}'(r,t)}{A'(r,t)} - \frac{\dot{A}(r,t)}{A(r,t)}\right)^2 \ . \tag{3.42}$$

By differentiating the Hubble function $H(r,t) = \dot{A}(r,t)/A(r,t)$ with respect to r, one finds that the two Hubble functions $H(r,t)$ and $H_r(r,t)$, defined in Eq. (3.40), are related at the reference time $t = t_0$ as

$$H_r(r,t_0) = H_0(r) + rH_0'(r) \ , \tag{3.43}$$

so that the expressions for the expansion scalar (3.39) and the shear (3.42) simplify to:

$$\theta(r,t_0) = 3H_0(r) + rH_0'(r) = \frac{1}{r^2}\frac{\partial}{\partial r}\left(r^3 H_0(r)\right) \ , \tag{3.44}$$

$$\sigma^2(r,t_0) = \frac{2}{3}(rH_0'(r))^2 \ . \tag{3.45}$$

We also have use for the LTB volume element:

$$\sqrt{\det[g_{ij}]}\,\mathrm{d}r\,\mathrm{d}\theta\,\mathrm{d}\varphi = \frac{A'(r,t)A^2(r,t)\sin\theta}{\sqrt{1-k(r)}}\,\mathrm{d}r\,\mathrm{d}\theta\,\mathrm{d}\varphi \ . \tag{3.46}$$

In the end, let us present some results that apply only to the flat LTB model considered in Paper 1.

When $k(r) = 0$, the line-element (3.13) takes the form

$$\mathrm{d}s^2 = -\mathrm{d}t^2 + (A'(r,t))^2\mathrm{d}r^2 + A^2(r,t)\left(\mathrm{d}\theta^2 + \sin^2\theta\mathrm{d}\varphi^2\right) \ . \tag{3.47}$$

The Einstein equations (3.18) and (3.24) for the metric (3.47) reduce to

$$H(r,t) = H_0(r)\left(\frac{A_0(r)}{A(r,t)}\right)^{3/2} \tag{3.48}$$

$$\rho_m(r,t) = \frac{3H_0^2(r)}{8\pi G}\left[1+\frac{2A_0(r)H_0'(r)}{3A_0'(r)H_0(r)}\right]\left(\frac{A_0^2(r)A_0'(r)}{A^2(r,t)A'(r,t)}\right) . \tag{3.49}$$

Substituting Eq. (3.27) into Eq. (3.48) gives the time evolution of the Hubble function as

$$H(r,t) = \frac{H_0(r)}{1+\frac{3H_0(r)}{2}(t-t_0)} . \tag{3.50}$$

Substituting Eq. (3.27) into Eq. (3.49) gives the explicit time evolution equation of the matter density as

$$\rho_m(r,t) = \frac{3H_0^2(r)+2rH_0'(r)H_0(r)}{8\pi G[1+\frac{3H_0(r)}{2}(t-t_0)][r(t-t_0)H_0'(r)+(1+\frac{3H_0(r)}{2}(t-t_0))]} , \tag{3.51}$$

where the choice $A_0(r) = r$ of Eq. (3.25) has been employed.

3.2.2 Light propagation in the LTB spacetime

In this Section, we derive the distance-redshift relations, discussed in Sect. 2.3.1, in the LTB model for an observer centered at the origin; a more general derivation for an off-center observer can be found e.g. in Ref. [67].

The spherical symmetry of the solution implies that light can travel radially, that is, there exist geodesics with $\mathrm{d}\theta = \mathrm{d}\phi = 0$. Moreover, since light always travels along null geodesics, we have $\mathrm{d}s^2 = 0$. Inserting these conditions into the equation for the line-element (3.13), we obtain the constraint equation for radial light rays

$$\frac{\mathrm{d}t}{\mathrm{d}u} = -\frac{\mathrm{d}r}{\mathrm{d}u}\frac{A'(r,t)}{\sqrt{1-k(r)}} , \tag{3.52}$$

where u is a curve parameter and the minus sign indicates we are studying radially incoming light rays.

Consider two light rays with solutions to Eq. (3.52) given by $t_1 = t(u)$ and $t_2 = t(u)+\lambda(u)$. Inserting these into Eq. (3.52), we obtain

$$\frac{\mathrm{d}}{\mathrm{d}u}t_1 = \frac{\mathrm{d}t(u)}{\mathrm{d}u} = -\frac{\mathrm{d}r}{\mathrm{d}u}\frac{A'(r,t)}{\sqrt{1-k(r)}} \tag{3.53}$$

$$\frac{\mathrm{d}}{\mathrm{d}u}t_2 = \frac{\mathrm{d}t(u)}{\mathrm{d}u}+\frac{d\lambda(u)}{\mathrm{d}u} = -\frac{\mathrm{d}r}{\mathrm{d}u}\frac{A'(r,t)}{\sqrt{1-k(r)}}+\frac{\mathrm{d}\lambda(u)}{\mathrm{d}u} . \tag{3.54}$$

On the other hand, we also have

$$\frac{\mathrm{d}}{\mathrm{d}u}t_2 = -\frac{\mathrm{d}r}{\mathrm{d}u}\frac{A'(r,t(u)+\lambda(u))}{\sqrt{1-k(r)}} = -\frac{\mathrm{d}r}{\mathrm{d}u}\frac{A'(r,t)+\dot{A}'(r,t)\lambda(u)}{\sqrt{1-k(r)}} , \tag{3.55}$$

where Taylor expansion has been used in the last step and only terms linear in $\lambda(u)$ have been kept. Equating the right hand sides of Eqs. (3.54) and (3.55) gives the relation

$$\frac{\mathrm{d}\lambda(u)}{\mathrm{d}u} = -\frac{\mathrm{d}r}{\mathrm{d}u}\frac{\dot{A}'(r,t)\lambda(u)}{\sqrt{1-k(r)}} \ . \tag{3.56}$$

Differentiating the definition of the redshift, $z \equiv (\lambda(0) - \lambda(u))/\lambda(u)$, we obtain

$$\frac{\mathrm{d}z}{\mathrm{d}u} = -\frac{\mathrm{d}\lambda(u)}{\mathrm{d}u}\frac{\lambda(0)}{\lambda^2(u)} = \frac{\mathrm{d}r}{\mathrm{d}u}\frac{(1+z)\dot{A}'(r,t)}{\sqrt{1-k(r)}} \ , \tag{3.57}$$

where in the last step we have used Eq. (3.56) and the definition of the redshift. Finally, we can combine Eqs. (3.21), (3.52) and (3.57) to obtain the pair of differential equations

$$\frac{\mathrm{d}t}{\mathrm{d}z} = \frac{-A'(r,t)}{(1+z)\dot{A}'(r,t)} \tag{3.58}$$

$$\frac{\mathrm{d}r}{\mathrm{d}z} = \frac{\sqrt{1+H_0^2(r)(1-\Omega_m(r)-\Omega_\Lambda(r))A_0^2(r)}}{(1+z)\dot{A}'(r,t)} \ , \tag{3.59}$$

that determine the relations between the coordinates and the observable redshift: $t(z)$ and $r(z)$.

Now that we have related the redshift to the inhomogeneities, we still need the relation of the redshift to the observable distance measures – the luminosity distance $d_L(z)$ and the angular diameter distance $d_A(z)$, defined in Sect. 2.3.1. In the LTB model, the angular diameter distance is related to the metric simply by [16]:

$$d_A(z) = A(r(z), t(z)) \ , \tag{3.60}$$

so due to Etherington's theorem (2.36), we also have

$$d_L(z) = (1+z)^2 A(r(z), t(z)) \ . \tag{3.61}$$

As the relations $t(z)$ and $r(z)$ are determined by Eqs. (3.58) and (3.59) and the scale function $A(r,t)$ by Eq. (3.26), using Eqs. (3.60) and (3.61), we can calculate the observables d_A and d_L for any given z. All of these relations have a manifest dependence on the inhomogeneities, i.e. on the functions $H_0(r)$ and $\Omega_m(r)$. What remains is a comparison of Eqs. (3.60) and (3.61) with the observed distance measures.

3.3 Averaging

In this Section, we consider how to implement coarse graining in the form of explicitly averaging the dynamical variables of general relativity.

3.3.1 Averaging relativistic systems

Several complications arise when considering how to explicitly average in general relativity. Despite the fact that the Einstein equation (2.8) is covariant, its average is hard to define in a covariant manner, as only the inherently invariant rank 0 tensors, that is scalars, appear to have

well-defined averages. As an example, the spatial average of a scalar quantity $S(x,t)$, which is a function of the spatial coordinates and time, can be defined as

$$\langle S(x,t)\rangle_{\mathcal{D}} \equiv \frac{\int_{\mathcal{D}} S(x,t)\sqrt{\det[g_{ij}]}\mathrm{d}^3x}{\int_{\mathcal{D}}\sqrt{\det[g_{ij}]}\mathrm{d}^3x} \,, \tag{3.62}$$

where $\mathcal{D}$ is an averaging domain and g_{ij} is the spatial metric in Eq. (3.70). Although this average of a scalar quantity is covariant, it does, however, depend on the choice of the averaging hypersurface, that is, on the spacetime foliation. However, the appropriate averaging hypersurface is a physical choice which should be chosen based on analysis of observables and cannot be predetermined by mathematics. On the other hand, the only practicable way to average tensors seems to be the manifestly coordinate-dependent averaging of components: $\langle G\rangle \equiv \langle G_{\mu\nu}\rangle$.

Also the nonlinearity of general relativity, arising from the fact that gravitational field couples to itself as gravitons have mutual interactions, brings its own complications. Indeed, the nonlinearity plays a key role both at the conceptual, and especially at the physical level, when trying to average the Einstein equation; we will now turn to this issue.

3.3.2 Averaging cosmological inhomogeneities

The justification for the use of the FRW models comes from the fact that as there is no reason to believe that we would live in a special place in the universe, it is assumed to be homogeneous and isotropic on large scales. Galaxy surveys seem to support this, indicating the lumpiness is homogenized and isotropized to a smooth distribution roughly at the scale of $100h^{-1}$ Mpc [55, 56]. However, this argumentation needs to be considered more carefully: The crucial point is the difference between exact and statistical homogeneity and isotropy. The FRW model is exactly homogeneous and isotropic. However, even though the early universe was nearly exactly homogeneous and isotropic, the late universe is far from exact local homogeneity and isotropy – the distribution can only remain statistically homogeneous and isotropic on large scales.

Statistical homogeneity and isotropy means that if the universe is divided into boxes whose sizes are larger than the homogeneity scale, the average quantities evaluated inside each box are equal (up to cosmic variance). However, the key thing is that the average quantities of the boxes are not necessarily the same as in a completely smooth spacetime, because there are structures in the box. In general, the feature that the average evolution of a clumpy space is not the same as the evolution of a smooth space is called backreaction.

In terms of general relativity, the backreaction manifests itself by the nonlinearity of the Einstein equation, in particular by the fact that the evaluation of the Einstein tensor does not commute with averaging: $\langle G(g)\rangle - G(\langle g\rangle) \neq 0$. On physical grounds, as the Einstein field $G(g, \partial g, \partial^2 g)$ is more closely related to physical quantities whereas the metric corresponds to a gravitational tensor potential whose derivatives determine the physics, it would seem more correct to first calculate the Einstein tensor for the exact metric g and only then take the average $\langle G(g)\rangle$. The issue was first pointed out by Shirokov and Fisher in 1962 [34] and later made more popular by Ellis and collaborators under the name fitting problem [35, 36, 99, 100]; for a recent review, see Refs. [37, 101]. However, this is not what is done in the standard FRW cosmology, where we use the average metric to calculate the Einstein tensor $G(\langle g\rangle)$. Indeed, if a clumpy distribution is first smoothed by describing it with the exactly homogeneous and isotropic RW metric and only then the Einstein equation is used to determine the time evolution, the result is not the same as

if we evolved the full clumpy distribution and took the average at the end. Of course, we do not have the exact metric of the universe at hand, but we can do better than use the RW metric, which describes only exactly homogeneous and isotropic universes.

Indeed, in the next Section we discuss an averaging mechanism in an irrotational dust universe in which the scalar parts of the Einstein equation are averaged. This formalism thus avoids the problem of tensorial averaging and also the spacetime foliation is physically well justified – the proper time of the dust determines it. As we shall see, this results in Friedmann-like equations with the backreaction term included (see Eqs. (3.106) – (3.108)). We have addressed the issue of quantifying the backreaction in the real universe in Papers 3 and 4, discussed in Sects. 4.3.2 and 4.3.3.

3.4 Buchert averaging

Let us now concentrate on the so-called Buchert averaging method, which we have utilized in Papers 1, 3 and 4. The method is based on spatial averaging of scalar quantities in an irrotational dust universe and was developed by Thomas Buchert in the late 1990's [38], and is nowadays the most widely used averaging method in inhomogeneous cosmology.

In the Buchert method the fact that the Einstein equation (2.8) can be split into a set of ten independent equations[4], three of which are scalar equations and the others are vector and traceless tensor equations [102, 103], is utilized and only the scalar parts are averaged. The obvious cost is thus that the equation set is not closed; the scalar parts do not contain the full information. However, averaging the scalar parts provides useful information for cosmology as the cosmological parameters of most interest are scalars.

Before deriving the actual Buchert equations, let us first provide a brief overview of the mathematical background for dealing with hypersurfaces in Sect. 3.4.1 and then extract the set of three exact scalar equations from the full Einstein equation (2.8) in Sect. 3.4.2.

3.4.1 Mathematical background

By a hypersurface we mean an $(n-1)$-dimensional submanifold Σ of an n-dimensional manifold $\mathcal{M}$. The so called projection tensor $P_{\mu\nu}$ for a hypersurface Σ with unit normal vector $n^\mu = \delta^\mu_0$ and the extrinsic curvature $K_{\mu\nu}$ (sometimes called the first fundamental form and the second fundamental form of the hypersurface, respectively) are useful tools:

$$P_{\mu\nu} \equiv g_{\mu\nu} - \sigma n_\mu n_\nu \ , \tag{3.63}$$

where $\sigma = n_\mu n^\mu$ ($\sigma = -1$ for spacelike surfaces and $\sigma = +1$ for timelike surfaces) and

$$K_{\mu\nu} \equiv \frac{1}{2} P^\alpha{}_\mu P^\beta{}_\nu (\nabla_\alpha n_\beta + \nabla_\beta n_\alpha) \ . \tag{3.64}$$

Given any vector V^μ in the tangent space at a point p in a manifold $\mathcal{M}$, $P_{\mu\nu}$ will project it tangent to the hypersurface. Acting on any two vectors that are already tangent to Σ, $P_{\mu\nu}$ acts like the metric.

[4]The Einstein equation contains ten algebraically independent component equations, since both sides are symmetric two-index tensors. The Bianchi identity reduces the number of independent differential equations to six.

3.4.2 The scalar equations

We are interested in the late universe where radiation can be neglected and thus consider an irrotational single-component pressureless ideal fluid or dust. The energy-momentum tensor (2.14) then takes the form

$$T_{\mu\nu} = \rho u_\mu u_\nu \ , \tag{3.65}$$

and the energy-momentum continuity equation (2.11) states that

$$\nabla_\mu(\rho u^\mu u^\nu) = 0 \ . \tag{3.66}$$

The four-velocity of the dust u^μ is normalized by definition:

$$u^\mu u_\mu = \frac{\mathrm{d}x^\mu}{\mathrm{d}\tau}\frac{\mathrm{d}x_\mu}{\mathrm{d}\tau} = \frac{\mathrm{d}s^2}{\mathrm{d}\tau^2} = -1 \ . \tag{3.67}$$

Due to the absence of pressure (gradients), the fluid particles follow geodesics so we also have

$$u^\mu \nabla_\mu u^\nu = 0 \ . \tag{3.68}$$

The Einstein equation (2.8) for the energy-momentum tensor (3.65) reads as

$$R_{\mu\nu} - \frac{1}{2}R g_{\mu\nu} = 8\pi G \rho u_\mu u_\nu \ , \tag{3.69}$$

with the line-element in the comoving synchronous form

$$\mathrm{d}s^2 = -\mathrm{d}t^2 + g_{ij}\mathrm{d}x^i\mathrm{d}x^j \ . \tag{3.70}$$

In these coordinates, the four-velocity is thus $u^\mu = \delta^\mu_0$.

In our case the submanifold Σ is the $t =$ const. hypersurface, with the four-velocity u^μ of the dust particles as the unit normal vector. The projection tensor (3.63) is thus

$$P_{\mu\nu} = g_{\mu\nu} + u_\mu u_\nu \ . \tag{3.71}$$

Since the integral curves of u^μ are geodesics (Eq. (3.68)), the extrinsic curvature (3.64) reduces to

$$K_{\mu\nu} = \frac{1}{2}\left(\nabla_\mu u_\nu + \nabla_\nu u_\mu\right) = \nabla_\mu u_\nu \ . \tag{3.72}$$

The extrinsic curvature is thus symmetric. Furthermore, it can be decomposed into a trace and a trace-free part as follows [58, 102]

$$K_{\mu\nu} = \sigma_{\mu\nu} + \frac{1}{3}\theta P_{\mu\nu} \ , \tag{3.73}$$

where

$$\theta = P^{\mu\nu}K_{\mu\nu} = \nabla_\mu u^\mu \ , \tag{3.74}$$

is the trace of $K_{\mu\nu}$ describing the expansion (or contraction) rate of the local volume element and $\sigma_{\mu\nu}$ is the trace-free (i.e. $\sigma^\mu{}_\mu = 0$) shear tensor describing the distortion in the local shape without a change in volume. In the synchronous coordinates of Eq. (3.70), the expansion scalar (3.74) has the expression:

$$\theta = \partial_\mu u^\mu + \Gamma^\mu_{\mu\nu}u^\nu = \Gamma^\mu_{\mu 0} = \frac{\partial_t\sqrt{\det[g_{ij}]}}{\sqrt{\det[g_{ij}]}} \ . \tag{3.75}$$

Gauss's equation relates the 4-dimensional Riemann curvature tensor (2.1) to the hypersurface Riemann curvature through [58]

$$ {}^{(3)}R^{\rho}{}_{\sigma\mu\nu} = P^{\rho}{}_{\alpha}P^{\beta}{}_{\sigma}P^{\gamma}{}_{\mu}P^{\delta}{}_{\nu}R^{\alpha}{}_{\beta\gamma\delta} - (K^{\rho}{}_{\mu}K_{\sigma\nu} - K^{\rho}{}_{\nu}K_{\sigma\mu}) \ . \tag{3.76} $$

From this we obtain the hypersurface Ricci scalar ${}^{(3)}R$ by projecting with the projection tensor (3.71) as follows:

$$ {}^{(3)}R = P^{\sigma\nu}\left({}^{(3)}R^{\lambda}{}_{\sigma\lambda\nu}\right) = R + 2R_{\mu\nu}u^{\mu}u^{\nu} - K^2 + K^{\mu\nu}K_{\mu\nu} \ , \tag{3.77} $$

where $K = g^{\mu\nu}K_{\mu\nu}$. From (3.73) we see that $K^2 = \theta^2$ and $K^{\mu\nu}K_{\mu\nu} = \sigma^{\mu\nu}\sigma_{\mu\nu} + (1/3)\theta^2$. Plugging these into Eq. (3.77) yields

$$ R_{\mu\nu}u^{\mu}u^{\nu} + \frac{1}{2}R = \frac{1}{2}{}^{(3)}R + \frac{1}{3}\theta^2 - \frac{1}{2}\sigma^{\mu\nu}\sigma_{\mu\nu} \ . \tag{3.78} $$

By contracting then the Einstein equation for dust (3.69) on both sides by $u^{\mu}u^{\nu}$, we obtain

$$ R_{\mu\nu}u^{\mu}u^{\nu} + \frac{1}{2}R = 8\pi G\rho \ . \tag{3.79} $$

Substituting Eq. (3.78) into Eq. (3.79) finally yields the first scalar equation

$$ \frac{1}{3}\theta^2 = 8\pi G\rho - \frac{1}{2}{}^{(3)}R + \frac{1}{2}\sigma^{\mu\nu}\sigma_{\mu\nu} \ , \tag{3.80} $$

known as the Hamiltonian constraint.

Let us then derive the second scalar equation. The definition of the Riemann curvature tensor (2.1) can be written as

$$ \nabla_{\mu}\nabla_{\nu}u^{\rho} - \nabla_{\nu}\nabla_{\mu}u^{\rho} = R^{\rho}{}_{\sigma\mu\nu}u^{\sigma} \ . \tag{3.81} $$

Setting $\rho = \mu$ in Eq. (3.81) and multiplying it by u^{ν} yields

$$ u^{\nu}\nabla_{\mu}\nabla_{\nu}u^{\mu} - u^{\nu}\nabla_{\nu}\theta = R_{\sigma\nu}u^{\sigma}u^{\nu} \ . \tag{3.82} $$

The first term on the left can be written as

$$ u^{\nu}\nabla_{\mu}\nabla_{\nu}u^{\mu} = \nabla_{\mu}(u^{\nu}\nabla_{\nu}u^{\mu}) - \nabla_{\nu}u^{\mu}\nabla_{\mu}u^{\nu} \ . \tag{3.83} $$

With the help of the geodesic equation (3.68), Eq. (3.83) simplifies to

$$ u^{\nu}\nabla_{\mu}\nabla_{\nu}u^{\mu} = -\nabla_{\mu}u_{\nu}\nabla^{\mu}u^{\nu} \ . \tag{3.84} $$

Moreover,

$$ \nabla_{\mu}u_{\nu}\nabla^{\mu}u^{\nu} = K_{\mu\nu}K^{\mu\nu} = \sigma^{\mu\nu}\sigma_{\mu\nu} + \frac{1}{3}\theta^2 \ . \tag{3.85} $$

Inserting Eqs. (3.84) and (3.85) into Eq. (3.82), we obtain

$$ -\dot{\theta} - \sigma^{\mu\nu}\sigma_{\mu\nu} - \frac{1}{3}\theta^2 = R_{\sigma\nu}u^{\sigma}u^{\nu} \ , \tag{3.86} $$

where $\dot{\theta} \equiv u^{\mu}\nabla_{\mu}\theta = \partial_t\theta$. Furthermore, substituting Eq. (3.86) into Eq. (3.79) yields

$$ \dot{\theta} = -\sigma^{\mu\nu}\sigma_{\mu\nu} - \frac{1}{3}\theta^2 - 4\pi G\rho \ , \tag{3.87} $$

where we have used $R = 8\pi G\rho$, which follows from the trace of the Einstein equation (3.69). Eq. (3.87) is called the Raychaudhuri equation [102].

We can obtain the third scalar equation simply by contracting the energy-momentum continuity equation (3.66) by u_ν and using the normalization equation (3.67) and the geodesic equation (3.68):

$$\dot{\rho} + \theta\rho = 0 \ , \tag{3.88}$$

where $\dot{\rho} \equiv u^\mu \nabla_\mu \rho = \partial_t \rho$.

Let us finally collect together the three exact, local, covariant equations (3.80), (3.87) and (3.88):

$$\frac{1}{3}\theta^2 = 8\pi G\rho - \frac{1}{2}{}^{(3)}R + \frac{1}{2}\sigma^{\mu\nu}\sigma_{\mu\nu} \tag{3.89}$$

$$\dot{\theta} = -\sigma^{\mu\nu}\sigma_{\mu\nu} - \frac{1}{3}\theta^2 - 4\pi G\rho \tag{3.90}$$

$$\dot{\rho} = -\theta\rho \ . \tag{3.91}$$

Note that all the quantities in Eqs. (3.89) – (3.91) have both spatial and temporal dependence and can contain arbitrary large inhomogeneities. The price to pay for reducing the Einstein tensor equation to a set of scalar equations is that the system is not closed: there are three equations for four independent variables.

3.4.3 The Buchert equations

The spatial average of a scalar quantity $S(x,t)$ is given by Eq. (3.62). The definition (3.62) implies the non-commutativity of time-evolution and averaging as a fundamental property for systems with a time-dependent integration measure $\partial_t \sqrt{\det[g_{ij}]} \neq 0$:

$$\frac{\partial}{\partial t}\langle S(x,t)\rangle \neq \langle \frac{\partial}{\partial t} S(x,t)\rangle \ . \tag{3.92}$$

Taking the time derivative of Eq. (3.62) yields

$$\begin{aligned} \partial_t \langle S\rangle_{\mathcal{D}} &= \frac{\int_{\mathcal{D}} \left[\sqrt{\det[g_{ij}]}\partial_t S + S\partial_t(\sqrt{\det[g_{ij}]})\right] \mathrm{d}^3x}{\int_{\mathcal{D}} \sqrt{\det[g_{ij}]}\mathrm{d}^3x} + \\ &- \frac{\int_{\mathcal{D}} S\sqrt{\det[g_{ij}]}\mathrm{d}^3x \int_{\mathcal{D}} \partial_t(\sqrt{\det[g_{ij}]})\mathrm{d}^3x}{(\int_{\mathcal{D}} \sqrt{\det[g_{ij}]}\mathrm{d}^3x)^2} \ , \end{aligned} \tag{3.93}$$

which can be written in terms of the expansion scalar (3.75) as

$$\partial_t \langle S\rangle_{\mathcal{D}} = \langle \partial_t S\rangle_{\mathcal{D}} + \langle S\theta\rangle_{\mathcal{D}} - \langle S\rangle_{\mathcal{D}}\langle\theta\rangle_{\mathcal{D}} \ . \tag{3.94}$$

In order to compare the average evolution with homogeneous and isotropic FRW models, we have to define a scale factor. The simplest extension of the notion of an overall scale factor to an inhomogeneous and anisotropic spacetime is to use the volume of the spatial hypersurface:

$$a_{\mathcal{D}}(t) \equiv \left(\frac{\int_{\mathcal{D}} \sqrt{\det[g_{ij}]}\mathrm{d}^3x}{\int_{\mathcal{D}} \sqrt{\det[g_{ij}(t=t_0)]}\mathrm{d}^3x}\right)^{\frac{1}{3}} \ . \tag{3.95}$$

By using the definition of the average in Eq. (3.62), we can write the average of the expansion scalar (3.75) in terms of the scale factor (3.95) as

$$\langle\theta\rangle_{\mathcal{D}} = \frac{\int_{\mathcal{D}} \partial_t(\sqrt{\det[g_{ij}]})\mathrm{d}^3x}{\int_{\mathcal{D}} \sqrt{\det[g_{ij}]}\mathrm{d}^3x} = 3\frac{\dot{a}_{\mathcal{D}}}{a_{\mathcal{D}}} \equiv 3\mathcal{H}_{\mathcal{D}} \ , \tag{3.96}$$

where we have introduced the domain dependent Hubble expansion function $\mathcal{H}_{\mathcal{D}}$.

Let us then take the average of the scalar equations (3.89) – (3.91) according to the definition (3.62) and commuting the time derivatives using Eq. (3.94). This gives us the averaged equations satisfied by the scale factor (3.95), derived by Buchert in 1999 [38].

1. We start with the Hamiltonian constraint (3.89):

$$\frac{1}{3}\langle\theta^2\rangle_{\mathcal{D}} = 8\pi G\langle\rho\rangle_{\mathcal{D}} - \frac{1}{2}\langle{}^{(3)}R\rangle_{\mathcal{D}} + \frac{1}{2}\langle\sigma^{\mu\nu}\sigma_{\mu\nu}\rangle_{\mathcal{D}} \ . \tag{3.97}$$

   By defining the backreaction,

$$\mathcal{Q}_{\mathcal{D}}(t) \equiv \frac{2}{3}(\langle\theta^2\rangle_{\mathcal{D}} - \langle\theta\rangle^2_{\mathcal{D}}) - \langle\sigma^{\mu\nu}\sigma_{\mu\nu}\rangle_{\mathcal{D}} \ , \tag{3.98}$$

   and using the relation between the average expansion rate and the scale factor (3.96), Eq. (3.97) simplifies to:

$$3\left(\frac{\dot{a}_{\mathcal{D}}}{a_{\mathcal{D}}}\right)^2 = 8\pi G\langle\rho\rangle_{\mathcal{D}} - \frac{1}{2}\langle{}^{(3)}R\rangle_{\mathcal{D}} - \frac{1}{2}\mathcal{Q}_{\mathcal{D}} \ . \tag{3.99}$$

   Eq. (3.99) is a generalization of the Friedmann equation (cf. Eq. (2.18)).

2. Next we consider the average of the Raychaudhuri equation (3.90):

$$\langle\partial_t\theta\rangle_{\mathcal{D}} = -2\langle\sigma^2\rangle_{\mathcal{D}} - \frac{1}{3}\langle\theta^2\rangle_{\mathcal{D}} - 4\pi G\langle\rho\rangle_{\mathcal{D}} \ . \tag{3.100}$$

   Commuting the time derivative in Eq. (3.100) according to the relation (3.94) yields

$$\partial_t\langle\theta\rangle_{\mathcal{D}} = -\langle\sigma^{\mu\nu}\sigma_{\mu\nu}\rangle_{\mathcal{D}} + \frac{2}{3}\langle\theta^2\rangle_{\mathcal{D}} - \langle\theta\rangle^2_{\mathcal{D}} - 4\pi G\langle\rho\rangle_{\mathcal{D}} \ . \tag{3.101}$$

   With the help of the backreaction (3.98), Eq. (3.101) can be written as

$$\partial_t\langle\theta\rangle_{\mathcal{D}} = \mathcal{Q}_{\mathcal{D}} - \frac{1}{3}\langle\theta\rangle^2_{\mathcal{D}} - 4\pi G\langle\rho\rangle_{\mathcal{D}} \ . \tag{3.102}$$

   Furthermore, using Eq. (3.96) yields the Buchert acceleration equation:

$$3\frac{\ddot{a}_{\mathcal{D}}}{a_{\mathcal{D}}} = -4\pi G\langle\rho\rangle_{\mathcal{D}} + \mathcal{Q}_{\mathcal{D}} \ . \tag{3.103}$$

3. Finally, the average of the third scalar equation (3.91) reads as

$$\langle\partial_t\rho\rangle_{\mathcal{D}} + \langle\theta\rho\rangle_{\mathcal{D}} = 0 \ . \tag{3.104}$$

   With the help of Eqs. (3.94) and (3.96), we obtain a continuity equation for the averages:

$$\partial_t\langle\rho\rangle_{\mathcal{D}} + 3\frac{\dot{a}_{\mathcal{D}}}{a_{\mathcal{D}}}\langle\rho\rangle_{\mathcal{D}} = 0 \ . \tag{3.105}$$

Let us collect together the Buchert equations (3.99), (3.103) and (3.105):

$$3\frac{\ddot{a}_{\mathcal{D}}(t)}{a_{\mathcal{D}}(t)} = -4\pi G\langle\rho\rangle_{\mathcal{D}}(t) + \mathcal{Q}_{\mathcal{D}}(t) \tag{3.106}$$

$$3\left(\frac{\dot{a}_{\mathcal{D}}(t)}{a_{\mathcal{D}}(t)}\right)^2 = 8\pi G\langle\rho\rangle_{\mathcal{D}}(t) - \frac{1}{2}\langle{}^{(3)}R\rangle_{\mathcal{D}}(t) - \frac{1}{2}\mathcal{Q}_{\mathcal{D}}(t) \tag{3.107}$$

$$\partial_t\langle\rho\rangle_{\mathcal{D}}(t) = -3\frac{\dot{a}_{\mathcal{D}}(t)}{a_{\mathcal{D}}(t)}\langle\rho\rangle_{\mathcal{D}}(t)\ . \tag{3.108}$$

The difference between the Buchert acceleration equation (3.106) and its dust FRW counterpart, Eq. (2.19) with $p = 0$, is given by the backreaction $\mathcal{Q}_{\mathcal{D}}(t)$, defned in Eq. (3.98).

In the context of cosmological averaging, with the overall dynamics of the universe given by Eqs. (3.106), (3.107) and (3.108), one can make the approximation that the average metric takes the form:

$$\mathrm{d}s^2 = -\mathrm{d}t^2 + a_{\mathcal{D}}^2(t)\left[\frac{\mathrm{d}r^2}{1-k_{\mathcal{D}}(t)r^2} + r^2(\mathrm{d}\theta^2 + \sin^2\theta\mathrm{d}\varphi^2)\right]\ , \tag{3.109}$$

which makes it possible to calculate estimates for the observable properties of light; see e.g. Refs. [12, 104]. Although, on spatial slices, the form of the metric (3.109) is the same as in the homogeneous and isotropic FRW universe, the time evolution of the scale factor $a_{\mathcal{D}}(t)$ and the spatial curvature $k_{\mathcal{D}}(t)$ are in general different from the FRW case, where $a(t)$ is determined by the Friedmann equation (2.18) and $k =$ constant.

In addition to the backreaction, compared to the corresponding FRW equations, there is also another difference in the averaged equations (3.106) – (3.108): the explicit dependence on the smoothing scale $\mathcal{D}$. We have studied the implications of the scale-dependence on the observations in Paper 1; see also Sect. 4.2.

Chapter 4

Effects of nonlinear cosmic structures

4.1 Backreaction

In Sect. 3.3, we discussed averaging in cosmology. By considering a general irrotational dust universe, we derived a set of averaged scalar equations, the Buchert equations (3.106) – (3.108), describing the average evolution of an inhomogeneous universe. These equations differ from the conventional FRW equations by the backreaction term (3.98) and by the dependence on the averaging scale. An important implication is that the averages of the inhomogeneous quantities do not evolve in time like the corresponding homogeneous quantities.

The backreaction (3.98) is given by the (positive) variance of the expansion rate minus the (positive) average shear. A commonly presented conjecture is that the backreaction of inhomogeneities could cause the acceleration of the average expansion and could thus account for the cosmological observations [12, 19, 105, 106]. Indeed, from Eq. (3.106) it is obvious that, regardless of the local deceleration at each point as is manifest from Eq. (3.90), with large enough backreaction $\mathcal{Q}_{\mathcal{D}}(t) > 4\pi G\langle\rho\rangle_{\mathcal{D}}(t)$, the global expansion can accelerate without an exotic fluid with negative pressure or a modification of gravity. Physically, the global acceleration is possible because the volume can become dominated by fast-expanding regions [107]. This is realized with large enough variance of the expansion rate, if the counterbalancing average shear is not too large. The variance becomes large when contracting ($\theta < 0$) and expanding ($\theta > 0$) regions coexist. This is exactly what happens in the late universe with structures forming via gravitational collapse [97, 108].

By partitioning the averaging domain $\mathcal{D}$ into a set of N mutually disjoint subregions $\mathcal{D}_i$ that satisfy $\bigcup_{i=1}^{N}\mathcal{D}_i = \mathcal{D}$, the total backreaction (3.98) can be written as

$$\mathcal{Q}_{\mathcal{D}} = \sum_{i=1}^{N} f_i \mathcal{Q}_{\mathcal{D}_i} + \frac{1}{3}\sum_{i=1}^{N}\sum_{j=1}^{N} f_i f_j \left(\langle\theta\rangle_{\mathcal{D}_i} - \langle\theta\rangle_{\mathcal{D}_j}\right)^2 \ , \tag{4.1}$$

where f_i is the volume fraction of the subregion $\mathcal{D}_i$, $f_i \equiv \mathrm{Vol}(\mathcal{D}_i)/\mathrm{Vol}(\mathcal{D})$. The expression (4.1) makes it explicit that the backreaction is an intensive, rather than extensive, quantity.

Although the cosmological backreaction is conceptually well-understood and the mechanism by which it could act is physically plausible, the complexity of the structure formation at the nonlinear level means its magnitude in the real universe is difficult to evaluate and is hence widely debated [37, 109]. Indeed, there have been contradictory outcomes in the literature:

some studies have found a significant amount of backreaction [19, 21, 107, 110–112], even to the extent of accounting for the observed cosmic acceleration entirely without additional effects [19, 107, 112], while others suggest backreaction to be insignificant [113–119]. As many of the current standard values for the cosmological parameters – not just the cosmological constant – rely on the hypothesis of negligible backreaction, its evaluation is a very important task [120,121].

A significant amount of backreaction is usually obtained via the simplification of partially or fully neglecting the shear on the interface between regions of different expansion rates, i.e. ignoring the matching conditions [19, 107, 111, 112], whereas in perturbative studies where the shear is present the backreaction is found to be small [122–124]. This suggests that the magnitude of the shear must be evaluated more carefully; we have elaborated this issue in Papers 3 and 4 within exact general relativity, see Sect. 4.3. Also the topic of Paper 2 is closely related to this; in Paper 2, we have shed light on the issue of the adequacy of the perturbative approach by calculating how perturbations affect the luminosity distance within the FRW model, see Sect. 4.3.3.

Besides the backreaction, there is also the explicit dependence of the averaged quantities on the averaging scale that makes the Buchert equations differ from the Friedmann equations. We have analyzed this issue in Paper 1 and discuss it in Sect. 4.2.

4.1.1 Averaging LTB models

We have studied averaging using the LTB models introduced in Sect. 3.2, so let us start by calculating some useful LTB averages. For simplicity, we usually do not explicitly write the subscript $\mathcal{D}$ to denote the averaging domain in the averages.

With the help of Eqs. (3.39) and (3.42), the backreaction (3.98) of the LTB solution simplifies to

$$\mathcal{Q}(t) = 2\left\langle \frac{\dot{A}^2(r,t)}{A^2(r,t)} \right\rangle + 4\left\langle \frac{\dot{A}(r,t)\dot{A}'(r,t)}{A(r,t)A'(r,t)} \right\rangle - \frac{2}{3}\left\langle 2\frac{\dot{A}(r,t)}{A(r,t)} + \frac{\dot{A}'(r,t)}{A'(r,t)} \right\rangle^2 , \tag{4.2}$$

which, when evaluated on the $t = t_0$ hypersurface using Eqs. (3.40), (3.43) and (3.44), reduces to

$$\mathcal{Q}(t_0) = 6\left(\left\langle H_0^2 \right\rangle - \left\langle H_0 \right\rangle^2\right) + 4\left(\left\langle rH_0'H_0 \right\rangle - \left\langle rH_0' \right\rangle \left\langle H_0 \right\rangle\right) - \frac{2}{3}\left\langle rH_0' \right\rangle^2 , \tag{4.3}$$

where $H_0 \equiv H_0(r)$.

The above result (4.2) is the general expression for the backreaction in LTB models, but let us calculate it explicitly for the flat case $k(r) = 0$. The integration measure (3.46) now reads as

$$\sqrt{\det[g_{ij}]}\mathrm{d}^3x = A'A^2 \sin\theta \mathrm{d}r\mathrm{d}\theta\mathrm{d}\varphi \ . \tag{4.4}$$

For symmetry and simplicity, we only consider averages over a spherical domain of radius R centered at the origin. From Eqs. (3.39) and (3.42) we have the following total derivatives:

$$\frac{2}{3}\theta^2 - \sigma^2 = 2\frac{\dot{A}^2}{A^2} + 4\frac{\dot{A}\dot{A}'}{AA'} = \frac{2}{A^2A'}\frac{\partial}{\partial r}\left(\dot{A}^2A\right) , \tag{4.5}$$

$$\theta = 2\frac{\dot{A}}{A} + \frac{\dot{A}'}{A'} = \frac{1}{A^2A'}\frac{\partial}{\partial r}\left(\dot{A}A^2\right) . \tag{4.6}$$

Using the definition of the average (3.62), we thus obtain

$$\left\langle \frac{2}{3}\theta^2 - \sigma^2 \right\rangle = \frac{3}{A^3} 2\dot{A}^2 A = 6\frac{\dot{A}^2(R,t)}{A^2(R,t)} \tag{4.7}$$

and

$$\frac{2}{3}\langle\theta\rangle^2 = \frac{2}{3}\left(\frac{3}{A^3}A^2\dot{A}\right)^2 = 6\frac{\dot{A}^2(R,t)}{A^2(R,t)} \ , \tag{4.8}$$

so the backreaction (3.98) is

$$\mathcal{Q} = \frac{2}{3}\left(\langle\theta^2\rangle - \langle\theta\rangle^2\right) - \langle\sigma^2\rangle = \left\langle \frac{2}{3}\theta^2 - \sigma^2 \right\rangle - \frac{2}{3}\langle\theta\rangle^2 = 0 \ . \tag{4.9}$$

The backreaction thus vanishes identically for the flat matter-dominated LTB model over a spherical domain (though not for domains of arbitrary shape).

As the spatial metric (3.47) reduces to the flat Euclidean form on a $t =$ const. hypersurface, the Ricci scalar (3.36) vanishes as well and hence we have $\langle {}^{(3)}R\rangle = 0$ in Eq. (3.107) for the flat matter-dominated LTB model. Note also that with the choice (3.25), the coordinate distances thus correspond to proper distances on the $t = t_0$ hypersurfaces.

The average of the expansion scalar (3.39) yields the following relation between the average Hubble function $\mathcal{H}(t)$, defined in Eq. (3.96), and the LTB Hubble function $H(r,t)$ in the flat LTB model:

$$\mathcal{H}(t) = \frac{1}{3}\langle\theta\rangle = \frac{A^2\dot{A}}{3}\frac{3}{A^3} = \frac{\dot{A}(R,t)}{A(R,t)} = H(R,t) \ . \tag{4.10}$$

4.2 Scale dependence in the Buchert averaging

One criticism towards the Buchert averaging method has been that, with the averaging done over a single domain, it would not be able to capture the effects of possible large scale inhomogeneities [19, 20]. Indeed, although the major part of the universe appears to be taken up by voids of size $10h^{-1} - 100h^{-1}$ Mpc, the observations seem to indicate the existence of large voids and superclusters, see e.g. Refs. [53, 125, 126]. In Paper 1, a generalization to the Buchert method was presented in the form of utilizing a scale-dependent averaging to study the capability of taking into account inhomogeneities on larger scales as well. This issue had not been examined carefully before, though some ideas of multiple averaging scales existed in the literature [12, 104].

Physically, the use of a scale-dependent averaging domain in calculating the observable distance measures (2.36) can be justified by the fact that as the distance the observed light travels depends on how far the object is, it would be reasonable to average over the proper distance of the objects $R(z)$ for each redshift z instead of using a fixed domain R. To test the possible effects of the scale-dependent averaging on the averaged observable quantities, we used the flat LTB model, introduced in Sect. 3.2.1, as a testing ground. This model is particularly useful in distinguishing the effect, as both the backreaction $\mathcal{Q}$ and the spatial curvature scalar ${}^{(3)}R$ vanish identically (for spherical integration domains $\mathcal{R}$) as noted in Sect. 4.1.1 and therefore the only difference from the homogeneous and flat matter-dominated FRW equations for the average scale factor

$a_{\mathcal{R}}(t)$ and the average matter density $\langle\rho\rangle_{\mathcal{R}}$ is the scale dependence of the averaged quantities:

$$\frac{\ddot{a}_{\mathcal{R}}}{a_{\mathcal{R}}} = -\frac{4\pi G}{3}\langle\rho\rangle_{\mathcal{R}} \tag{4.11}$$

$$\left(\frac{\dot{a}_{\mathcal{R}}}{a_{\mathcal{R}}}\right)^2 = \frac{8\pi G}{3}\langle\rho\rangle_{\mathcal{R}} \tag{4.12}$$

$$\frac{\partial}{\partial t}\langle\rho\rangle_{\mathcal{R}} = -3\frac{\dot{a}_{\mathcal{R}}}{a_{\mathcal{R}}}\langle\rho\rangle_{\mathcal{R}}\ , \tag{4.13}$$

where $\mathcal{R}$ denotes a spherical integration domain.

Solving Eqs. (4.11), (4.12) and (4.13) gives the Friedmann solution, $a_{\mathcal{R}}(t) = (t/t_0(R))^{2/3}$, with scale-dependent age of the universe $t_0(R)$. Thus, the template metric (3.109) reduces to

$$\mathrm{d}s^2 = -\mathrm{d}t^2 + (t/t_0(R))^{4/3}\left[\mathrm{d}r^2 + r^2(\mathrm{d}\theta^2 + \sin^2\theta\mathrm{d}\varphi^2)\right]\ . \tag{4.14}$$

The observable distance measures can thus be directly obtained from the corresponding FRW results. Utilizing the fact that the RW metric is just a special case of the LTB metric in the limit $A(r,t) \to a(t)r$ and $k(r) \to kr^2$ together with Eqs. (2.33), (3.58) and (3.59), we obtain the proper distance of the flat FRW model

$$r(z) = \frac{2}{H_0}\left(1 - \frac{1}{\sqrt{1+z}}\right)\ . \tag{4.15}$$

Using Eqs. (3.58) and (4.15), the distance-redshift relations (3.60) and (3.61) thus become

$$d_A(z) = a(t(z))r(z) = \frac{2}{H_0}\frac{1}{(1+z)}\left(1 - \frac{1}{\sqrt{1+z}}\right) \tag{4.16}$$

$$d_L(z) = (1+z)^2 a(t(z))r(z) = \frac{2}{H_0}(1+z)\left(1 - \frac{1}{\sqrt{1+z}}\right)\ . \tag{4.17}$$

From Eqs. (4.10) and (4.15), we obtain for the averaged distance

$$\bar{r}(z) = \frac{2}{\mathcal{H}_{\mathcal{R}}(t_0)}\left(1 - \frac{1}{\sqrt{1+z}}\right) = \frac{2}{H_0(R)}\left(1 - \frac{1}{\sqrt{1+z}}\right)\ , \tag{4.18}$$

so that the averaged distance-redshift relations can be written as:

$$\bar{d}_A(z) = a_{\mathcal{R}}(\bar{t}(z))\bar{r}(z) = \frac{2H_0^{-1}(R(z))}{(1+z)}\left(1 - \frac{1}{\sqrt{1+z}}\right) \tag{4.19}$$

$$\bar{d}_L(z) = (1+z)^2 a_{\mathcal{R}}(\bar{t}(z))\bar{r}(z) = 2H_0^{-1}(R(z))(1+z)\left(1 - \frac{1}{\sqrt{1+z}}\right)\ . \tag{4.20}$$

Note that instead of a single scale R, we have allowed for a running averaging scale $R(z)$ in Eqs. (4.19) and (4.20). In this case, the averaged equations (4.11), (4.12) and (4.13) hold true for each scale $R(z)$ separately. In practice, this means that we have a different FRW model for each redshift.

Using both a single scale $R(z) = \text{const.} \equiv R$ and a redshift dependent scale $R(z)$, we examined the deviation of Eqs. (4.19) and (4.20) from their exact LTB counterparts (3.60) and (3.61). Note that averaging over a single scale is equivalent to using the perfectly homogeneous EdS model; in that case, the freedom to choose the averaging scale R only corresponds to fixing the value of the effective Hubble constant $H_0(R)$ in Eqs. (4.19) and (4.20):

- A single averaging scale R – **Single scale**

  In this case, the observables are determined by Eqs. (4.19) and (4.20) with $R(z) =$ constant $\equiv R$:

$$\bar{d}_L(z) = 2H_0^{-1}(R)(1+z)\left(1 - \frac{1}{\sqrt{1+z}}\right). \tag{4.21}$$

  When considering a model that fits the supernova observations (see Sect. 4.2.1) the averaging scale R was taken to be the present-day physical distance to the object with the highest redshift in the supernova sample, $R = r_{\mathrm{LTB}}(z_{\max})$, numerically computed from Eqs. (3.58) and (3.59) with the scale function from Eq. (3.27). For periodic inhomogeneities in Sect. 4.2.2, the scale was chosen to be $R = 2\pi r_0$, where r_0 is the wavelength of the inhomogeneities.

There are two conceptual steps in coarse graining needed to calculate the observables [104]. Firstly, the step from the exact Einstein equations to the Buchert equations, and secondly, the step from the exact metric (3.47) to the average metric (4.14). In order to quantify the approximation in the latter step, we considered the following two cases separately – the case in which both the field equations and the metric have been averaged, and the case where only the field equations have been averaged, but the exact metric is used to determine the geodesics:

- $R(z) = \bar{r}(z)$ – **Running scale with averaged geodesics**

  In this case, the running averaging scale $R(z)$ was taken to be the present-day physical distance to each redshift, as determined by the averaged geodesics (4.18), in which $R = r_{\mathrm{LTB}}(z_{\max})$ or $R = 2\pi r_0$. Choosing again $R = \bar{r}(z)$ in Eq. (4.18) would lead to the iterative use of Eq. (4.18), perhaps ultimately converging to $r_{\mathrm{LTB}}(z)$ and making it no different from the case of exact geodesics. Although not used here, this could be a practical way of computing the distance in more complex models where the exact result is unattainable. The observables are determined by

$$\bar{d}_L(z) = 2H_0^{-1}\left(2H_0^{-1}(R)\left(1 - \frac{1}{\sqrt{1+z}}\right)\right)(1+z)\left(1 - \frac{1}{\sqrt{1+z}}\right). \tag{4.22}$$

- $R(z) = r_{\mathrm{LTB}}(z)$ – **Running scale with exact geodesics**

  Here the running averaging scale $R(z)$ was taken to be the present-day physical distance to each redshift, as determined by the geodesics of the exact metric, Eqs. (3.58) and (3.59), yielding for the observables:

$$\bar{d}_L(z) = 2H_0^{-1}(r_{\mathrm{LTB}}(z))(1+z)\left(1 - \frac{1}{\sqrt{1+z}}\right). \tag{4.23}$$

In order to make comparison between the coarse-grained observables of Eqs. (4.21), (4.22) and (4.23) and the exact expressions (3.60) and (3.61), we first considered low redshifts analytically by Taylor expanding the observables. The advantage in using the expansions is that as the LTB function $H_0(r)$ can be left unspecified, the comparison is independent of the profile. The superiority of a running scale versus a single scale for generic inhomogeneity profiles was explicit in the expansions and we demonstrated the improvement in accuracy up to redshifts $z \sim 0.2$ also by testing the expansions numerically for physically motivated inhomogeneity profiles $H_0(r)$. Furthermore, we performed direct numerical comparisons using two different LTB profiles $H_0(r)$:

a model fitting the supernova observations presented in Ref. [20], that gives a good fit to the Riess et. al. gold sample of 157 supernovae [65], and a periodic inhomogeneity profile representing a toy model for structures. Let us review the outcomes of the two models in Sects. 4.2.1 and 4.2.2.

4.2.1 Acceleration without backreaction

The expansion of the dust dominated flat LTB universe can have neither local nor average acceleration by virtue of Eq. (4.9), but nevertheless can, as shown e.g. in Sect. 3.2 of Ref. [20], fit the supernova observations. Thus, from the observational point of view, the model can have effective acceleration or acceleration along our line of sight. Since the backreaction vanishes in this model, the only possibility to account for the effect within the Buchert averaging formalism seems to be the running smoothing scale.

The boundary condition function of this model is given by

$$H_0(r) = H + \Delta H e^{-r/r_0} \ , \tag{4.24}$$

where the parameters have the values $H + \Delta H = 65.5$ km/s/Mpc, $\Delta H = 16.8$ km/s/Mpc and $r_0 = 1400$ Mpc.

The relative deviations $(\bar{d}_A(z) - d_A(z))/d_A(z)$ are displayed in Figs. 4.1 and 4.2, where $d_A(z)$ is the exact result of Eq. (3.60) and $\bar{d}_A(z)$ stands for the averaged expressions (4.21), (4.22), (4.23). Due to the general relation (2.36), the figures 4.1 and 4.2 represent the relative deviations of the luminosity distance as well.

As an additional measure of the deviation, we performed the χ^2 analysis to the Riess et. al. supernova data. The χ^2 (see e.g. Ref. [127]) is given by

$$\chi^2 \equiv \frac{1}{157} \sum_{n=1}^{157} \left(\frac{d_L^{\mathrm{obs}}(z_n) - d_L(z_n)}{\sigma_n} \right)^2 \ , \tag{4.25}$$

where σ_n is the estimated error of the measured luminosity distance $d_L^{\mathrm{obs}}(z_n)$ to a source with redshift z_n. The χ^2 tells the goodness of the fit: the smaller the χ^2, the better the fit. Indeed, the result of this analysis confirms the huge deviation of the single scale from the exact result ($\chi^2 = 4.35$ versus $\chi^2 = 1.12$), whereas the running scale gives an excellent fit $\chi^2 = 1.11$, which is within one percent of the correct result $\chi^2 = 1.12$.

However, as is evident from Fig. 4.2, also the accuracy of the running scale starts to fail when going beyond the supernova fits to higher redshifts. Indeed, Fig. 4.2 reveals that at $z \gtrsim 2$ the running scale falls short of the $\mathcal{O}(1\%)$ accuracy compared to the exact observables. There is a plausible physical explanation for this: the inhomogeneities in the employed LTB model are decaying modes, and thus more important at higher redshifts and cannot be encapsulated in the present-day spatial averages. One can still argue that in a more realistic model the problem would be alleviated, since the inhomogeneities of the real universe are expected to grow forwards in time. Overall, we suppose the averaging with the running scale would be conceivable at least up to $z \sim 2$; for higher redshifts, one could then use coarser approximations, such as the perturbed FRW models.

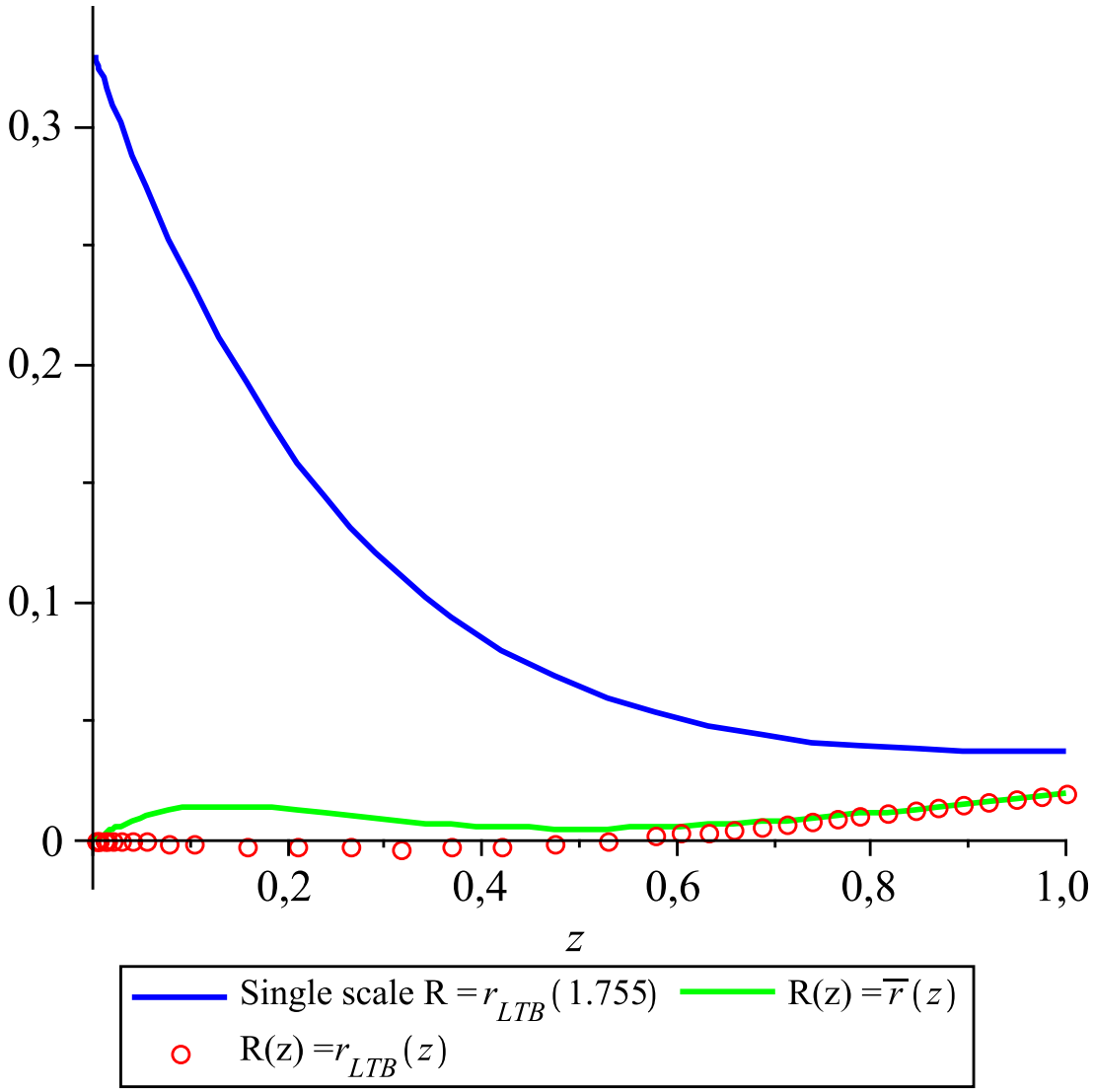

Figure 4.1: The relative deviation $(\bar{d}_A(z) - d_A(z))/d_A(z) = (\bar{d}_L(z) - d_L(z))/d_L(z)$ of the averaged angular diameter (or luminosity) distance $\bar{d}_A(z)$ from the exact value $d_A(z)$ for the bubble model of Sect. 4.2.1 in the following cases: Blue − a single averaging scale, chosen to be $r_{\,\mathrm{LTB}}(1.755) = 4944$ Mpc, where $z = 1.755$ is the redshift of the farthest supernova in the sample. Green − the averaged physical distance $\bar{r}(z)$ as the running smoothing scale. Red − the exact physical distance $r_{\mathrm{LTB}}(z)$ as the running smoothing scale.

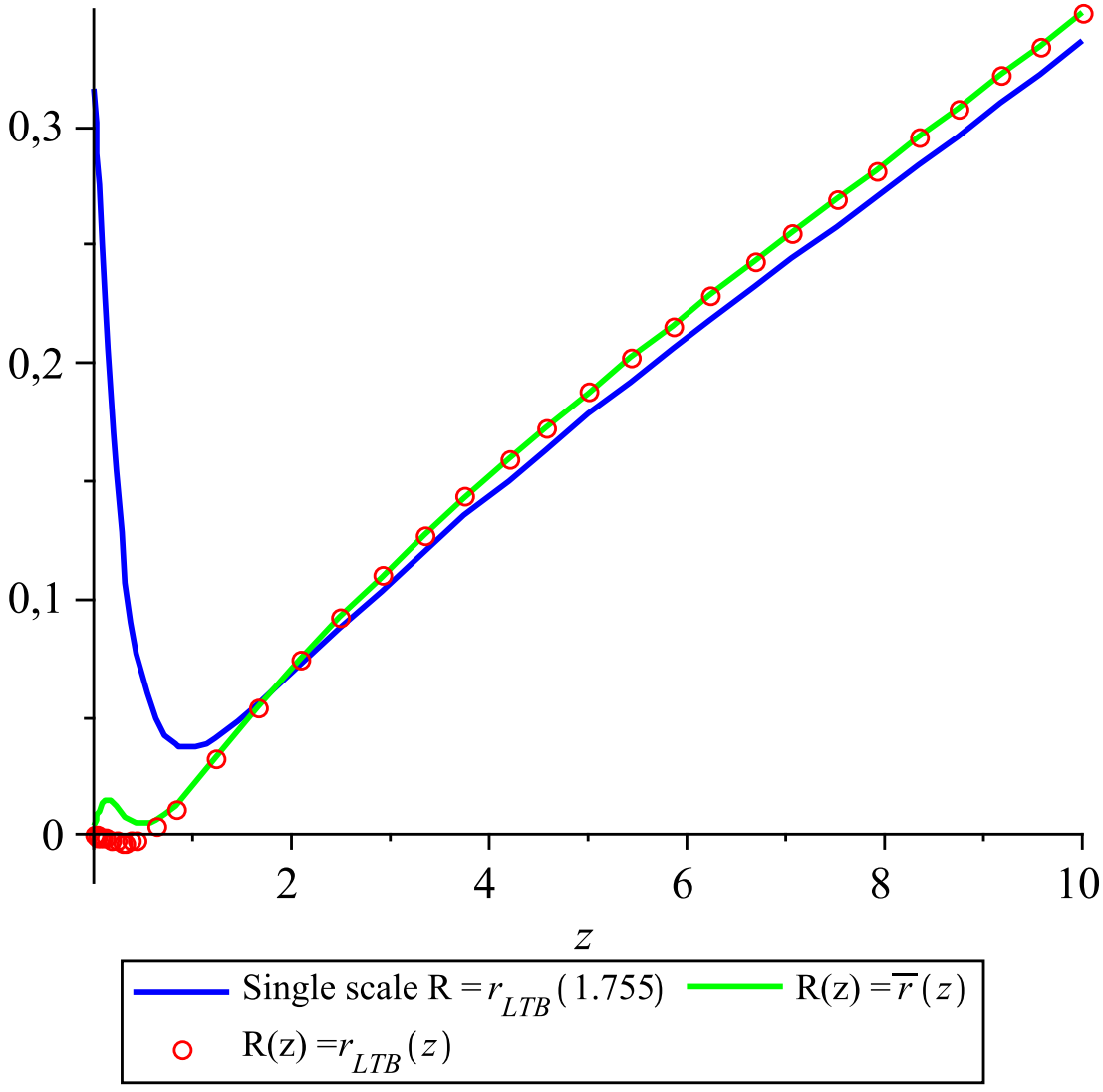

Figure 4.2: Same as in Figure 4.1, but for larger redshift range, $z = 0...10$.

4.2.2 Periodic inhomogeneities as a toy model for structure

Perhaps the closest representative of structure under the assumption of spherical symmetry is achieved with a periodic boundary condition function $H_0(r)$ [128]. Hence, we considered a profile

$$H_0(r) = H + \Delta H \sin r/r_0 \ , \tag{4.26}$$

where the values $H = 65.5\,\mathrm{km/s/Mpc}$, $\Delta H = 1.64\,\mathrm{km/s/Mpc}$ and $r_0 = 95\,\mathrm{Mpc}$ have been chosen to make the plots as illustrative as possible. We did not consider more intense inhomogeneities in order to keep the relation $r_{\mathrm{LTB}}(z)$ single-valued up to the redshift $z = 1$. The relative deviations $(\bar{d}_A(z) - d_A(z))/d_A(z)$ calculated using this profile are shown in Fig. 4.3.

4.2.3 Comments on the running scale averaging

Our studies of the scale dependence in the Buchert averaging method, using the flat LTB model as a testing ground, suggest that a single averaging scale R gives too coarse predictions for the observable distance-redshift relations $d(z)$ an exact LTB observer would make. Instead, using a redshift dependent scale $R(z)$, where $R(z)$ is the distance of the objects for each redshift z, improves the accuracy to $\mathcal{O}(1\%)$ precision at $z < 2$ in the averaged distance measures of Eqs. (4.22) and (4.23) as compared to the exact expression of Eq. (3.61).

The failure of the single averaging scale is most evident in Fig. 4.3: even though the model of Sect. 4.2.2 with periodic inhomogeneities is homogeneous on large scales, the single averaging scale still leads to unwanted deviations. Whether it is an artefact of the spherical symmetry, with light inevitably propagating through all the layers of structure, or a more general phenomenon, cannot be resolved within the employed LTB models. Altogether, the results of Paper 1 confirm the conclusion that averaging over a single scale gives a too coarse-grained description at least for the flat LTB universe. The inadequacy of the averaging procedure to account for the observations in the LTB universe was already suggested in Ref. [20], but the results of Paper 1 bring out the fact that the conclusion is valid only under the assumption of a single smoothing scale.

What comes to the running scale case, there are only minor deviations in the observables between the use of the averaged and the exact geodesics, though the exact physical distance evidently still gives the most accurate approximation. Anyway, due to the good congruence of the results between the averaged and the exact geodesics, the feasibility becomes the deciding factor. Indeed, in more realistic models of the universe, the exact geodesics are beyond computation. Overall, perhaps the best solution in practice is to use the averaged geodesics and, if needed, use Eq. (4.18) iteratively.

Another important point to note is that when considering the model that fits the supernova observations, see Sect. 4.2.1, we found that the running smoothing scale can account for the apparent acceleration even without backreaction. Consequently, it could be as important factor as the backreaction in the Buchert averaging formalism, especially when considering large scale inhomogeneities where the single-scale Buchert method fails. Although considered merely under the assumption of spherical symmetry, we expect the running scale to show its full advantage only when applied to more irregular large scale inhomogeneities, such as the observed large voids. In addition to its computational simplicity, a virtue of the method is that it provides a unified scheme to take into account both the global backreaction and the local deviations from the averages within the same formalism.

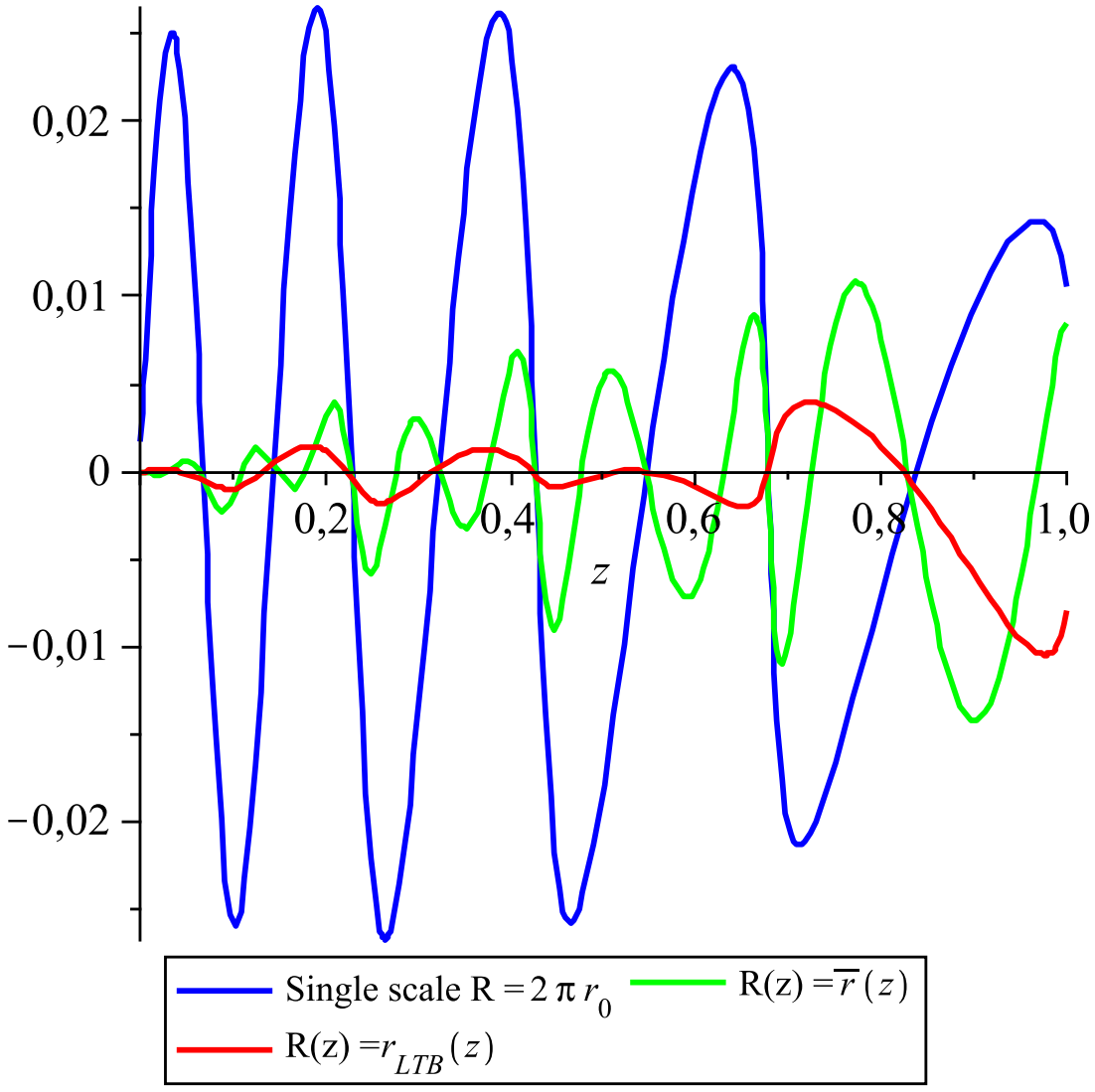

Figure 4.3: The relative deviation $(\bar{d}_A(z) - d_A(z))/d_A(z) = (\bar{d}_L(z) - d_L(z))/d_L(z)$ of the averaged angular diameter (or luminosity) distance $\bar{d}_A(z)$ from the exact value $d_A(z)$ for the model of Sect. 4.2.2 in the following cases: Blue − a single averaging scale, chosen to be one oscillation period $2\pi r_0 = 598$ Mpc. Green − the averaged physical distance $\bar{r}(z)$ as the running smoothing scale. Red − the exact physical distance $r_{\mathrm{LTB}}(z)$ as the running smoothing scale.

4.3 The role of the shear

In this section, we discuss the shear, which may – as we have exemplified in Papers 3 and 4 – play an important role in the dynamics of the nonlinear structures, although usually assumed to be negligible in the nonperturbative estimates for the backreaction [19, 107, 111, 112]. Note that we have only compared the shear in different models at fixed times, so the question of its explicit time evolution has not been considered here.

4.3.1 A void-wall pair: the disjoint FRW approximation

As the (observable) universe is made of a network of voids surrounded by walls, a simple way to estimate the backreaction for this kind of a configuration is to consider two disjoint FRW solutions: the voids represented by the Milne solution $\Omega = 0$

$$a = a_0 \left(\frac{t}{t_0} \right) \tag{4.27}$$

$$\theta_v = 3H(t) = \frac{3}{t} \, , \tag{4.28}$$

and the walls represented by the EdS solution $\Omega = 1$

$$a = a_0 \left(\frac{t}{t_0} \right)^{2/3} \tag{4.29}$$

$$\theta_v = 3H(t) = \frac{2}{t} \, , \tag{4.30}$$

where we have used the Friedmann equation (2.33) and the definition of the expansion scalar (3.75). As in the FRW models the shear is zero by construction, the backreaction (3.98) is thus just given by the variance

$$\mathcal{Q}_{\rm FRW} = \frac{2}{3} \left(\langle \theta^2 \rangle - \langle \theta \rangle^2 \right) \, , \tag{4.31}$$

where, due to the homogeneity of the voids and walls, the volume integrals reduce to the sums:

$$\langle \theta^2 \rangle = \frac{V_{\rm w} \theta_w^2 + V_{\rm v} \theta_v^2}{V_{\rm w} + V_{\rm v}} \tag{4.32}$$

and

$$\langle \theta \rangle = \frac{V_{\rm w} \theta_w + V_{\rm v} \theta_v}{V_{\rm w} + V_{\rm v}} \, . \tag{4.33}$$

By inserting Eqs. (4.28) and (4.30) in Eqs. (4.32) and (4.33), the backreaction (4.31) becomes

$$\mathcal{Q}_{\rm FRW} = \frac{2}{3} t_0^{-2} f_v (1 - f_v) \, , \tag{4.34}$$

where f_v is the void volume fraction:

$$f_v \equiv \frac{V_{\rm v}}{V_{\rm v} + V_{\rm w}} \, . \tag{4.35}$$

Since $0 \leqslant f_v \leqslant 1$, Eq. (4.34) implies that the maximum backreaction for the configuration is obtained with a void fraction $f_v = 1/2$, regardless of the void size, yielding the value

$$\mathcal{Q}_{\rm FRW}^{\rm max} = \frac{1}{6} t_0^{-2} \, . \tag{4.36}$$

Let us next calculate the void volume V_v. With $\Omega = 0$ and $t = t_0$, Eq. (2.27) gives $k = -a_0^2 H_0^2$, so by performing the coordinate transformation $\chi = a_0 H_0 r$, the RW metric (2.13) becomes

$$\mathrm{d}s^2 = -\mathrm{d}t^2 + \left(\frac{a(t)}{a_0 H_0}\right)^2 \left[\frac{\mathrm{d}\chi^2}{1+\chi^2} + \chi^2 \left(\mathrm{d}\theta^2 + \sin^2\theta \mathrm{d}\varphi^2\right)\right] \ . \tag{4.37}$$

The volume element for the metric (4.37) reads as

$$\sqrt{[\det g_{ij}]}\mathrm{d}\chi\mathrm{d}\theta\mathrm{d}\varphi = \left(\frac{a(t)}{a_0 H_0}\right)^3 \frac{\chi^2}{\sqrt{1+\chi^2}} \sin\theta \mathrm{d}\chi\mathrm{d}\theta\mathrm{d}\varphi \ , \tag{4.38}$$

from which the integration over the void $0 \leqslant \chi \leqslant a_0 H_0 r_0$ on the $t = t_0$ hypersurface yields

$$V_\mathrm{v} = 2\pi t_0^3 \left[\left(\frac{r_0}{t_0}\right)\sqrt{1+\left(\frac{r_0}{t_0}\right)^2} - \mathrm{arsinh}\left(\frac{r_0}{t_0}\right)\right] \ , \tag{4.39}$$

where we have used Eq. (4.28) to substitute $H_0 = t_0^{-1}$ and the freedom to set $a_0 = 1$. For realistic-sized voids, $r_0 \ll t_0$, expanding Eq. (4.39) gives

$$V_\mathrm{v} = \frac{4}{3}\pi r_0^3 \left[1 + \mathcal{O}\left(\frac{r_0}{t_0}\right)^2\right] \simeq \frac{4}{3}\pi r_0^3 \ . \tag{4.40}$$

For the flat wall, the volume is simply

$$V_\mathrm{w} = \frac{4}{3}\pi\left(R^3 - r_0^3\right) \ . \tag{4.41}$$

By inserting Eqs. (4.40) and (4.41) in (4.34), the backreaction for small voids $r_0 \ll t_0$ becomes

$$\mathcal{Q}_\mathrm{FRW} = \frac{2}{3} t_0^{-2} \left(\frac{r_0}{R}\right)^3 \left[1 - \left(\frac{r_0}{R}\right)^3\right] \ , \tag{4.42}$$

yielding the maximum backreaction of Eq. (4.36) when the void volume fraction is $R = 2^{1/3} r_0$.

However, this disjoint FRW approximation might give too coarse estimates for the backreaction: in particular, considering that on physical grounds, shear is expected to occur on the boundaries between regions of different expansion rates, what would be needed is an exact solution to match voids and walls together. We have studied this issue in Papers 3 and 4 using the exact LTB solution discussed in Sect. 3.2. Whereas in Paper 3 we only considered empty voids (with $\Omega_\mathrm{v} \simeq 0$ and $Ht \simeq 1$) matched together with flat walls (with $\Omega_\mathrm{w} \simeq 1$ and $Ht \simeq 2/3$), together with the condition that the void size r_0 compared to the horizon size t_0 is small $r_0 \ll t_0$, in Paper 4 we generalized the results to arbitrary void-wall pairs within $0 \leq \Omega_\mathrm{v} \leq \Omega_\mathrm{w} \leq 1$ and also relaxed the assumption of small voids. In Paper 4, we also considered a network of voids with different densities Ω_v and radii r_0, thus giving rise to relative variance of the expansion rate between the different void-wall pairs. To directly address the role of the shear, we then compared our results to the disjoint FRW case. Let us next discuss the results of the Papers.

4.3.2 Dependence on the void size and the transition sharpness

In Paper 3, we studied the behaviour of the shear and the backreaction within an LTB model consisting of two different regions: a void where $\Omega_0 \simeq 0$ and a wall where $\Omega_0 \simeq 1$, with a smooth transition in between. For this we chose the $\Omega_0(r)$ profile as follows:

$$\Omega_0(r) = \left(1 - e^{-(r/r_0)^n}\right)^2 \ , \tag{4.43}$$

where r_0 determines the size of the void and n the sharpness of the spatial transition between the void and the wall. By virtue of the (nearly) simultaneous Big Bang condition (3.38), Eq. (4.43) implies

$$H_0(r) = \frac{t_0^{-1}}{3}\left(2 + e^{-(r/r_0)^n}\right) \ , \tag{4.44}$$

which tells us that the void expands faster than the wall by a factor of 3/2.

Using LTB models with the void-wall profile (4.43), many voids can be straightforwardly joined together to construct a model for a network of voids. This is because LTB solutions with the profile (4.43) are, up to terms of order $e^{-(R/r_0)^n}$, $\Omega_0 = 1$ FRW dust solutions outside the void at $R > r_0$, all with t_0 as the age of the universe, implying that the different LTB solutions naturally join together in the wall region.

As the cosmological observations suggest that voids in the cosmic matter distribution satisfy $r_0 \ll t_0$ [51], in Paper 3 we limited ourselves to consider only subhorizon voids with $r_0 \ll t_0$. With the conditions (3.25) and (3.38), the curvature function $k(r)$ of Eq. (3.21) thus becomes

$$k(r) = -\left(\frac{r}{t_0}\right)^2 \underbrace{\left(1 - \frac{1}{3}\sqrt{\Omega_0(r)}\right)^2 (1 - \Omega_0(r))}_{\leq 1} \ . \tag{4.45}$$

As the function (4.43) rapidly approaches the value $\Omega_0 = 1$ outside the void, we have

$$\max\left(|k(r)|\right) < \left(\frac{r_0}{t_0}\right)^2 \ll 1 \ . \tag{4.46}$$

Thus, $k(r)$ satisfies $|k(r)| \ll 1 \ \forall \ r$. Note, however, that the condition $|k(r)| \ll 1$ does not imply that the spatial curvature (3.36) is small in the void.

The advantage of $k(r)$ being small is that calculations become simpler as the part of the LTB volume element (3.46) containing $k(r)$ can be expanded as follows

$$\frac{1}{\sqrt{1 - k(r)}} = 1 + \frac{1}{2}k(r) + \mathcal{O}(k^2(r)) \ . \tag{4.47}$$

Furthermore, Eqs. (3.13), (3.25) and (4.46) imply that the coordinate r closely measures the proper distance on the spatial hypersurface defined by $t = t_0$.

Given the LTB volume element (3.46), we can expand Eq. (3.62) for small $k(r)$ using the result (4.47) to obtain:

$$\langle S \rangle = \langle S \rangle_0 + \frac{1}{2}\left(\langle Sk \rangle_0 - \langle S \rangle_0 \langle k \rangle_0\right) + \mathcal{O}(k^2) \ , \tag{4.48}$$

where the subscript 0 now refers to averages where $k(r) = 0$ in the integration measure, that is $\sqrt{[\det g_{ij}]_0} \equiv A'(r,t)A^2(r,t)\sin\theta$.

When applying the expansion (4.48) to the shear

$$\langle\sigma^2\rangle = \langle\sigma^2\rangle_0 + \underbrace{\frac{1}{2}\left(\langle\sigma^2 k\rangle_0 - \langle\sigma^2\rangle_0\langle k\rangle_0\right)}_{\equiv\langle\sigma^2\rangle_1} \ , \tag{4.49}$$

we obtained the following analytic expression for the average shear in the zeroth order of $k(r)$:

$$\langle\sigma^2\rangle_0 = \frac{t_0^{-2}}{6}\left(\frac{r_0}{R}\right)^3\left(1+\frac{3}{n}\right)\Gamma\left(\frac{3}{n}\right)2^{-3/n} \ , \tag{4.50}$$

where Γ stands for Euler's gamma function. We also calculated the first-order term and found it is suppressed by the overall factor $(r_0/t_0)^2$ relative to the leading order term (4.50). Since the shear falls off rapidly in the wall outside the void, the following approximation has been used when calculating Eq. (4.50):

$$\int_0^R \sigma^2(r,t_0)r^2\,\mathrm{d}r \simeq \int_0^\infty \sigma^2(r,t_0)r^2\,\mathrm{d}r \ , \tag{4.51}$$

where $R > r_0$ is the (coordinate) radius of the spherical averaging region.

As long as the volume-ratio $(r_0/R)^3$ is kept fixed, the average shear (4.50) for subhorizon size voids is independent of the size of the void and thus also gives the average shear for the network of subhorizon size voids where each void can have a different value of r_0. This is because, as we noted earlier, the LTB void-wall profiles (4.43) naturally match together outside the voids.

In the step function limit $n \to \infty$, Eq. (4.50) diverges with the following asymptotics:

$$\langle\sigma^2(r,t_0)\rangle \sim \frac{1}{18}t_0^{-2}\left(\frac{r_0}{R}\right)^3 n \ , \tag{4.52}$$

telling that the sharper the transition between the void and the wall, the higher the value of the average shear. This can be traced back to the thin infinite compensating shell that forms in the limit $n \to \infty$.

Let us consider the backreaction (3.98) next. As shown in Eq. (4.9), the backreaction vanishes in the flat LTB model, i.e. in the zeroth order of $k(r)$. This implies that the variance of the expansion rate must be equal to the average shear (4.50) to the leading order. Therefore, we must go beyond the zeroth order to obtain the leading order term of the backreaction.

Using the result (4.48), the first-order term reads as

$$\mathcal{Q} = 3H_0^2(R)\langle k\rangle_0 + \left\langle\left(\frac{\theta^2}{3}-\frac{\sigma^2}{2}\right)k\right\rangle_0 - 2H_0(R)\langle\theta k\rangle_0 \ , \tag{4.53}$$

where we have written $\langle\theta\rangle_0$ in terms of $H_0(R)$ using the result (4.8). Using the approximation (4.51) for the integrals in Eq. (4.53) that contain $k(r)$ as a common factor yields

$$\begin{aligned}\mathcal{Q} \ &= \ \frac{1}{9}t_0^{-2}\left(\frac{r_0}{R}\right)^3\left(\frac{r_0}{t_0}\right)^2\frac{1}{n}\Gamma\left(\frac{5}{n}\right)\left\{\frac{8}{9}\cdot 3^{-5/n} - \frac{2}{3}\cdot 4^{-5/n} + \frac{2}{3}\cdot 5^{-5/n} + \frac{4}{9}\cdot 6^{-5/n} + \right. \\ &+ \ e^{-2(R/r_0)^n}\left(-8 - 4\cdot 2^{-5/n} + 2\cdot 3^{-5/n} + 4^{-5/n}\right) + \\ &+ \ \left. e^{-(R/r_0)^n}\left(\frac{8}{3}\cdot 2^{-5/n} + \frac{32}{9}\cdot 3^{-5/n} - \frac{7}{3}\cdot 4^{-5/n} - \frac{4}{3}\cdot 5^{-5/n}\right)\right\} \ . \end{aligned} \tag{4.54}$$

In the limit $n \to \infty$, Eq. (4.54) gives

$$\mathcal{Q} = \frac{4}{135} t_0^{-2} \left(\frac{r_0}{R}\right)^3 \left(\frac{r_0}{t_0}\right)^2 \ , \tag{4.55}$$

showing that although both the average shear and the variance of the expansion rate diverge as $n \to \infty$, the backreaction, given by their difference, has a finite limit. The result (4.54) also shows that the dependence of the backreaction on the sharpness of the transition between the void and the wall is weak, so that the qualitative behaviour is the same for all n. In the step function limit, when the void is exactly compensated – that is, the solution becomes exactly FRW outside the void – the result (4.55) is also valid for a network of voids as long as the ratios r_0/R and r_0/t_0 are kept fixed.

We have numerically tested the effect of replacing the condition (3.38) with the exact simultaneous Big Bang condition (3.37) for different values of the parameters n and r_0. Although not significant, the relative error in the backreaction was found to be larger the smaller the value of n, peaking at $\mathcal{O}(0.1)$ for small n. The decrease of the error with increasing n can be understood as a consequence of the fact that the approximation (3.38) is exact at the extreme values $\Omega_0 = 0$ and $\Omega_0 = 1$ so, in the step function limit $n \to \infty$ where $\Omega_0(r)$ only takes these values, it does not matter whether the exact condition (3.37) or the approximation (3.38) is used.

When comparing the LTB result (4.55) with $R = 2^{1/3} r_0$ to the disjoint FRW result (4.36), we obtain:

$$\mathcal{Q} = \frac{4}{45} \left(\frac{r_0}{t_0}\right)^2 \mathcal{Q}_{\mathrm{FRW}} \ . \tag{4.56}$$

The result (4.56) demonstrates how important it can be to take into account the shear: for a realistic-sized void with $r_0 = 0.01 t_0$, the FRW approximation overestimates the backreaction by the tremendous factor of 10^5. The suppressive factor $(r_0/t_0)^2$ appears to be consistent with the results from perturbative analysis in Refs. [129, 130].

4.3.3 More general void-wall profiles and a network of different voids

Given the result (4.54) for the backreaction found in Paper 3 is qualitatively similar for all values of n, i.e. the dependence of the backreaction on the transition sharpness is weak, in Paper 4 we considered a more general LTB profile with a step function transition between voids and walls:

$$\Omega_0(r) = \left(\sqrt{\Omega_{\mathrm{v}}} + (\sqrt{\Omega_{\mathrm{w}}} - \sqrt{\Omega_{\mathrm{v}}})\Theta(r - r_0)\right)^2 \ , \tag{4.57}$$

where Θ stands for the Heaviside step function and r_0 determines the size of the void. Because of the constraint (3.38), the density profile (4.57) implies the expansion profile

$$H_0(r) = \frac{t_0^{-1}}{3} \left(3 - \sqrt{\Omega_{\mathrm{v}}} + (\sqrt{\Omega_{\mathrm{v}}} - \sqrt{\Omega_{\mathrm{w}}})\Theta(r - r_0)\right) \ . \tag{4.58}$$

In the case $\Omega_{\mathrm{v}} = 0$ and $\Omega_{\mathrm{w}} = 1$, the profile considered reduces to the step function limit $n \to \infty$ of Eqs. (4.43) and (4.44) studied in Paper 3. To calculate the backreaction for the void-wall model defined by Eqs. (4.57) and (4.58), we also need the first derivative of the expansion profile:

$$H_0'(r) = -\frac{1}{3} t_0^{-1} (\sqrt{\Omega_{\mathrm{w}}} - \sqrt{\Omega_{\mathrm{v}}})\delta(r - r_0) \ , \tag{4.59}$$

where δ stands for the Dirac delta function.

The advantage of describing the void-wall transition by a step function is that analytic calculations are possible. The result for the backreaction (4.3) with the profile (4.57) and (4.58) reads as

$$\mathcal{Q} = t_0^{-2} \frac{(\sqrt{\Omega_\mathrm{w}} - \sqrt{\Omega_\mathrm{v}})^2}{v^2} \left\{ \frac{2}{3}\mathcal{I}_0\mathcal{I}_1 + \frac{4}{9}\big[(\mathcal{I}_0 + \mathcal{I}_1)\,\mathcal{B} - \mathcal{I}_1\mathcal{A}\big]\varepsilon^3 - \frac{2}{27}\mathcal{A}^2\varepsilon^6 \right\} , \tag{4.60}$$

with the following definitions:

- The reduced dimensionless volume v:

$$v = \int_0^{\varepsilon x} \frac{y^2 \mathrm{d}y}{\sqrt{1 + y^2\alpha(\Theta)}} , \tag{4.61}$$

  where $\varepsilon \equiv r_0/t_0$, $x \equiv R/r_0 > 1$, $\Theta \equiv \Theta(r - r_0)$ and

$$\alpha(\Theta) \equiv \left(1 - \frac{1}{3}\left[\sqrt{\Omega_\mathrm{v}} + (\sqrt{\Omega_\mathrm{w}} - \sqrt{\Omega_\mathrm{v}})\Theta\right]\right)^2 \left(1 - \left[\sqrt{\Omega_\mathrm{v}} + (\sqrt{\Omega_\mathrm{w}} - \sqrt{\Omega_\mathrm{v}})\Theta\right]^2\right) . \tag{4.62}$$

- The integral $\mathcal{I}$:

$$\mathcal{I}(\mu, \nu, \alpha) \equiv \int_\mu^\nu \frac{y^2 \mathrm{d}y}{\sqrt{1 + y^2\alpha}} , \tag{4.63}$$

  which can be calculated analytically to yield

$$\mathcal{I}(\mu, \nu, \alpha) = \frac{1}{2\alpha^{3/2}} \left[\sqrt{\alpha}(\nu\sqrt{1 + \alpha\nu^2} - \mu\sqrt{1 + \alpha\mu^2}) + \ln\left(\frac{\sqrt{\alpha}\mu + \sqrt{1 + \alpha\mu^2}}{\sqrt{\alpha}\nu + \sqrt{1 + \alpha\nu^2}} \right) \right] . \tag{4.64}$$

  For example the volume (4.61) can be written in terms of the function (4.63) as

$$v = \int_0^{\varepsilon} \frac{y^2 \mathrm{d}y}{\sqrt{1 + y^2\alpha(0)}} + \int_\varepsilon^{\varepsilon x} \frac{y^2 \mathrm{d}y}{\sqrt{1 + y^2\alpha(1)}} = \underbrace{\mathcal{I}(0, \varepsilon, \alpha(0))}_{\equiv \mathcal{I}_0} + \underbrace{\mathcal{I}(\varepsilon, \varepsilon x, \alpha(1))}_{\equiv \mathcal{I}_1} , \tag{4.65}$$

  where α is defined in Eq. (4.62).

- The integrals $\mathcal{A}$ and $\mathcal{B}$

$$\mathcal{A} \equiv \int_0^1 \frac{\mathrm{d}\vartheta}{\sqrt{1 + \varepsilon^2\alpha(\vartheta)}} \tag{4.66}$$

$$\mathcal{B} \equiv \int_0^1 \frac{\vartheta \mathrm{d}\vartheta}{\sqrt{1 + \varepsilon^2\alpha(\vartheta)}} . \tag{4.67}$$

The backreaction (4.60) can be calculated numerically or as an expansion in powers of ε or ε^{-1}. When considering small voids $r_0 \ll t_0$, the sixth order expansion of Eq. (4.60) for the values $\Omega_\mathrm{v} = 0$, $\Omega_\mathrm{w} = 1$ and $(r_0/R)^3 = 1/2$ yields

$$\mathcal{Q} = t_0^{-2} \left\{ \frac{2}{135}\left(\frac{r_0}{t_0}\right)^2 - \frac{137107}{12247200}\left(\frac{r_0}{t_0}\right)^4 + \frac{33336241}{3940536600}\left(\frac{r_0}{t_0}\right)^6 - \mathcal{O}\left(\frac{r_0}{t_0}\right)^8 \right\} . \tag{4.68}$$

We see that the first term agrees with the result of Paper 3 as given by Eq. (4.55). In case of small voids $r_0 \lesssim 0.3\,t_0$, the values $\Omega_\mathrm{v} = 0$ and $\Omega_\mathrm{w} = 0.7$ were found to maximize the backreaction, however, the increase being only $\sim 10\%$ relative to the case where $\Omega_\mathrm{v} = 0$ and $\Omega_\mathrm{w} = 1$.

By inspecting the power series (4.68), we found a very simple but accurate fitting formula for the backreaction in terms of elementary functions, given by

$$\mathcal{Q} = \frac{2}{135} t_0^{-2} \left(\frac{r_0}{t_0}\right)^2 \frac{1}{1 + \frac{3}{4}\left(\frac{r_0}{t_0}\right)^2} \,. \tag{4.69}$$

Testing the fitting formula (4.69) numerically shows that it is very accurate up to horizon sized voids $r_0 \sim t_0$ (for $r_0 < t_0$ we have $|\text{error}| < 1\%$) and an excellent approximation even beyond. To illustrate this, we have plotted the fitting formula (4.69) against the exact backreaction (4.60) and the leading order term of the expansion (4.68) in Figure 4.4. The figure also shows that the mere leading order term gives an accurate approximation for the backreaction even up to voids of size $r_0 \sim t_0/3$.

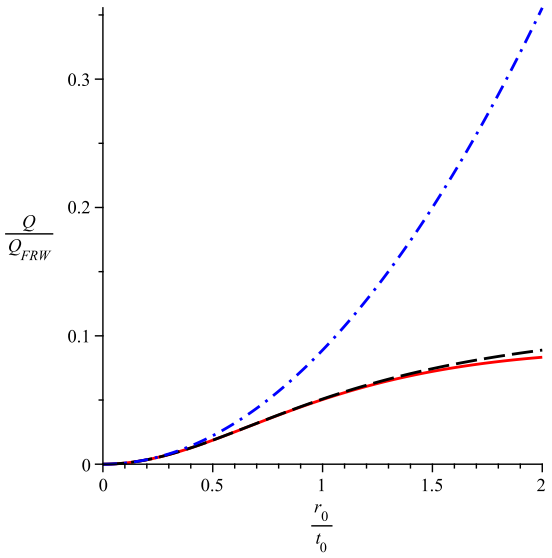

Figure 4.4: The backreaction as a function of r_0/t_0 for the profile (4.57) with $\Omega_\mathrm{v} = 0$, $\Omega_\mathrm{w} = 1$ and $(r_0/R)^3 = 1/2$ calculated using the exact result (4.60) (red solid curve), the leading order term of the expansion (4.68) (blue dash dotted curve) and the fitting formula (4.69) (black dashed curve).

We also studied the behaviour of the backreaction for a network of subhorizon voids. Whereas the first-order result (4.55) calculated in Paper 3 applies also to a network presuming all the voids have the same size r_0, in Paper 4 we used the general form (4.1) for the total backreaction to calculate an upper limit for a network of voids with different sizes r_0 and densities Ω_v. In order to do this, the following matching condition must be met: the different void-wall pairs must have the same wall-density Ω_w and the same age of the universe t_0. This provides an exact solution, because, outside the void at $R > r_0$, the void-wall LTB profiles are identical to the homogeneous Friedmann dust solution with Ω_w as the density parameter and t_0 as the age of the universe and thus naturally match together.

The total backreaction (4.1) consists of the volume-weighted average of the backreactions $\mathcal{Q}_i$ of the individual void-wall pairs i plus a sum over the relative variances of the expansion rates between all the different pairs. The relative variance term makes the configuration particularly interesting as it seems to offer a way to increase the variance of the expansion rate without having to introduce any counterbalancing extra shear. However, the upper limit for the variance term in the total backreaction (4.1) was found to be

$$\frac{1}{3}\sum_{i=1}^{N}\sum_{j=1}^{N} f_i f_j \left(\langle\theta\rangle_{\mathcal{D}_i} - \langle\theta\rangle_{\mathcal{D}_j}\right)^2 \leq 10^{-3} t_0^{-2} \left(\frac{r_0}{t_0}\right)^4 , \tag{4.70}$$

where r_0 is the radius of the largest void in the network and we have assumed that the volume fractions f_i are constant $f_i \equiv f = 1/N$. Eq. (4.70) shows that the relative variance term is at most of the order $(r_0/t_0)^4$ so the backreaction for a network of LTB voids with profile defined by Eqs. (4.57) and (4.58) is essentially given just by the volume-weighted average of the backreactions of the individual void-wall pairs and thus remains of order $(r_0/t_0)^2$.

4.3.4 Comments on the shear studies

In Papers 3 and 4, we pinpointed the issue of small versus large cosmological backreaction to the question of matching conditions: while the variance of the expansion rate alone can induce significant backreaction as demonstrated by using the disjoint FRW approximation presented in Sect. 4.3.1, the shear arising from matching together the regions with different expansion rates seems to bring down the backreaction by at least five orders of magnitude for voids of the observed size.

Apart from the profiles considered, the systematic study of the role of shear makes our approach different from the previous studies on the backreaction in the LTB model which have focused on finding profiles that exhibit acceleration of the average expansion [105, 108, 131–133], on general properties of the backreaction [134–136] or on scale-dependence of the averages as analyzed in Paper 1.

The void-wall profiles (4.43) and (4.57) have a compensating overdense peak in the physical matter density $\rho_0(r)$ between the void and the wall regions. The peak is required to make the wall (very close to) the FRW solution. One might thus ask whether this is the reason for the suppressed backreaction. To address this issue, we also considered uncompensated profiles and demonstrated that the suppression of the backreaction is not due to an overdense or collapsing region between the void and the wall but truly an effect of the shear; our numerical computations show that the dependence of the backreaction on r_0 is $\mathcal{Q} \propto r_0^2$ also for uncompensated voids. However, extrapolating the result from a void-wall pair to the network of voids is harder for the uncompensated voids than for the compensated ones. The reason is that, without the compensating overdensity, the solution approaches RW metric slower: although the matter density is constant outside the void ($r > r_0$), the spatial curvature becomes (nearly) constant only much further ($r \gtrsim 10 r_0$) from the void. It thus appears that in order to match together uncompensated voids in the simple fashion, the separation between the voids must be so large that only a few voids fit inside the horizon. Therefore, more sophisticated junction conditions need to be applied in joining together uncompensated voids to obtain a global void-fraction more consistent with observations such as the ones quoted in Ref. [51].

The crucial question is whether the suppression of the backreaction due to the shear is a general property of all realistic cosmological solutions of general relativity or just a special property of

the matching in the considered particular solutions. This issue has to be addressed with solutions more sophisticated than the LTB-based models employed here. The generalization would include breaking the spherical symmetry, rotation (which has an opposite effect to shear) and a network of uncompensated voids.

4.4 Perturbed FRW models

We have been studying backreaction that emerges from averaging the Einstein equation. The backreaction is a manifestation of the nonlinearity of general relativity. In standard cosmology, the growth of structure is described by linear perturbations around the FRW model. This standard cosmological perturbation theory [72] fails to describe structures at the full nonlinear level, but is nevertheless prevalently considered to be a working description of the overall dynamics of the universe, with dark energy included at late times.

However, it has been suggested in the literature that the linearly perturbed FRW model would actually remain valid even for strongly nonlinear density perturbations, implying that the nonlinear effects of the structures on the average dynamics would be small [113–115, 122, 137–142]. The argument is that even in the regime when the density perturbation becomes large, the corresponding metric perturbation ϕ in Eq. (4.94) in the Newtonian gauge would remain small. This is the case e.g. in the solar system.

However, the argumentation is not free of problems; see Refs. [143,144] for discussion and further references. Most importantly, it is not in general enough for the linear perturbation theory to remain valid that ϕ would remain small when the density perturbation becomes large: the observables are not calculated from the metric alone, but involve first and second derivatives of the metric as well, which can become large when the density becomes nonlinear. In this case, the linear equations as such are therefore no longer consistent. Indeed, in the standard perturbation theory the assumption that the metric perturbation $h_{\mu\nu}$ of Eq. (4.82) and its first and second derivatives $\partial_\rho h_{\mu\nu}$ and $\partial_\rho\partial_\sigma h_{\mu\nu}$ remain small implies that the density perturbation must be small as well. In practice, in case the density perturbation is allowed to be large, one would thus need to find a second-order correction to the perturbation equations. However, trying to find a second-order correction is a very involved task: Directly expanding the equations to second order in ϕ is inconsistent, unless the intrinsic second-order terms in the metric are included as well. Indeed, the proper second-order calculation would be much more complicated, as the metric cannot be written in the simple diagonal form of Eq. (4.94) [145]. Altogether, as the second derivatives of the metric perturbations have variations of order unity after structures become nonlinear, the smallness of the metric perturbations alone is not a sufficient condition for the correction to the average expansion to be small.

It is important to note that in addition to the effects on the average expansion rate, nonlinear structures can affect light propagation also via other mechanisms, which may have to be considered separately. We have addressed the validity of the perturbed matter-dominated FRW model in the context of light propagation in Paper 2, to be discussed in Sect. 4.4.2. Before that, let us give a brief overview of the basics of the standard cosmological perturbation theory in Sect. 4.4.1.

4.4.1 Standard cosmological perturbation theory and gauge transformations

In standard cosmology, the evolution of structures in the universe is described in terms of linear (first-order) perturbation theory. The basic assumption is that although the structures evidently become nonlinear, the large-scale distribution of nonlinear objects can be treated in terms of linear theory. Furthermore, the effect of the perturbations on the observable distance measures is considered to be negligible, as the perturbations are assumed to average out during the journey of light over cosmological distances.

In this Section, we review the basic formalism of the cosmological perturbation theory with emphasis on gauge transformations; for further details and analysis of the actual perturbation equations, we refer the reader e.g. to [72, 146] .

All the quantities are written as a sum of the background value, corresponding to the homogeneous and isotropic FRW model, and a perturbation, which is the deviation from the background value. For example, the energy density is written as

$$\rho(t, x^i) = \bar{\rho}(t) + \delta\rho(t, x^i) \ , \tag{4.71}$$

where the perturbation $\delta\rho(t, x^i)$ is a first-order small. The linearized – that is, containing only the zeroth order (background) and the first-order terms – Einstein equation then determines the evolution of the perturbations.

In the standard cosmological perturbation theory [72, 146], the background spacetime is the spatially flat FRW universe, represented by the metric (2.13) with $k = 0$. For convenience, we introduce here the so-called conformal time, defined as

$$\mathrm{d}\eta = \frac{\mathrm{d}t}{a(t)} \ . \tag{4.72}$$

The background metric $\bar{g}$ thus reads as

$$\bar{g}_{\mu\nu}\mathrm{d}x^\mu\mathrm{d}x^\nu = a^2(\eta)(-\mathrm{d}\eta^2 + \mathrm{d}x^2 + \mathrm{d}y^2 + \mathrm{d}z^2) = a^2(\eta)\eta_{\mu\nu}\mathrm{d}x^\mu\mathrm{d}x^\nu \ , \tag{4.73}$$

where $\eta_{\mu\nu}\mathrm{d}x^\mu\mathrm{d}x^\nu$ is the Minkowski metric. As an example of the use of the conformal time (4.72), consider the EdS case, where the Friedmann equation (2.33) yields $a(t) = (t/t_0)^{2/3}$ so that $H = 2/(3t)$. In conformal time, these become:

$$t = \frac{\eta}{3} \tag{4.74}$$

$$a = \left(\frac{\eta}{\eta_0}\right)^2 \tag{4.75}$$

$$\mathcal{H} \equiv \frac{\partial_\eta a}{a} = aH = \frac{2}{\eta} \ . \tag{4.76}$$

In terms of the redshift (2.32), we have from the Fridmann equation (2.33) that

$$H = H_0(1+z)^{3/2} \ , \tag{4.77}$$

so that, by virtue of Eq. (4.76)

$$\mathcal{H} = H_0\sqrt{1+z} \ . \tag{4.78}$$

Furthermore, the FRW limit $A \to ar$ and $k(r) = kr^2$ of the LTB results (3.58) and (3.59) yields

$$\frac{\mathrm{d}t}{\mathrm{d}z} = -a\frac{\mathrm{d}r}{\mathrm{d}z} = -\frac{1}{H_0(1+z)^{5/2}} \ , \tag{4.79}$$

where we have used Eq. (4.77). In terms of the conformal time (4.72), we obtain

$$\frac{\mathrm{d}\eta}{\mathrm{d}z} = -\frac{\mathrm{d}r}{\mathrm{d}z} = -\frac{1}{H_0(1+z)^{3/2}} \ , \tag{4.80}$$

so that

$$\Delta\eta = r = \frac{2}{H_0}\left(1 - \frac{1}{\sqrt{1+z}}\right) \ , \tag{4.81}$$

for the EdS model.

The metric of the perturbed universe can be written as

$$g_{\mu\nu} = \bar{g}_{\mu\nu} + \delta g_{\mu\nu} = a^2(\eta_{\mu\nu} + h_{\mu\nu}) \ , \tag{4.82}$$

where $h_{\mu\nu}$ and its first and second derivatives are assumed to be small to first order. The perturbation $h_{\mu\nu}$ and the metric $\eta_{\mu\nu}$ are not tensors in the perturbed spacetime. However, raising and lowering the indices of h is defined through $\eta_{\mu\nu}$, for example:

$$h^{\mu}_{\nu} \equiv \eta^{\mu\alpha}h_{\alpha\nu} \ . \tag{4.83}$$

The usual decomposition of $h_{\mu\nu}$ is

$$[h_{\mu\nu}] \equiv \begin{bmatrix} -2A & -B_i \\ -B_i & -2D\delta_{ij} + 2E_{ij} \end{bmatrix} \ , \tag{4.84}$$

so that the line-element for the metric (4.82) is

$$\mathrm{d}s^2 = a^2(\eta)\left\{-(1+2A)\mathrm{d}\eta^2 - 2B_i\mathrm{d}\eta\mathrm{d}x^i + [(1-2D)\delta_{ij} + 2E_{ij}]\mathrm{d}x^i\mathrm{d}x^j\right\} \ . \tag{4.85}$$

The function $A(\eta, x^i)$ is called the lapse function, and $B_i(\eta, x^i)$ the shift vector.

In order to do operations such as summation and differentiation, we need a correspondence between the background spacetime and the perturbed spacetime: the point $\bar{P}$ in the background spacetime and the point P in the perturbed spacetime which have the same coordinate values, are taken to correspond to each other. However, this correspondence is not unique; there exist many possible coordinate systems in the perturbed spacetime that correspond to a given coordinate system of the background spacetime. The choice among these coordinate systems in the perturbed spacetime is called the gauge choice[1].

We denote the coordinates of the background by x^α, and the two different coordinate systems in the perturbed spacetime by $\hat{x}^\alpha$ and $\tilde{x}^\alpha$. The correspondence is given by

$$\tilde{x}^\alpha(\tilde{P}) = \hat{x}^\alpha(\hat{P}) = x^\alpha(\bar{P}) \ . \tag{4.86}$$

[1] An alternative but equivalent way to think of the gauge is a diffeomorphic mapping between the perturbed and the background spacetimes.

A gauge transformation means a coordinate transformation between the coordinate systems in the perturbed spacetime for a given point, for example:

$$\begin{aligned} \tilde{x}^\alpha(\tilde{P}) &= \hat{x}^\alpha(\tilde{P}) + \xi^\alpha \\ \tilde{x}^\alpha(\hat{P}) &= \hat{x}^\alpha(\hat{P}) + \xi^\alpha \ , \end{aligned} \tag{4.87}$$

where ξ^α is a first-order small.

Using Eqs. (4.86) and (4.87), the relation between the coordinates of the two different points in a given coordinate system is given by

$$\begin{aligned} \hat{x}^\alpha(\tilde{P}) &= \hat{x}^\alpha(\hat{P}) - \xi^\alpha \\ \tilde{x}^\alpha(\tilde{P}) &= \tilde{x}^\alpha(\hat{P}) - \xi^\alpha \ . \end{aligned} \tag{4.88}$$

We would like to know how tensors transform in the gauge transformation (4.87). Whereas the usual coordinate transformation rule of general relativity applies at a given point, now the aim is to relate quantities at different points to each other. An implication of this is that scalars are not invariant under gauge transformations. Consider a tensor $C_{\alpha\beta} = \bar{C}_{\alpha\beta} + \delta C_{\alpha\beta}$ as an example. The perturbation $\delta C_{\alpha\beta}$ is not unique, it depends on the gauge and is defined via

$$\begin{aligned} \widehat{\delta C}_{\alpha\beta}(x^\gamma) &\equiv C_{\hat{\alpha}\hat{\beta}}(\hat{P}) - \bar{C}_{\alpha\beta}(\bar{P}) \\ \widetilde{\delta C}_{\alpha\beta}(x^\gamma) &\equiv C_{\tilde{\alpha}\tilde{\beta}}(\tilde{P}) - \bar{C}_{\alpha\beta}(\bar{P}) \ . \end{aligned} \tag{4.89}$$

The usual GR transformation rule reads as

$$C_{\tilde{\mu}\tilde{\nu}}(\tilde{P}) = \frac{\partial \hat{x}^\rho}{\partial \tilde{x}^\mu} \frac{\partial \hat{x}^\sigma}{\partial \tilde{x}^\nu} C_{\hat{\rho}\hat{\sigma}}(\tilde{P}) = \left(\delta^\rho_\mu - \xi^\rho{}_\mu\right) \left(\delta^\sigma_\nu - \xi^\sigma{}_\nu\right) C_{\hat{\rho}\hat{\sigma}}(\tilde{P}) \ , \tag{4.90}$$

where we have used Eq. (4.87). We can write

$$C_{\hat{\alpha}\hat{\beta}}(\tilde{P}) = C_{\hat{\alpha}\hat{\beta}}(\hat{P}) + \frac{\partial C_{\hat{\alpha}\hat{\beta}}}{\partial \hat{x}^\lambda} \left[\hat{x}^\lambda(\tilde{P}) - \hat{x}^\lambda(\hat{P})\right] = C_{\hat{\alpha}\hat{\beta}}(\hat{P}) - \frac{\partial \bar{C}_{\alpha\beta}}{\partial x^\lambda}(\bar{P}) \xi^\lambda \ , \tag{4.91}$$

where we have used Eq. (4.88). Inserting Eq. (4.91) into Eq. (4.90) yields

$$C_{\hat{\alpha}\hat{\beta}}(\tilde{P}) = C_{\hat{\alpha}\hat{\beta}}(\hat{P}) - \xi^\rho{}_\alpha \bar{C}_{\rho\beta}(\bar{P}) - \xi^\sigma{}_\beta \bar{C}_{\alpha\sigma}(\bar{P}) - \frac{\partial \bar{C}_{\alpha\beta}}{\partial x^\lambda}(\bar{P}) \xi^\lambda \ . \tag{4.92}$$

Finally, subtracting the background value at $\bar{C}_{\alpha\beta}(\bar{P})$ from Eq. (4.92), we obtain the gauge transformation rule for the tensor perturbation $\delta C_{\alpha\beta}$:

$$\widetilde{\delta C}_{\alpha\beta} = C_{\hat{\alpha}\hat{\beta}}(\tilde{P}) - \bar{C}_{\alpha\beta}(\bar{P}) = \widehat{\delta C}_{\alpha\beta} - \xi^\rho{}_\alpha \bar{C}_{\rho\beta} - \xi^\sigma{}_\beta \bar{C}_{\alpha\sigma} - \bar{C}_{\alpha\beta,\lambda} \xi^\lambda \ , \tag{4.93}$$

where we have used the definitions (4.89).

There are only six physical degrees of freedom in the metric (4.82), which can be divided into 2 scalar, 2 vector and 2 tensor perturbations, referring to their transformation properties under rotations in the background space. The scalar, vector and tensor parts do not interact in first-order perturbation theory, and can thus be considered separately. Vector perturbations couple to rotational velocity perturbations in the cosmic fluid and decay in time. Tensor perturbations obey a wave equation corresponding to gravitational waves, and they are gauge-invariant. In cosmology, scalar perturbations are the most important, as they couple to density and pressure

perturbations and are thus responsible for the formation of structure in the universe from small initial perturbations.

In standard cosmology, perhaps the most commonly used gauge is the Newtonian gauge (also known as the conformal-Newtonian gauge or the longitudinal gauge) that contains only the scalar perturbations. In this gauge, the line-element reads as

$$\mathrm{d}s^2 = a^2(\eta)\left[-(1+2\phi)\mathrm{d}\eta^2 + (1-2\psi)\delta_{ij}\mathrm{d}x^i\mathrm{d}x^j\right] \ , \tag{4.94}$$

where the function ϕ is often called the Newtonian potential, since in the Newtonian limit, it becomes equal to the Newtonian potential perturbation, and ψ is called the Newtonian curvature perturbation, because it determines the curvature of the 3-dimensional $t = \text{const.}$ spatial sections, which are flat in the unperturbed universe. In the case of perfect fluid, $\phi = \psi$, so we have

$$\mathrm{d}s^2 = a^2(\eta)\left[-(1+2\psi)\mathrm{d}\eta^2 + (1-2\psi)\delta_{ij}\mathrm{d}x^i\mathrm{d}x^j\right] \ . \tag{4.95}$$

4.4.2 Perturbations in the luminosity distance and the supernova data

To address the question of whether the effects of inhomogeneities are too large to be describable within the perturbed FRW description, in Paper 2 we considered an $\Omega = 1$ dust FRW model with small spherically symmetric perturbations in the gravitational potential ψ. Whereas in the standard cosmological perturbation theory the observable distance-redshift relations are calculated from the background solution, we took into account the effect of the perturbations on the luminosity distance to first order. To check the validity of the perturbative approach, the idea was to deduce the perturbation profile by requiring that the perturbed luminosity distance equals the luminosity distance inferred from the SNIa data – taken to be the standard ΛCDM luminosity distance for simplicity.

The other aim of Paper 2 was to contrast the result with LTB models, which, under certain conditions have been shown to be physically equivalent to perturbed FRW models [115,142,147]. Our study in Paper 2 addresses only the issue of whether the nonlinear effects of structures on the light propagation can be captured within the perturbative framework, whereas the question of other nonlinear effects such as the backreaction of the average expansion is not explicitly considered. Of course, these effects might or might not be distinct in the real universe – a better overall understanding would be needed.

We start by assuming that the spacetime can be described by a perturbed FRW model in the Newtonian gauge, as given by the line-element (4.95). The effect of linear perturbations on the luminosity distance has been calculated in the past [148–151]. We follow the notation of Bonvin, Durrer and Gasparini [151], who find the luminosity distance $d_L(\eta_s, \hat{\mathbf{n}})$ of a source at conformal time η_s in a universe described by the metric (4.95) as given by [151]

$$\begin{aligned}\frac{d_L(\eta_s,\hat{\mathbf{n}})}{1+z} \quad - \quad & \Delta\eta = (\mathbf{v}_o\cdot\hat{\mathbf{n}} - \psi_o)\,\Delta\eta - 2\Delta\eta\mathbf{v}\cdot\hat{\mathbf{n}} + 2\int_{\eta_s}^{\eta_o}\mathrm{d}\lambda\,\psi + 2\Delta\eta\int_{\eta_s}^{\eta_o}\mathrm{d}\lambda\,\hat{\mathbf{n}}\cdot\nabla\psi + \\ + \quad & 2\int_{\eta_s}^{\eta_o}\mathrm{d}\lambda\int_{\eta_s}^{\lambda}\mathrm{d}\bar{\lambda}\,\hat{\mathbf{n}}\cdot\nabla\psi - \int_{\eta_s}^{\eta_o}\mathrm{d}\lambda\int_{\eta_s}^{\lambda}\mathrm{d}\bar{\lambda}\,(\bar{\lambda}-\eta_s)\left(\nabla^2\psi - \hat{\mathbf{n}}\cdot\nabla\left(\hat{\mathbf{n}}\cdot\nabla\psi\right)\right), \end{aligned} \tag{4.96}$$

where $\hat{\mathbf{n}} = -\hat{\mathbf{e}}_r$ refers to the spatial direction of light propagating towards the observer, η_s is the conformal time at emission, and $\Delta\eta \equiv \eta_o - \eta_s$. The integrands of the above integrals are taken

to depend on λ ($\bar{\lambda}$) as well as on $\mathbf{x} = \mathbf{x}_o - \hat{\mathbf{n}}\,(\eta_o - \lambda)$, i.e. they are evaluated on the past light cone. The subscript o refers to the observer today.

Let $k^\mu \equiv \mathrm{d}x^\mu/\mathrm{d}\lambda$ be the photon momentum, that is the light-like geodesic for the metric with affine parameter λ. The geodesic equation reads as

$$\frac{\mathrm{d}k^\mu}{\mathrm{d}\lambda} + \Gamma^\mu_{\rho\sigma} k^\rho k^\sigma = 0 \ . \tag{4.97}$$

For simplicity, let us consider the metric

$$\mathrm{d}s^2 = -(1+2\psi)\mathrm{d}\eta^2 + (1-2\psi)\delta_{ij}\mathrm{d}x^i\mathrm{d}x^j \ . \tag{4.98}$$

The Christoffel symbols (2.2) for the metric (4.98) are given in Eq. (A.2) of Appendix A. To first order, the four-velocity $u^\mu = \mathrm{d}x^\mu/\mathrm{d}\tau$ of the cosmic fluid is given by

$$(u^\mu) = (1-\psi, v^i) \ . \tag{4.99}$$

Since the background metric of Eq. (4.98) is Minkowski, the background photon momentum is constant and we may normalize the affine parameter such that $\bar{k}^0 = 1$ and $\bar{k}^i = n^i$ with $\sum_{i=1}^3 n^i n^i = 1$. As usual, the overbars denote background quantities. For the perturbed 4-velocity of the photon we may still assume $k^0_s = 1$. The geodesic equation (4.97) then yields for k^0 (to first order)

$$k^0(\lambda_o) - k^0(\lambda_s) = k^0(\lambda_o) - 1 = -2\int_{\lambda_s}^{\lambda_o} \mathrm{d}\lambda \hat{\mathbf{n}}\cdot\nabla\psi \ , \tag{4.100}$$

from which we also have

$$k^0(\lambda) = \frac{\mathrm{d}\eta}{\mathrm{d}\lambda} = 1 - 2\int_{\lambda_s}^{\lambda} \mathrm{d}\lambda' \hat{\mathbf{n}}\cdot\nabla\psi \ , \tag{4.101}$$

so that $\mathrm{d}\lambda = \mathrm{d}\eta$ to first order. As we interpret the function $\psi(\eta, \mathbf{x})$ along the light cone, i.e.

$$\psi(\eta, \mathbf{x}) = \psi(\eta(\lambda), \mathbf{x}(\eta(\lambda))) \equiv \psi(\eta(\lambda)) \equiv \psi(\lambda) \ , \tag{4.102}$$

we can write (to first order)

$$\frac{\mathrm{d}\psi}{\mathrm{d}\lambda} = \frac{\mathrm{d}\psi}{\mathrm{d}\eta} = \frac{\mathrm{d}x^\mu}{\mathrm{d}\eta}\frac{\partial\psi}{\partial x^\mu} = \dot{\psi} + \hat{\mathbf{n}}\cdot\nabla\psi \ , \tag{4.103}$$

where $\dot{\psi} \equiv \partial_\eta\psi$. Inserting Eq. (4.103) into (4.100) then yields

$$k^0(\lambda_o) - 1 = -2(\psi_o - \psi_s) + 2\int_{\lambda_s}^{\lambda_o} \mathrm{d}\lambda\dot{\psi} \ . \tag{4.104}$$

For k^i, integrating the geodesic equation (4.97) gives

$$k^i(\lambda_o) - k^i(\lambda_s) = 2n^i(\psi_o - \psi_s) - 2\int_{\lambda_s}^{\lambda_o} \mathrm{d}\lambda\partial_i\psi \ . \tag{4.105}$$

Using Eqs. (4.99), (4.103), (4.104) and (4.105), the redshift of a photon emitted at spacetime position s and observed at o then becomes

$$1 + z_m = \frac{(g_{\mu\nu}k^\mu u^\nu)_s}{(g_{\mu\nu}k^\mu u^\nu)_o} = 1 + \psi_s - \psi_o + (\mathbf{v}_o - \mathbf{v}_s)\cdot\hat{\mathbf{n}} + 2\int_{\eta_s}^{\eta_o} \mathrm{d}\eta\hat{\mathbf{n}}\cdot\nabla\psi \ , \tag{4.106}$$

where the subscript m refers to the perturbed Minkowski metric (4.98). The redshift z deduced from the metric (4.95) and the redshift of Eq. (4.106) are related by

$$1 + z = (1 + \bar{z})(1 + z_m) \ , \tag{4.107}$$

where

$$z = \bar{z} + \delta z \ , \tag{4.108}$$

with

$$1 + \bar{z} = \frac{1}{a} \ , \tag{4.109}$$

referring to the unperturbed redshift of the EdS model.

In Eq. (4.96), η_s refers to the background conformal time corresponding to the emission of light from the source. However, in the presence of perturbations a fixed value of η does not correspond to a spatially homogeneous value of the redshift z. Furthermore, it is z, not η, which is measurable and by considering any quantity as a function of redshift effectively one slices the universe in slices of constant z, not η. We would thus like to have the luminosity distance in Eq. (4.96) as a function of the redshift z. With the help of Eq. (4.108), we obtain

$$d_L(z, \hat{\mathbf{n}}) = d_L(\bar{z}, \hat{\mathbf{n}}) + \frac{\mathrm{d}d_L(z, \hat{\mathbf{n}})}{\mathrm{d}z}\Big|_{\bar{z}} \delta z \equiv d_L(\eta_s, \hat{\mathbf{n}}) + \frac{\mathrm{d}d_L(z, \hat{\mathbf{n}})}{\mathrm{d}z}\Big|_{\bar{z}} \delta z \ , \tag{4.110}$$

where we can write

$$\frac{\mathrm{d}d_L(z, \hat{\mathbf{n}})}{\mathrm{d}z}\Big|_{\bar{z}} = \frac{\partial d_L(\bar{z}, \hat{\mathbf{n}})}{\partial \bar{z}} + \frac{\partial d_L(\bar{z}, \hat{\mathbf{n}})}{\partial \eta_s} \frac{\partial \eta_s}{\partial a_s} \frac{\partial a_s}{\partial \bar{z}} \ , \tag{4.111}$$

as the term is multiplied by the small quantity δz in Eq. (4.110). For the background luminosity distance $d_L(\bar{z})$, we obtain from Eqs. (2.36) and (4.81) that

$$d_L(\bar{z}) = (1 + \bar{z})(\eta_0 - \eta_s) \ , \tag{4.112}$$

so Eq. (4.111) thus becomes

$$\frac{\mathrm{d}d_L(z, \hat{\mathbf{n}})}{\mathrm{d}z}\Big|_{\bar{z}} = \Delta\eta + \frac{1}{\mathcal{H}_s} + \text{first order} \ , \tag{4.113}$$

where we have used Eq. (4.109). From Eq. (4.107), we can calculate that

$$\frac{\delta z}{1 + z} = \frac{z_m}{1 + z_m} = z_m \ , \tag{4.114}$$

to first order. Altogether, by combining Eqs. (4.106), (4.110), (4.113) and (4.114) we obtain

$$\frac{d_L(z, \hat{\mathbf{n}})}{1 + z} - \Delta\eta = \frac{d_L(\eta_s, \hat{\mathbf{n}})}{1 + z} - \Delta\eta + \left(\Delta\eta + \frac{1}{\mathcal{H}_s}\right) \left[\psi_s - \psi_o + (\mathbf{v}_o - \mathbf{v}_s) \cdot \hat{\mathbf{n}} + 2 \int_{\eta_s}^{\eta_o} \mathrm{d}\lambda \, \hat{\mathbf{n}} \cdot \nabla\psi\right] \ . \tag{4.115}$$

Inserting Eq. (4.96) into Eq. (4.115) finally yields for the luminosity distance

$$\begin{aligned} \frac{d_L(z, \hat{\mathbf{n}})}{1 + z} - \Delta\eta \ &= \ \left(2\Delta\eta + \frac{1}{\mathcal{H}_s}\right)(\mathbf{v}_o \cdot \hat{\mathbf{n}} - \psi_o) - \left(3\Delta\eta + \frac{1}{\mathcal{H}_s}\right)\mathbf{v}_s \cdot \hat{\mathbf{n}} + \left(\Delta\eta + \frac{1}{\mathcal{H}_s}\right)\psi_s \\ &+ \ 2\int_{\eta_s}^{\eta_o} \mathrm{d}\lambda \, \psi + 2\left(2\Delta\eta + \frac{1}{\mathcal{H}_s}\right)\int_{\eta_s}^{\eta_o} \mathrm{d}\lambda \, \hat{\mathbf{n}} \cdot \nabla\psi + 2\int_{\eta_s}^{\eta_o} \mathrm{d}\lambda \int_{\eta_s}^{\lambda} \mathrm{d}\bar{\lambda} \, \hat{\mathbf{n}} \cdot \nabla\psi \\ &- \ \int_{\eta_s}^{\eta_o} \mathrm{d}\lambda \int_{\eta_s}^{\lambda} \mathrm{d}\bar{\lambda} \, (\bar{\lambda} - \eta_s) \left(\nabla^2\psi - \hat{\mathbf{n}} \cdot \nabla\left(\hat{\mathbf{n}} \cdot \nabla\psi\right)\right) \ . \end{aligned} \tag{4.116}$$

Eq. (4.116) can be used to determine the fluctuations of the luminosity distance induced by a Gaussian perturbation [151], such as the one commonly assumed to arise from inflation and describing structure formation in the concordance cosmology. However, we turned the reasoning the other way round and asked: assuming the lhs of Eq. (4.116) is a measured function from SNIa observations – here taken to be the $d_L(z)$ relation corresponding to the ΛCDM universe with $\Omega_\Lambda \simeq 0.7$ and $\Omega_m \simeq 0.3$ – and that the underlying model for the background universe is the EdS model, can we determine the perturbation ψ (or $\mathbf{v}$) needed to give the observed luminosity distance? In other words, can a local gravitational perturbation fool us into thinking that light has propagated in a universe with the estimated value for the cosmological constant? We will answer this question by assuming that the perturbation ψ exhibits spherical symmetry for simplicity.

Assuming linear theory, one can relate the velocity field $\mathbf{v}$ with respect to the EdS background and the Newtonian potential by [146]

$$\mathbf{v} = -\frac{2}{3\mathcal{H}}\nabla\psi \ . \tag{4.117}$$

For the radial component v_r, Eq. (4.117) yields

$$\hat{\mathbf{e}}_r \cdot \mathbf{v} = v_r = -\frac{2}{3\mathcal{H}}\hat{\mathbf{e}}_r \cdot \nabla\psi = -\frac{2}{3\mathcal{H}}\frac{\partial}{\partial r}\psi \ . \tag{4.118}$$

From Eq. (4.116), it is convenient to derive a second-order equation for the radial velocity v_r – assuming that it is the dominant component $\mathbf{v} \simeq v_r\hat{\mathbf{e}}_r$ – by acting with two derivatives along the past light cone:

$$\frac{\mathrm{d}}{\mathrm{d}\eta} \equiv \frac{\partial}{\partial\eta} + \hat{\mathbf{n}} \cdot \nabla = \frac{\partial}{\partial\eta} - \hat{\mathbf{e}}_r \cdot \nabla \ . \tag{4.119}$$

Indeed, if the radial component is to be able to account for the observed $d_L(z)$ relation, it will have to be be much larger than the other velocity components related to the standard small Gaussian density fluctuations. Given v_r, the potential can be determined via Eq. (4.117).

Let us calculate the $\nabla^2\psi$ term in Eq. (4.116). For the flat matter-dominated universe, we have $\partial_\eta\psi = 0$ [146]. Assuming the radial velocity is dominant, we can write

$$\nabla \cdot \mathbf{v} = \left(\frac{2}{r} + \hat{\mathbf{e}}_r \cdot \nabla\right) v_r = \left(\frac{2}{r} + \frac{\partial}{\partial\eta} - \frac{\mathrm{d}}{\mathrm{d}\eta}\right) v_r \, , \tag{4.120}$$

where we have used Eq. (4.119). Substituting v_r from Eq. (4.118) into Eq. (4.120) and using Eq. (4.76) and the result $\Delta\eta = r$ given by Eq. (4.81) yields

$$\nabla \cdot \mathbf{v} = \frac{2v_r}{\Delta\eta} - \frac{\mathrm{d}}{\mathrm{d}\eta}v_r + \frac{\mathcal{H}v_r}{2} \ , \tag{4.121}$$

so that we obtain from Eq. (4.117)

$$-\Delta\eta\nabla^2\psi = \frac{3\mathcal{H}}{2}\Delta\eta\nabla \cdot \mathbf{v} = \frac{3\mathcal{H}^2}{2}\left(\frac{\Delta\eta}{2} + \frac{2}{\mathcal{H}}\right) v_r - \frac{3\mathcal{H}\Delta\eta}{2}\frac{\mathrm{d}}{\mathrm{d}\eta}v_r \, . \tag{4.122}$$

Taking the two derivatives (4.119) of Eq. (4.116), with the help of Eq. (4.122), yields

$$\begin{aligned} \frac{\mathrm{d}^2}{\mathrm{d}\eta_s^2}\left[\frac{d_L}{1+z} - \Delta\eta\right] &= \left(3\Delta\eta + \frac{1}{\mathcal{H}_s}\right)\frac{\mathrm{d}^2}{\mathrm{d}\eta_s^2}v_{sr} - \frac{3\mathcal{H}_s}{2}\left(7\Delta\eta + \frac{13}{3\mathcal{H}_s}\right)\frac{\mathrm{d}}{\mathrm{d}\eta_s}v_{sr} + \\ &+ \frac{15\mathcal{H}_s^2}{4}\left(\frac{7}{5}\Delta\eta + \frac{3}{\mathcal{H}_s}\right)v_{sr} \ , \end{aligned} \tag{4.123}$$

where $v_{sr} \equiv \hat{\mathbf{e}}_r \cdot \mathbf{v}_s = -\hat{\mathbf{n}} \cdot \mathbf{v}_s$. We can now express Eq. (4.123) in terms of the redshift z, which, as each term in Eq. (4.123) is first order, becomes just the background EdS redshift. Thus, by using Eqs. (4.78), (4.80) and (4.81), we finally obtain

$$\left(6 - \frac{5}{\sqrt{1+z}}\right)(1+z)^3 \frac{\mathrm{d}^2 v_{sr}}{\mathrm{d}z^2} + \frac{3}{2}\left(20 - \frac{44}{3\sqrt{1+z}}\right)(1+z)^2 \frac{\mathrm{d}v_{sr}}{\mathrm{d}z} +$$
$$+ \quad \frac{3}{4}\left(14 + \frac{1}{\sqrt{1+z}}\right)(1+z) v_{sr} = H_0 \left[(1+z)^2 \frac{\mathrm{d}^2}{\mathrm{d}z^2} d_L - \frac{1}{2}(1+z)\frac{\mathrm{d}}{\mathrm{d}z} d_L + \frac{1}{2} d_L\right] . \quad (4.124)$$

Assuming that the observed d_L is described by the corresponding theoretical relation for a ΛCDM universe

$$d_L = \frac{1+z}{H_0^{\Lambda\mathrm{CDM}}} \int_1^{1+z} \frac{\mathrm{d}x}{\sqrt{\alpha x^3 + \beta}} \ , \quad (4.125)$$

where $\alpha \simeq 0.3$, $\beta \simeq 0.7$ and $H_0^{\Lambda\mathrm{CDM}} = 70$ km/s/Mpc, the rhs of Eq. (4.124) becomes

$$H_0 \left[(1+z)^2 \frac{\mathrm{d}^2}{\mathrm{d}z^2} d_L - \frac{1}{2}(1+z)\frac{\mathrm{d}}{\mathrm{d}z} d_L + \frac{1}{2} d_L\right] = \frac{3}{2} \frac{H_0}{H_0^{\Lambda\mathrm{CDM}}} \frac{(1+z)^2 \beta}{(\alpha(1+z)^3 + \beta)^{3/2}} \ . \quad (4.126)$$

In Fig. 4.5, we have plotted the solution to the equation of motion for the velocity field, given by Eq. (4.124), that gives rise to the luminosity distance given in Eq. (4.125). We have also plotted the gravitational potential ψ, assuming that it is zero at large redshifts. As the solution demonstrates, a spherically symmetric small perturbation in the gravitational potential can indeed explain the observed acceleration. Note that the value H_0 in the hypothetical $\Omega = 1$ dust universe is not really an observable since the model is unlikely to fit all cosmological data. For the purposes of the present approach, it is an adjustable parameter. Here we have chosen $H_0 = 50$ km/s/Mpc for illustrative purposes only. As is obvious from the gravitational potential of Fig. 4.5, physically the perturbation corresponds to a spherical underdensity around us.

The density profile on the light cone can be immediately obtained via the poisson equation [146]

$$4\pi a^2 G \delta\rho = \nabla^2 \psi - 3\mathcal{H}^2 \psi \ . \quad (4.127)$$

Using Eqs. (4.122), (4.78) and (4.81), we obtain the total matter density $\rho = \bar{\rho} + \delta\rho$, where $\bar{\rho} = \bar{\rho}_{\mathrm{crit}}(z) = 3H_0^2/(8\pi G)(1+z)^3$, along the light cone:

$$8\pi G \rho(z) = 3H_0^2 (1+z)^3 \Big[1 - \frac{1}{2}\frac{(1+1/\sqrt{1+z})}{(1-1/\sqrt{1+z})} v_{sr}(z) - (1+z)\frac{\mathrm{d}v_{sr}(z)}{\mathrm{d}z} - 2\psi(z)\Big] \ . \quad (4.128)$$

In Fig. 4.6, we plot $\rho(z)/\bar{\rho}_{\mathrm{crit}}(z)$. The density contrast

$$\delta(z) \equiv \delta\rho(z)/\bar{\rho}(z) \ , \quad (4.129)$$

which we plot in Fig. 4.7, remains small during the whole evolution. It is thus important to note that the supernova data does not require a large density perturbation, but the large effect comes solely from the perturbations in the luminosity distance. The magnitude of the density contrast (4.129) at the last scattering surface is $|\delta(1100)| \simeq 10^{-5}$, consistent with the CMB observations.

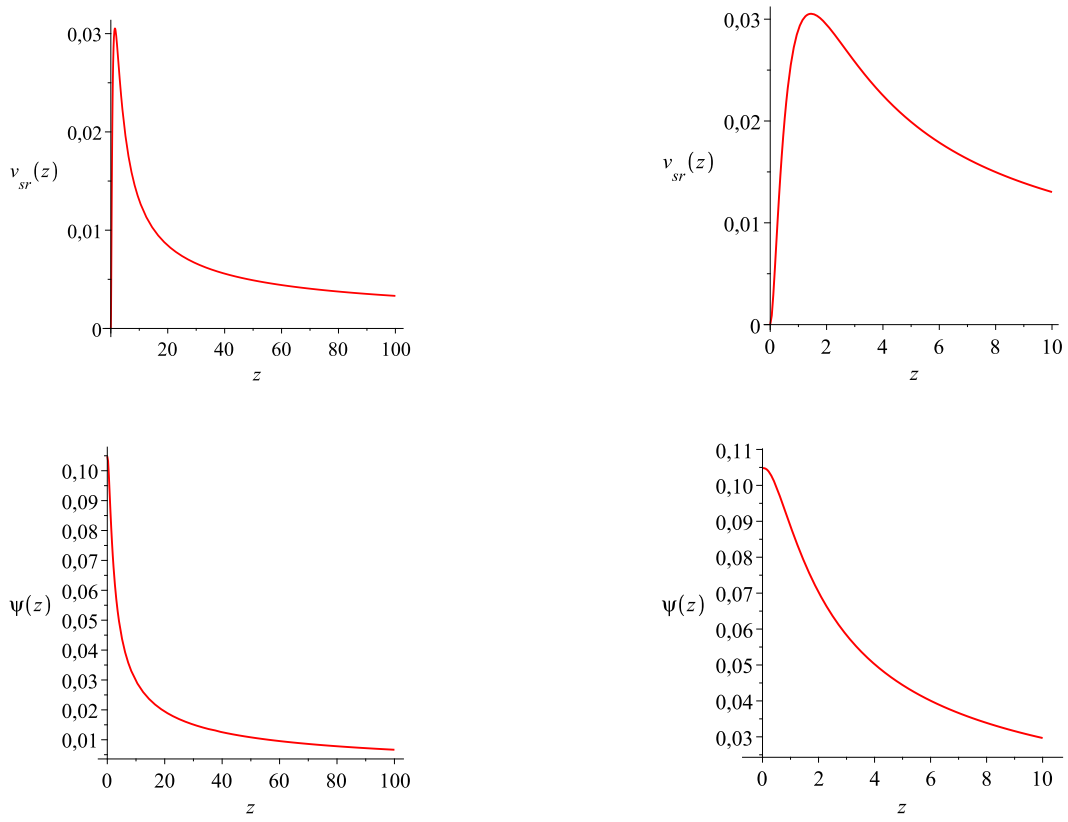

Figure 4.5: The velocity field $v_{sr}(z)$ and the gravitional potential $\psi(z)$ of the perturbed FRW universe. The plots on the right are close-ups of those on the left for redshifts $z < 10$.

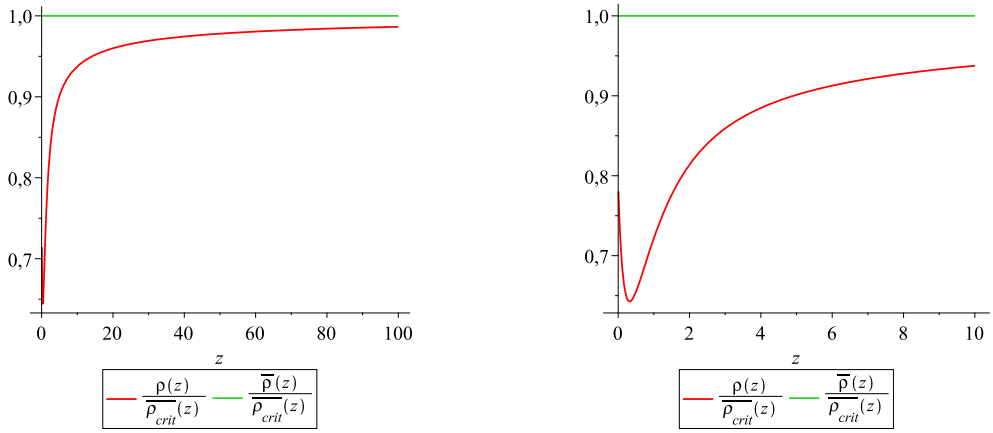

Figure 4.6: The density profile $\rho(z)/\bar{\rho}_{\rm crit}(z)$ (the red line). The green line corresponds to the background EdS, where $\bar{\rho}(z)/\bar{\rho}_{\rm crit}(z) = 1$. The plot on the right is a close-up of that on the left for redshifts $z < 10$.

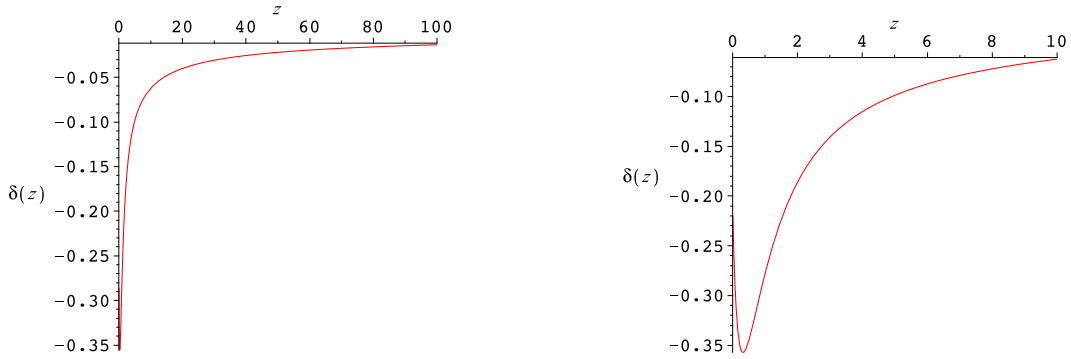

Figure 4.7: The density contrast $\delta(z) = \delta\rho(z)/\bar{\rho}(z)$. The plot on the right is a close-up of that on the left for redshifts $z < 10$.

In the second part of Paper 2 we considered the question of how LTB models relate to the perturbed FRW models. We just showed that the perturbed FRW model provides a fit to the supernova data, but we also know that LTB models can do that as well. Indeed, it has been shown that under certain conditions, the LTB metric (3.13) can be brought to the perturbed FRW form (4.95) via the following nonlinear gauge transformation [142, 147]:

$$r = \frac{A(\tilde{t},\tilde{r})}{a(\tilde{t})}(1+\xi(\tilde{t},\tilde{r})) \tag{4.130}$$

$$t = \tilde{t}+\xi^0(\tilde{t},\tilde{r}) \ , \tag{4.131}$$

where tildes now refer to the LTB coordinates and $a(\tilde{t}) \equiv (\tilde{t}/\tilde{t}_0)^{2/3}$ is a fictitious FRW scale factor corresponding to the background EdS universe, while θ and φ remain unchanged. If the LTB model is to be close to the FRW, the functions $\xi(\tilde{t},\tilde{r})$ and $\xi^0(\tilde{t},\tilde{r})$ must satisfy $|\xi|, |\xi^0 H| \ll 1$. The aim was to show whether these conditions are satisfied for our case on the past light cone.

Eq. (4.130) defines the FRW distance r in terms of the physical distance A, a prescribed FRW scale factor $a(\tilde{t}) \equiv \left(\tilde{t}/\tilde{t}_0\right)^{2/3}$ and a function ξ which is chosen to ensure that on the light cone r takes the standard FRW form (4.81) in terms of the redshift:

$$\frac{A(\tilde{t}(z),\tilde{r}(z))}{a(z)}(1+\xi(\tilde{t}(z),\tilde{r}(z))) = 2H_0^{-1}(1-1/\sqrt{1+z}) \ . \tag{4.132}$$

Furthermore, we choose the arbitrary $\tilde{r}$ such that, on the light cone:

$$\partial_{\tilde{r}} A(z) = a(z) \ . \tag{4.133}$$

Let us now determine the functions $H\xi^0$ and ξ along the light cone. We could proceed by using the gauge transformation equations for the metric components [115], calculated analogously to the standard cosmological perturbation theory as explained in Sect. 4.4.1. However, here we do not need the full gauge transformations, as the sufficient information is obtained by the fact that if the perturbed FRW and LTB metrics are to describe the same spacetime, just written in different coordinates, the observable distance-redshift relations should be the same: $d_A^{\mathrm{LTB}} = d_A^{\Lambda\mathrm{CDM}}$. So, by having the distance-redshift relations we can readily read off $A(\tilde{t},\tilde{r})$ along the past light cone of the LTB model, that is $A(z)$. The function ξ can then be determined directly from (4.132).

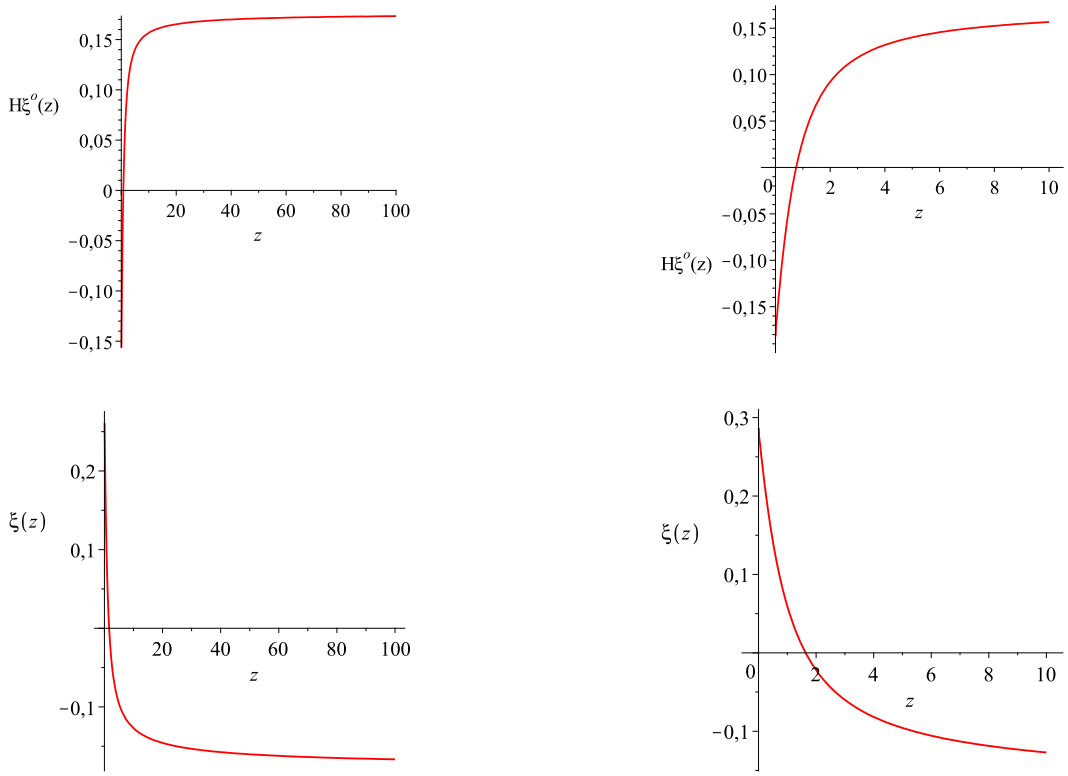

Figure 4.8: The functions $H\xi^0(z)$ and $\xi(z)$ relating the perturbed FRW and LTB clock times. The plots on the right are close-ups of those on the left for redshifts $z < 10$.

The $\theta\theta$ component of the gauge transformation of the metric yields (to first order):

$$A(\tilde{t},\tilde{r}) \simeq a(t)r\left[1-\psi(t,r)\right] \simeq a(\tilde{t})r\left[1-\psi(\tilde{t},\tilde{r})+H(\tilde{t})\xi^0(\tilde{t},\tilde{r})\right] \ , \tag{4.134}$$

where we have used Eq. (4.131). Using Eqs. (4.130), (4.132) and (3.60), we can thus obtain the small quantity $H\xi^0$ from Eq. (4.134) along our line of sight:

$$d_A(z) \ = \frac{2}{H_0(1+z)}\Big(1-\frac{1}{\sqrt{1+z}}\Big)\Big(1-\psi(z)+H(z)\xi^0(z)\Big) \tag{4.135}$$

$$\Longrightarrow \quad H(z)\xi^0(z) = \frac{d_A(z)(1+z)H_0}{2(1-\frac{1}{\sqrt{1+z}})}+\psi(z)-1 \ , \tag{4.136}$$

where d_A is obtained from Eqs. (2.36) and (4.125).

The outcome is shown in Fig. 4.8, where we display the shift between t and $\tilde{t}$ in units of the inverse Hubble rate as well as ξ. As can be seen both $H\xi^0$ and ξ are less than one. In principle, we could have kept higher orders in our expansions, but other than changing the numerical values of $\xi^0(z)$ by $\mathcal{O}(30)\%$, we do not expect any qualitative change in this picture. Thus, the conclusion is that an LTB model fitting the SNIa data can be mapped into a perturbed FRW model by a nonlinear coordinate transformation of the form (4.130), (4.131), at least on the light cone.

4.4.3 Comments on the perturbative FRW studies

In Paper 2, we established that the FRW $\Omega = 1$ dust universe with spherically symmetric perturbation $\psi(z)$ can fit the SNIa data. Physically, the perturbation corresponds to a void around us with EdS asymptotics along the past light cone so that the early universe was very homogeneous. Although the model as such is likely to be too simplistic to explain all the relevant cosmological data (though see Ref. [152] for a consideration of the CMB peak positions as well), the interesting point is that even in the absence of dark energy, the SNIa data does not require large deviations from FRW. Indeed, we also demonstrated that if the non-perturbative, spherically symmetric LTB model fits the SNIa data, it can be mapped into the perturbed FRW model by a nonlinear coordinate transformation (4.130) and (4.131), at least on the light cone. This is consistent with the results of Refs. [115,142]. It would be interesting to study whether the perturbative nature of the model persists inside the past light cone. A generalization including anisotropic density perturbations was considered in [153], resulting in possible observational constraints on large void models.

Our result is also consistent with the study of [154], where the so-called "inverse-problem" was considered – finding a map from a given luminosity distance to the corresponding LTB model; see also Refs. [155–157]. In [154], an LTB model whose luminosity distance is equivalent to that of the ΛCDM model was constructed. On the other hand, the results obtained in [141] seem to contradict ours. Their study is based on considering a Gpc sized LTB void model approaching spatially to EdS solution, and indeed, such case indicates a breakdown of the perturbative description: the peculiar velocity in their model becomes large at redshifts $z \gtrsim 500$, when the void represents a nonlinear superhorizon density fluctuation. However, when confronted with the CMB observations, a universe dominated by a Gpc sized void seems unlikely.

Although perturbations can have a large effect on the luminosity distance, as our studies demonstrate and has also been suggested in [144, 158] (for a recent discussion considering how inhomogeneities can affect the optical properties of the universe in the context of various close to FRW models, see Ref. [159]), the claim is that if the metric of the universe remains close to FRW at all times, then the backreaction of the average expansion, being a genuine nonlinear effect, would have to be small. We refer the reader to Refs. [106, 143, 144], where the issue of the applicability of the linearly perturbed RW metric and its possible implications about the magnitude of the backreaction are extensively discussed. Indeed, it was shown in [144] that in the case the metric can be written in a perturbed RW form, the average expansion rate – and thus the backreaction – and the redshift remain close to the background (with non-restricted second spatial derivatives of ψ and under certain assumptions about the observer four-velocity). However, the question of the magnitude of the backreaction as well as other possible nonlinear mechanisms in the real universe still remains unresolved; the metric is not an observable quantity, and on the other hand, it is supported by observations that there are large local variations in the expansion rate [68,160]. The question is thus whether the effects of these local variations cancel in reality when considering the average expansion rate, the redshift and the distance.

Chapter 5

Summary

The main purpose of this thesis has been to study the dynamics of cosmological structures in the context of the interpretation of observations such as the distance-redshift relations. The standard way in cosmology is to describe the universe by the homogeneous and isotropic FRW models, with linear perturbations representing the structures. However, the validity of the standard approach needs to be carefully evaluated: Firstly, there are nonlinear structures in the universe and their role must be understood for correct interpretation of the cosmological data. Secondly, in order to match with the observations, a mysterious dark energy component is needed in the standard cosmology, starting to affect the dynamics of the universe in the same era when nonlinear cosmological structures start to form. Indeed, these observations combined with the theoretical fact that general relativity is a nonlinear theory have provided the main motivation for this thesis work. The fact that dark energy is both theoretically problematic and observationally coincidental, provides further motivation to study the cosmological inhomogeneities.

In cosmology, the complexity of both the universe and the underlying theory of gravity forces to make some simplifying assumptions. The required simplifications can be embodied by symmetries in the exact solutions of the Einstein equation or by explicit averaging of the Einstein equation. Our emphasis has mainly been to study the issue from the latter perspective. Due to the nonlinearity of general relativity, the average evolution of a clumpy space is not the same as the evolution of a smooth space – a feature known as the backreaction [38]. This issue was considered already in the 1960's by Shirokov and Fisher [34], and elaborated by Ellis in the 1980's [36], but has gained more attention during the last decade in the context of the dark energy debate [37].

The task then is to evaluate the magnitude of the backreaction in the universe. Various attempts have been made to do this, however, with contradictory outcomes; in some estimates the backreaction is found to be large while others conclude it to be negligible. Here we do not make an attempt to fully quantify the backreaction in the real universe, but instead investigate various aspects of how it could be done in practice. The backreaction in the Buchert equations is a quantity that depends on the variance of the average expansion rate minus the average shear. The shear has often been neglected in the backreaction estimates, so that the effect would come solely from the variance term, which is indeed known to be present in the cosmic web. However, as we found in Papers 3 and 4, it can be of equal importance to take into account the shear as well, as shear is expected to occur at the boundaries of regions with different expansion rates. Indeed, we pinpointed the issue of small versus large backreaction to the question of matching conditions. Using the exact spherically symmetric but inhomogeneous LTB solution to represent voids and walls, we demonstrated that the shear can bring down the backreaction by at least five

orders of magnitude for voids of the observed size, relative to the case where the shear is neglected altogether. To address the question of whether the result is a general property of all realistic cosmological solutions of general relativity, one needs to construct more sophisticated models for the cosmic web beyond spherical symmetry. Indeed, a dense enough network of uncompensated voids would give rise to large global negative spatial curvature absent in our models, which is known to be important for large backreaction [12]. It may be of importance to include collapsing regions as well, as they have been suggested to play an essential role in the average dynamics of the universe due to the large contribution they can have to the variance of the expansion rate [19, 107].

Besides the backreaction, the explicit dependence on the averaging scale in the averaged Einstein equations makes them differ from the Friedmann equations. In Paper 1, we analyzed the scale-dependence using the flat LTB model as a testing ground. By allowing for a redshift dependent averaging scale in calculating the observable luminosity and angular diameter distances, we found an $\mathcal{O}(1\%)$ precision at redshifts $z < 2$ compared to their exact values, whereas using a single scale gives too coarse predictions for the observables. The choice of the averaging scale could thus be as important as the backreaction term in a realistic application of the averaging method in the real universe. Although considered merely under the assumption of spherical symmetry for testing purposes, we expect the scale-dependent averaging method to show its full advantage only when applied to more irregularly shaped large scale inhomogeneities.

In Paper 2, we found that a spherically symmetric linear perturbation around the Einstein-de Sitter model can provide an equally good fit to the supernova data as the standard ΛCDM model. Whereas in the standard cosmological perturbation theory, the effect of the perturbations on the observable distance measures is assumed to average out, we obtained the large effect by not making this assumption. The density profile was found to represent a void around our location, with the density contrast remaining small along the light cone. Although likely to be a too simple model to explain all the relevant cosmological data, the point was in demonstrating the possible effect inhomogeneities can have already at the perturbative level. Furthermore, the model was confirmed to be equivalent to a nonperturbative LTB model along the past light cone, suggesting that the supernova data does not imply the presence of additional nonperturbative effects. On the other hand, while perturbations can considerably affect the distance-redshift relations, the backreaction remains small in close to FRW spacetimes [106, 144]. The question is whether a close to FRW spacetime represents ours – that is, whether the effects of the known large local variations of the dynamical quantities in the cosmic web cancel when considering the average expansion rate and ultimately the observables such as the redshift and the distance.

So far, it has been demonstrated in various works that the effects of the structures not present in the standard cosmology can account for at least most of the current cosmological observations without dark energy. In this thesis, the focus was to take steps towards better theoretical understanding of different mechanisms as to how the cosmic structures may affect the observable dynamics of the universe. The destiny of dark energy remains to be seen, but what is certain is that more accurate theoretical calculations combined with the improving observational data with less model-dependent assumptions are required to further clarify the dynamics of the cosmic web.

Appendix A

Christoffel symbols for the LTB metric and the perturbed Minkowski metric

The nonzero Christoffel symbols (2.2) for the metric (3.2) are:

$$\begin{aligned}
\Gamma^0_{11} &= X\dot{X}, \quad \Gamma^0_{22} = A\dot{A}, \quad \Gamma^0_{33} = A\dot{A}\sin^2\theta, \quad \Gamma^1_{11} = \frac{X'}{X}, \quad \Gamma^1_{01} = \Gamma^1_{10} = \frac{\dot{X}}{X} \ , \\
\Gamma^1_{22} &= -\frac{AA'}{X^2}, \quad \Gamma^1_{33} = -\frac{AA'\sin^2\theta}{X^2}, \quad \Gamma^2_{02} = \Gamma^2_{20} = \Gamma^3_{03} = \Gamma^3_{30} = \frac{\dot{A}}{A} \ , \\
\Gamma^2_{12} &= \Gamma^2_{21} = \Gamma^3_{13} = \Gamma^3_{31} = \frac{A'}{A}, \quad \Gamma^2_{33} = -\sin\theta\cos\theta, \quad \Gamma^3_{23} = \Gamma^3_{32} = \frac{\cos\theta}{\sin\theta} \ ,
\end{aligned} \tag{A.1}$$

where $' \equiv \partial_r f$ and $\dot{} \equiv \partial_t$.

The Christoffel symbols (2.2) for the metric (4.98), to first order in the gravitational potential ψ, are:

$$\begin{aligned}
\Gamma^0_{00} &= \dot{\psi}, \quad \Gamma^0_{0i} = \partial_i\psi, \quad \Gamma^0_{ij} = -\dot{\psi}\delta_{ij} \ , \\
\Gamma^i_{00} &= \delta^{ik}\partial_k\psi, \quad \Gamma^i_{0j} = -\dot{\psi}\delta^i_j, \quad \Gamma^i_{jk} = \delta^{li}\partial_l\psi\delta_{jk} - \delta^i_j\partial_k\psi - \delta^i_k\partial_j\psi \ ,
\end{aligned} \tag{A.2}$$

where $\dot{} \equiv \partial_\eta$.

Bibliography

[1] A. Einstein, "The Field Equations of Gravitation," *Sitzungsber. Preuss. Akad. Wiss. Berlin (Math. Phys.)* **1915** (1915) 844–847.

[2] A. H. Guth, "The Inflationary Universe: A Possible Solution to the Horizon and Flatness Problems," *Phys. Rev.* **D23** (1981) 347–356.

[3] A. D. Linde, "A New Inflationary Universe Scenario: A Possible Solution of the Horizon, Flatness, Homogeneity, Isotropy and Primordial Monopole Problems," *Phys. Lett.* **B108** (1982) 389–393.

[4] **Supernova Search Team** Collaboration, A. G. Riess *et al.*, "Observational Evidence from Supernovae for an Accelerating Universe and a Cosmological Constant," *Astron. J.* **116** (1998) 1009–1038, arXiv:astro-ph/9805201.

[5] **Supernova Cosmology Project** Collaboration, S. Perlmutter *et al.*, "Measurements of Omega and Lambda from 42 High-Redshift Supernovae," *Astrophys. J.* **517** (1999) 565–586, arXiv:astro-ph/9812133.

[6] A. G. Riess *et al.*, "New Hubble Space Telescope Discoveries of Type Ia Supernovae at $z > 1$: Narrowing Constraints on the Early Behavior of Dark Energy," *Astrophys. J.* **659** (2007) 98–121, arXiv:astro-ph/0611572.

[7] **WMAP** Collaboration, E. Komatsu *et al.*, "Seven-Year Wilkinson Microwave Anisotropy Probe (WMAP) Observations: Cosmological Interpretation," *Astrophys. J. Suppl.* **192** (2011) 18, arXiv:1001.4538 [astro-ph.CO].

[8] **SDSS** Collaboration, D. J. Eisenstein *et al.*, "Detection of the Baryon Acoustic Peak in the Large-Scale Correlation Function of SDSS Luminous Red Galaxies," *Astrophys. J.* **633** (2005) 560–574, arXiv:astro-ph/0501171.

[9] J. Frieman, M. Turner, and D. Huterer, "Dark Energy and the Accelerating Universe," *Ann.Rev.Astron.Astrophys.* **46** (2008) 385–432, arXiv:0803.0982 [astro-ph].

[10] E. J. Copeland, M. Sami, and S. Tsujikawa, "Dynamics of dark energy," *Int. J. Mod. Phys.* **D15** (2006) 1753–1936, arXiv:hep-th/0603057.

[11] S. Nojiri and S. D. Odintsov, "Introduction to modified gravity and gravitational alternative for dark energy," *eConf* **C0602061** (2006) 06, arXiv:hep-th/0601213 [hep-th].

[12] T. Buchert, "Dark Energy from Structure - A Status Report," *Gen. Rel. Grav.* **40** (2008) 467–527, arXiv:0707.2153 [gr-qc].

[13] M.-N. Celerier, "The Accelerated Expansion of the Universe Challenged by an Effect of the Inhomogeneities. A Review," arXiv:astro-ph/0702416.

[14] S. Rasanen, "Backreaction: directions of progress," *Class.Quant.Grav.* **28** (2011) 164008, arXiv:1102.0408 [astro-ph.CO]. * Temporary entry *.

[15] A. Krasiński, *Inhomogeneous cosmological models*. Cambridge University Press, 1997. http://books.google.com/books?id=8ZNMOMc92ugC.

[16] J. Plebanski and A. Krasinski, "An introduction to general relativity and cosmology,". Cambridge, UK: Univ. Pr. (2006) 534 p.

[17] M.-N. Celerier, "Do we really see a cosmological constant in the supernovae data ?," *Astron. Astrophys.* **353** (2000) 63–71, arXiv:astro-ph/9907206.

[18] H. Alnes, M. Amarzguioui, and O. Gron, "An inhomogeneous alternative to dark energy?," *Phys.Rev.* **D73** (2006) 083519, arXiv:astro-ph/0512006 [astro-ph].

[19] S. Rasanen, "Accelerated expansion from structure formation," *JCAP* **0611** (2006) 003, arXiv:astro-ph/0607626.

[20] K. Enqvist and T. Mattsson, "The effect of inhomogeneous expansion on the supernova observations," *JCAP* **0702** (2007) 019, arXiv:astro-ph/0609120 [astro-ph].

[21] T. Mattsson, "Dark energy as a mirage," *Gen.Rel.Grav.* **42** (2010) 567–599, arXiv:0711.4264 [astro-ph].

[22] K. Enqvist, M. Mattsson, and G. Rigopoulos, "Supernovae data and perturbative deviation from homogeneity," *JCAP* **0909** (2009) 022, arXiv:0907.4003 [astro-ph.CO].

[23] P. Bull and T. Clifton, "Local and non-local measures of acceleration in cosmology," arXiv:1203.4479 [astro-ph.CO].

[24] M. Tanimoto and Y. Nambu, "Luminosity distance-redshift relation for the LTB solution near the center," *Class. Quant. Grav.* **24** (2007) 3843–3857, arXiv:gr-qc/0703012.

[25] S. Alexander, T. Biswas, A. Notari, and D. Vaid, "Local Void vs Dark Energy: Confrontation with WMAP and Type Ia Supernovae," *JCAP* **0909** (2009) 025, arXiv:0712.0370 [astro-ph].

[26] J. Garcia-Bellido and T. Haugboelle, "Confronting Lemaitre-Tolman-Bondi models with Observational Cosmology," *JCAP* **0804** (2008) 003, arXiv:0802.1523 [astro-ph].

[27] J. Garcia-Bellido and T. Haugboelle, "The radial BAO scale and Cosmic Shear, a new observable for Inhomogeneous Cosmologies," *JCAP* **0909** (2009) 028, arXiv:0810.4939 [astro-ph].

[28] T. Clifton, P. G. Ferreira, and K. Land, "Living in a Void: Testing the Copernican Principle with Distant Supernovae," *Phys. Rev. Lett.* **101** (2008) 131302, arXiv:0807.1443 [astro-ph].

[29] S. February, J. Larena, M. Smith, and C. Clarkson, "Rendering Dark Energy Void," *Mon. Not. Roy. Astron. Soc.* **405** (2010) 2231, arXiv:0909.1479 [astro-ph.CO].

[30] K. Kainulainen and V. Marra, "SNe observations in a meatball universe with a local void," *Phys. Rev.* **D80** (2009) 127301, arXiv:0906.3871 [astro-ph.CO].

[31] T. Biswas, A. Notari, and W. Valkenburg, "Testing the Void against Cosmological data: fitting CMB, BAO, SN and H0," *JCAP* **1011** (2010) 030, arXiv:1007.3065 [astro-ph.CO].

[32] V. Marra and M. Paakkonen, "Observational constraints on the LLTB model," *JCAP* **1012** (2010) 021, arXiv:1009.4193 [astro-ph.CO].

[33] V. Marra and A. Notari, "Observational constraints on inhomogeneous cosmological models without dark energy," *Class. Quant. Grav.* **28** (2011) 164004, arXiv:1102.1015 [astro-ph.CO].

[34] M. F. Shirokov and I. Z. Fisher, "Isotropic Space with Discrete Gravitational-Field Sources. On the Theory of a Nonhomogeneous Isotropic Universe," *AZh* **39** (1962) 899.

[35] G. F. R. Ellis, "Relativistic cosmology - Its nature, aims and problems," in *General Relativity and Gravitation Conference*, B. Bertotti, F. de Felice, & A. Pascolini, ed., pp. 215–288. 1984.

[36] G. Ellis and W. Stoeger, "The 'fitting problem' in cosmology," *Class.Quant.Grav.* **4** (1987) 1697–1729.

[37] C. Clarkson, G. Ellis, J. Larena, and O. Umeh, "Does the growth of structure affect our dynamical models of the universe? The averaging, backreaction and fitting problems in cosmology," *Rept. Prog. Phys.* **74** (2011) 112901, arXiv:1109.2314 [astro-ph.CO].

[38] T. Buchert, "On average properties of inhomogeneous fluids in general relativity. I: Dust cosmologies," *Gen. Rel. Grav.* **32** (2000) 105–125, arXiv:gr-qc/9906015.

[39] T. Mattsson and M. Mattsson, "Exploiting scale dependence in cosmological averaging," *JCAP* **0802** (2008) 004, arXiv:0708.3673 [astro-ph].

[40] M. Mattsson and T. Mattsson, "On the role of shear in cosmological averaging," *JCAP* **1010** (2010) 021, arXiv:1007.2939 [astro-ph.CO].

[41] M. Mattsson and T. Mattsson, "On the role of shear in cosmological averaging II: large voids, non-empty voids and a network of different voids," arXiv:1012.4008 [astro-ph.CO].

[42] E. Hubble, "A relation between distance and radial velocity among extra–galactic nebulae," *Proc. Nat. Acad. Sci.* **15** (1929) 168–173.

[43] R. A. Alpher, H. Bethe, and G. Gamow, "The origin of chemical elements," *Phys. Rev.* **73** (1948) 803–804.

[44] R. A. Alpher and R. C. Herman, "On the Relative Abundance of the Elements," *Physical Review* **74** (Dec., 1948) 1737–1742.

[45] A. A. Penzias and R. W. Wilson, "A Measurement of excess antenna temperature at 4080- Mc/s," *Astrophys. J.* **142** (1965) 419–421.

[46] J. C. Mather, D. J. Fixsen, R. A. Shafer, C. Mosier, and D. T. Wilkinson, "Calibrator Design for the COBE Far Infrared Absolute Spectrophotometer (FIRAS)," *Astrophys. J.* **512** (1999) 511–520, arXiv:astro-ph/9810373.

[47] G. F. Smoot *et al.*, "Structure in the COBE differential microwave radiometer first year maps," *Astrophys. J.* **396** (1992) L1–L5.

[48] E. W. Kolb and M. S. Turner, "The Early universe," *Front. Phys.* **69** (1990) 1–547.

[49] A. R. Liddle and D. H. Lyth, "Cosmological inflation and large-scale structure,". ISBN-13-9780521828499.

[50] S. Tsujikawa, "Introductory review of cosmic inflation," arXiv:hep-ph/0304257 [hep-ph].

[51] F. Hoyle and M. S. Vogeley, "Voids in the 2dF Galaxy Redshift Survey," *Astrophys. J.* **607** (2004) 751–764, arXiv:astro-ph/0312533.

[52] J. R. Gott, III *et al.*, "A Map of the Universe," *Astrophys. J.* **624** (2005) 463, arXiv:astro-ph/0310571.

[53] A. V. Tikhonov, "Voids in the SDSS Galaxy Survey," *Astron. Lett.* **33** (2007) 499–511, arXiv:0707.4283 [astro-ph].

[54] A. M. von Benda-Beckmann and V. Mueller, "Void Statistics and Void Galaxies in the 2dFGRS," arXiv:0710.2783 [astro-ph].

[55] **The 2dFGRS** Collaboration, S. Cole *et al.*, "The 2dF Galaxy Redshift Survey: Power-spectrum analysis of the final dataset and cosmological implications," *Mon. Not. Roy. Astron. Soc.* **362** (2005) 505–534, arXiv:astro-ph/0501174.

[56] **SDSS** Collaboration, M. Tegmark *et al.*, "Cosmological Constraints from the SDSS Luminous Red Galaxies," *Phys. Rev.* **D74** (2006) 123507, arXiv:astro-ph/0608632.

[57] C. M. Will, "The confrontation between general relativity and experiment," *Living Rev. Rel.* **9** (2005) 3, arXiv:gr-qc/0510072.

[58] S. M. Carroll, "Spacetime and geometry: An introduction to general relativity,". San Francisco, USA: Addison-Wesley (2004) 513 p.

[59] W. H. Smith, "LHC Startup," arXiv:0808.3131 [hep-ex].

[60] D. Branch and G. Tammann, "Type ia supernovae as standard candles," *Ann.Rev.Astron.Astrophys.* **30** (1992) 359–389.

[61] I. M. H. Etherington, "On the Definition of Distance in General Relativity.," *Philosophical Magazine* **15** (1933) 761–+.

[62] G. F. R. Ellis, "relativistic cosmology.," in *General Relativity and Cosmology*, R. K. Sachs, ed., pp. 104–182. 1971.

[63] **Supernova Search Team** Collaboration, J. L. Tonry *et al.*, "Cosmological results from high-z supernovae," *Astrophys.J.* **594** (2003) 1–24, arXiv:astro-ph/0305008 [astro-ph].

[64] **Supernova Cosmology Project** Collaboration, R. A. Knop *et al.*, "New constraints on Omega(M), Omega(lambda), and w from an independent set of eleven high-redshift supernovae observed with HST," *Astrophys.J.* **598** (2003) 102, arXiv:astro-ph/0309368 [astro-ph].

[65] **Supernova Search Team** Collaboration, A. G. Riess *et al.*, "Type Ia Supernova Discoveries at z>1 From the Hubble Space Telescope: Evidence for Past Deceleration and Constraints on Dark Energy Evolution," *Astrophys. J.* **607** (2004) 665–687, arXiv:astro-ph/0402512.

[66] **The SNLS Collaboration** Collaboration, P. Astier *et al.*, "The Supernova legacy survey: Measurement of omega(m), omega(lambda) and W from the first year data set," *Astron.Astrophys.* **447** (2006) 31–48, arXiv:astro-ph/0510447 [astro-ph].

[67] H. Alnes and M. Amarzguioui, "CMB anisotropies seen by an off-center observer in a spherically symmetric inhomogeneous universe," *Phys. Rev.* **D74** (2006) 103520, arXiv:astro-ph/0607334.

[68] D. L. Wiltshire, P. R. Smale, T. Mattsson, and R. Watkins, "Hubble flow variance and the cosmic rest frame," arXiv:1201.5371 [astro-ph.CO].

[69] A. Vilenkin and L. H. Ford, "Gravitational Effects upon Cosmological Phase Transitions," *Phys. Rev.* **D26** (1982) 1231.

[70] A. D. Linde, "Scalar Field Fluctuations in Expanding Universe and the New Inflationary Universe Scenario," *Phys. Lett.* **B116** (1982) 335.

[71] A. A. Starobinsky, "Dynamics of Phase Transition in the New Inflationary Universe Scenario and Generation of Perturbations," *Phys. Lett.* **B117** (1982) 175–178.

[72] S. Dodelson, *Modern cosmology*. Academic Press, New York, NY, 2003.

[73] S. Hassani, *Mathematical physics: a modern introduction to its foundations*. Springer, 1999. http://books.google.com/books?id=BCMLOp6DyFIC.

[74] M. Kerscher, K. Mecke, J. Schmalzing, C. Beisbart, T. Buchert, *et al.*, "Morphological fluctuations of large scale structure: The PSCz survey," *Astron.Astrophys.* **373** (2001) 1–11, arXiv:astro-ph/0101238 [astro-ph].

[75] L. Pietronero and F. S. Labini, "Statistical physics for complex cosmic structures," *AIP Conf.Proc.* **822** (2006) 294–300, arXiv:astro-ph/0406202 [astro-ph].

[76] D. W. Hogg, D. J. Eisenstein, M. R. Blanton, N. A. Bahcall, J. Brinkmann, *et al.*, "Cosmic homogeneity demonstrated with luminous red galaxies," *Astrophys.J.* **624** (2005) 54–58, arXiv:astro-ph/0411197 [astro-ph].

[77] F. S. Labini, "Characterizing the large scale inhomogeneity of the galaxy distribution," *AIP Conf. Proc.* **1241** (2010) 981–990, arXiv:0910.3833 [astro-ph.CO].

[78] F. S. Labini and L. Pietronero, "The complex universe: recent observations and theoretical challenges," *J. Stat. Mech.* **1011** (2010) P11029, arXiv:1012.5624 [astro-ph.CO].

[79] F. S. Labini, "Inhomogeneities in the universe," *Class. Quant. Grav.* **28** (2011) 164003, arXiv:1103.5974 [astro-ph.CO].

[80] A. Einstein, "Cosmological Considerations in the General Theory of Relativity," *Sitzungsber. Preuss. Akad. Wiss. Berlin (Math. Phys.)* **1917** (1917) 142–152.

[81] G. Lemaitre, "The expanding universe," *Gen. Rel. Grav.* **29** (1997) 641–680.

[82] Y. B. Zeldovich, "Cosmological Constant and Elementary Particles," *JETP Lett.* **6** (1967) 316.

[83] Y. B. Zel'dovich, "The Cosmological constant and the theory of elementary particles," *Sov. Phys. Usp.* **11** (1968) 381–393.

[84] L. A. Kofman, N. Y. Gnedin, and N. A. Bahcall, "Cosmological constant, COBE cosmic microwave background anisotropy, and large scale clustering," *Astrophys.J.* **413** (1993) 1–9.

[85] **SDSS** Collaboration, B. A. Reid *et al.*, "Baryon Acoustic Oscillations in the Sloan Digital Sky Survey Data Release 7 Galaxy Sample," *Mon. Not. Roy. Astron. Soc.* **401** (2010) 2148–2168, arXiv:0907.1660 [astro-ph.CO].

[86] **ESSENCE** Collaboration, W. M. Wood-Vasey *et al.*, "Observational Constraints on the Nature of the Dark Energy: First Cosmological Results from the ESSENCE Supernova Survey," *Astrophys. J.* **666** (2007) 694–715, arXiv:astro-ph/0701041.

[87] N. Jarosik *et al.*, "Seven-Year Wilkinson Microwave Anisotropy Probe (WMAP) Observations: Sky Maps, Systematic Errors, and Basic Results," arXiv:1001.4744 [astro-ph.CO].

[88] J. A. Peacock, "Cosmological physics,". Cambridge, UK: Univ. Pr. (1999) 682 p.

[89] A. G. Riess *et al.*, "A Redetermination of the Hubble Constant with the Hubble Space Telescope from a Differential Distance Ladder," *Astrophys. J.* **699** (2009) 539–563, arXiv:0905.0695 [astro-ph.CO].

[90] N. Straumann, "Dark energy: Recent developments," *Mod. Phys. Lett.* **A21** (2006) 1083–1098, arXiv:hep-ph/0604231.

[91] T. P. Sotiriou, "Modified Actions for Gravity: Theory and Phenomenology," arXiv:0710.4438 [gr-qc].

[92] T. Koivisto, *Formation of Structure in Dark Energy Cosmologies.* PhD Thesis, Helsinki University Print, 2006.

[93] K. Bolejko, M.-N. Celerier, and A. Krasinski, "Inhomogeneous cosmological models: exact solutions and their applications," *Class. Quant. Grav.* **28** (2011) 164002, arXiv:1102.1449 [astro-ph.CO].

[94] G. Lemaître, "L'Univers en expansion," *Annales de la Societe Scietifique de Bruxelles* **53** (1933) 51–+.

[95] R. C. Tolman, "Effect of imhomogeneity on cosmological models," *Proc.Nat.Acad.Sci.* **20** (1934) 169–176.

[96] H. Bondi, "Spherically symmetrical models in general relativity," *Mon.Not.Roy.Astron.Soc.* **107** (1947) 410–425.

[97] P. S. Apostolopoulos, N. Brouzakis, N. Tetradis, and E. Tzavara, "Cosmological Acceleration and Gravitational Collapse," *JCAP* **0606** (2006) 009, arXiv:astro-ph/0603234.

[98] J. Silk, "Large-scale inhomogeneity of the Universe - Spherically symmetric models," *A&A.* **59** (July, 1977) 53–58.

[99] G. F. R. Ellis and T. Buchert, "The universe seen at different scales," *Phys. Lett.* **A347** (2005) 38–46, arXiv:gr-qc/0506106.

[100] G. F. R. Ellis, "83 years of general relativity and cosmology: Progress and problems," *Class. Quant. Grav.* **16** (1999) A37–A75.

[101] T. Buchert, "Toward physical cosmology: focus on inhomogeneous geometry and its non-perturbative effects," *Class. Quant. Grav.* **28** (2011) 164007, arXiv:1103.2016 [gr-qc].

[102] J. Ehlers, "Contributions to the relativistic mechanics of continuous media," *Gen. Rel. Grav.* **25** (1993) 1225–1266.

[103] G. F. R. Ellis and H. van Elst, "Cosmological models," *NATO Adv. Study Inst. Ser. C. Math. Phys. Sci.* **541** (1999) 1–116, arXiv:gr-qc/9812046.

[104] A. Paranjape and T. P. Singh, "Explicit Cosmological Coarse Graining via Spatial Averaging," *Gen. Rel. Grav.* **40** (2008) 139–157, arXiv:astro-ph/0609481.

[105] A. Paranjape and T. P. Singh, "The Possibility of Cosmic Acceleration via Spatial Averaging in Lemaitre-Tolman-Bondi Models," *Class. Quant. Grav.* **23** (2006) 6955–6969, arXiv:astro-ph/0605195.

[106] T. Buchert and S. Rasanen, "Backreaction in late-time cosmology," arXiv:1112.5335 [astro-ph.CO].

[107] S. Rasanen, "Evaluating backreaction with the peak model of structure formation," *JCAP* **0804** (2008) 026, arXiv:0801.2692 [astro-ph].

[108] T. Kai, H. Kozaki, K.-i. nakao, Y. Nambu, and C.-M. Yoo, "Can inhomogeneties accelerate the cosmic volume expansion?," *Prog. Theor. Phys.* **117** (2007) 229–240, arXiv:gr-qc/0605120.

[109] G. Ellis, "Patchy solutions," *Nature* **452** (2008) 158–161.

[110] E. W. Kolb, S. Matarrese, and A. Riotto, "On cosmic acceleration without dark energy," *New J. Phys.* **8** (2006) 322, arXiv:astro-ph/0506534.

[111] D. L. Wiltshire, "Cosmic clocks, cosmic variance and cosmic averages," *New J. Phys.* **9** (2007) 377, arXiv:gr-qc/0702082.

[112] A. Wiegand and T. Buchert, "Multiscale cosmology and structure-emerging Dark Energy: A plausibility analysis," *Phys. Rev.* **D82** (2010) 023523, arXiv:1002.3912 [astro-ph.CO].

[113] A. Ishibashi and R. M. Wald, "Can the acceleration of our universe be explained by the effects of inhomogeneities?," *Class.Quant.Grav.* **23** (2006) 235–250, arXiv:gr-qc/0509108 [gr-qc].

[114] J. Behrend, I. A. Brown, and G. Robbers, "Cosmological Backreaction from Perturbations," *JCAP* **0801** (2008) 013, arXiv:0710.4964 [astro-ph].

[115] A. Paranjape and T. Singh, "Cosmic Inhomogeneities and the Average Cosmological Dynamics," *Phys.Rev.Lett.* **101** (2008) 181101, arXiv:0806.3497 [astro-ph].

[116] T. Clifton and P. G. Ferreira, "Archipelagian Cosmology: Dynamics and Observables in a Universe with Discretized Matter Content," *Phys. Rev.* **D80** (2009) 103503, arXiv:0907.4109 [astro-ph.CO].

[117] T. Clifton, "Cosmology Without Averaging," *Class. Quant. Grav.* **28** (2011) 164011, arXiv:1005.0788 [gr-qc].

[118] D. Alonso, J. Garcia-Bellido, T. Haugbolle, and J. Vicente, "Large scale structure simulations of inhomogeneous LTB void models," *Phys. Rev.* **D82** (2010) 123530, arXiv:1010.3453 [astro-ph.CO].

[119] S. R. Green and R. M. Wald, "A new framework for analyzing the effects of small scale inhomogeneities in cosmology," *Phys. Rev.* **D83** (2011) 084020, arXiv:1011.4920 [gr-qc].

[120] S. Sarkar, "Is the evidence for dark energy secure?," *Gen. Rel. Grav.* **40** (2008) 269–284, arXiv:0710.5307 [astro-ph].

[121] A. Blanchard, "Evidence for the Fifth Element Astrophysical status of Dark Energy," *Astron. Astrophys. Rev.* **18** (2010) 595–645, arXiv:1005.3765 [astro-ph.CO].

[122] I. A. Brown, G. Robbers, and J. Behrend, "Averaging Robertson-Walker Cosmologies," *JCAP* **0904** (2009) 016, arXiv:0811.4495 [gr-qc].

[123] C. Clarkson, K. Ananda, and J. Larena, "The influence of structure formation on the cosmic expansion," *Phys. Rev.* **D80** (2009) 083525, arXiv:0907.3377 [astro-ph.CO].

[124] O. Umeh, J. Larena, and C. Clarkson, "The Hubble rate in averaged cosmology," *JCAP* **1103** (2011) 029, arXiv:1011.3959 [astro-ph.CO].

[125] L. Rudnick, S. Brown, and L. R. Williams, "Extragalactic Radio Sources and the WMAP Cold Spot," *Astrophys. J.* **671** (2007) 40–44, arXiv:0704.0908 [astro-ph].

[126] J. Einasto *et al.*, "Clusters and Superclusters in the Sloan Digital Sky Survey," *Astron. Astrophys.* **405** (2003) 425–444, arXiv:astro-ph/0212312.

[127] W. H. Press, S. A. Teukolsky, W. T. Vetterling, and B. P. Flannery, *Numerical recipes in Fortran 90 (2nd ed.): the art of parallel scientific computing.* Cambridge University Press, New York, NY, USA, 1996.

[128] T. Biswas, R. Mansouri, and A. Notari, "Nonlinear Structure Formation and Apparent Acceleration: an Investigation," *JCAP* **0712** (2007) 017, arXiv:astro-ph/0606703.

[129] A. Gruzinov, M. Kleban, M. Porrati, and M. Redi, "Gravitational Backreaction of Matter Inhomogeneities," *JCAP* **0612** (2006) 001, arXiv:astro-ph/0609553.

[130] D. Baumann, A. Nicolis, L. Senatore, and M. Zaldarriaga, "Cosmological Non-Linearities as an Effective Fluid," arXiv:1004.2488 [astro-ph.CO].

[131] Y. Nambu and M. Tanimoto, "Accelerating universe via spatial averaging," arXiv:gr-qc/0507057.

[132] C.-H. Chuang, J.-A. Gu, and W.-Y. P. Hwang, "Inhomogeneity-Induced Cosmic Acceleration in a Dust Universe," *Class. Quant. Grav.* **25** (2008) 175001, arXiv:astro-ph/0512651.

[133] K. Bolejko and L. Andersson, "Apparent and average acceleration of the Universe," *JCAP* **0810** (2008) 003, arXiv:0807.3577 [astro-ph].

[134] R. A. Sussman, "On the spatial volume averaging in Lemaitre-Tolman-Bondi dust models. 1. Back reaction, spatial curvature and binding energy," arXiv:0807.1145 [gr-qc].

[135] R. A. Sussman, "Quasi-local variables, non-linear perturbations and back- reaction in spherically symmetric spacetimes," arXiv:0809.3314 [gr-qc].

[136] R. A. Sussman, "Back-reaction and effective acceleration in generic LTB dust models," *Class. Quant. Grav.* **28** (2011) 235002, arXiv:1102.2663 [gr-qc].

[137] M. Kasai, H. Asada, and T. Futamase, "Toward a no-go theorem for accelerating universe by nonlinear backreaction," *Prog.Theor.Phys.* **115** (2006) 827–832, arXiv:astro-ph/0602506 [astro-ph].

[138] A. Paranjape, "Backreaction of Cosmological Perturbations in Covariant Macroscopic Gravity," *Phys.Rev.* **D78** (2008) 063522, arXiv:0806.2755 [astro-ph].

[139] A. Paranjape, "Nonlinear Structure Formation, Backreaction and Weak Gravitational Fields," arXiv:0811.2619 [astro-ph].

[140] A. Paranjape, "The Averaging Problem in Cosmology," arXiv:0906.3165 [astro-ph.CO].

[141] E. W. Kolb, V. Marra, and S. Matarrese, "On the description of our cosmological spacetime as a perturbed conformal Newtonian metric and implications for the backreaction proposal for the accelerating universe," *Phys.Rev.* **D78** (2008) 103002, arXiv:0807.0401 [astro-ph].

[142] K. Van Acoleyen, "LTB solutions in Newtonian gauge: From Strong to weak fields," *JCAP* **0810** (2008) 028, arXiv:0808.3554 [gr-qc].

[143] S. Rasanen, "Applicability of the linearly perturbed FRW metric and Newtonian cosmology," *Phys. Rev.* **D81** (2010) 103512, arXiv:1002.4779 [astro-ph.CO].

[144] S. Rasanen, "Light propagation and the average expansion rate in near- FRW universes," arXiv:1107.1176 [astro-ph.CO].

[145] S. Matarrese, S. Mollerach, and M. Bruni, "Second order perturbations of the Einstein-de Sitter universe," *Phys.Rev.* **D58** (1998) 043504, arXiv:astro-ph/9707278 [astro-ph].

[146] H. Kurki-Suonio, *Introduction to cosmological perturbation theory.* Lecture Notes, 2011.

[147] A. Paranjape and T. P. Singh, "Structure Formation, Backreaction and Weak Gravitational Fields," *JCAP* **0803** (2008) 023, arXiv:0801.1546 [astro-ph].

[148] M. Sasaki, "The Magnitude - Redshift relation in a perturbed Friedmann universe," *Mon. Not. Roy. Astron. Soc.* **228** (1987) 653–669.

[149] T. Pyne and M. Birkinshaw, "The Luminosity Distance in Perturbed FLRW Spacetimes," *Mon. Not. Roy. Astron. Soc.* **348** (2004) 581, arXiv:astro-ph/0310841.

[150] E. Barausse, S. Matarrese, and A. Riotto, "The Effect of Inhomogeneities on the Luminosity Distance- Redshift Relation: is Dark Energy Necessary in a Perturbed Universe?," *Phys. Rev.* **D71** (2005) 063537, arXiv:astro-ph/0501152.

[151] C. Bonvin, R. Durrer, and M. A. Gasparini, "Fluctuations of the luminosity distance," *Phys. Rev.* **D73** (2006) 023523, arXiv:astro-ph/0511183.

[152] C.-M. Yoo, K.-i. Nakao, and M. Sasaki, "CMB observations in LTB universes: Part I: Matching peak positions in the CMB spectrum," *JCAP* **1007** (2010) 012, arXiv:1005.0048 [astro-ph.CO].

[153] R. Nishikawa, C.-M. Yoo, and K.-i. Nakao, "Evolution of density perturbations in large void universe," arXiv:1202.1582 [astro-ph.CO].

[154] C.-M. Yoo, T. Kai, and K.-i. Nakao, "Solving Inverse Problem with Inhomogeneous Universe," *Prog. Theor. Phys.* **120** (2008) 937–960, arXiv:0807.0932 [astro-ph].

[155] H. Iguchi, T. Nakamura, and K.-i. Nakao, "Is dark energy the only solution to the apparent acceleration of the present universe?," *Prog. Theor. Phys.* **108** (2002) 809–818, arXiv:astro-ph/0112419.

[156] D. J. H. Chung and A. E. Romano, "Mapping Luminosity-Redshift Relationship to LTB Cosmology," *Phys. Rev.* **D74** (2006) 103507, arXiv:astro-ph/0608403.

[157] K. Bolejko, C. Hellaby, and A. H. A. Alfedeel, "The Metric of the Cosmos from Luminosity and Age Data," *JCAP* **1109** (2011) 011, arXiv:1102.3370 [astro-ph.CO].

[158] K. Bolejko, "The effect of inhomogeneities on the distance to the last scattering surface and the accuracy of the CMB analysis," *JCAP* **1102** (2011) 025, arXiv:1101.3338 [astro-ph.CO].

[159] K. Bolejko and P. G. Ferreira, "Ricci focusing, shearing, and the expansion rate in an almost homogeneous Universe," arXiv:1204.0909 [astro-ph.CO].

[160] N. Li and D. J. Schwarz, "Scale dependence of cosmological backreaction," *Phys. Rev.* **D78** (2008) 083531, arXiv:0710.5073 [astro-ph].